ANNUAL REPORT 2004
ZWE FRM-II

Neutron multiplication with respect to the external neutron source — Onset of criticality

Countrate of the 3 neutron detectors outside of the moderator tank, relative units, logarithmic scale

All shutdown rods and control rod in shutdown position

All shutdown rods fully withdrawn

Start of moving-out of the control rod

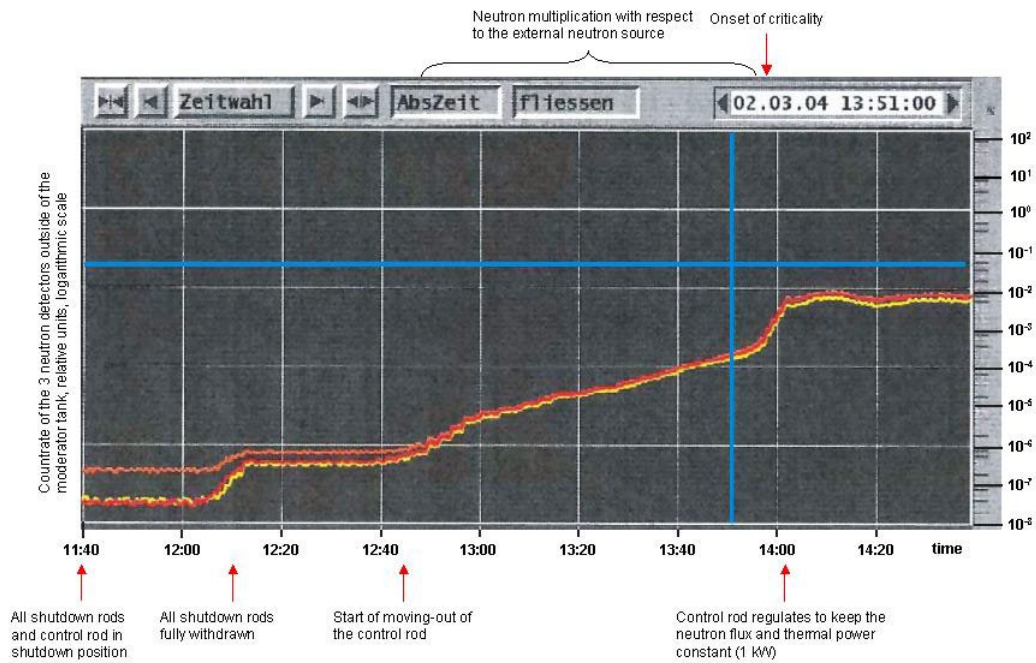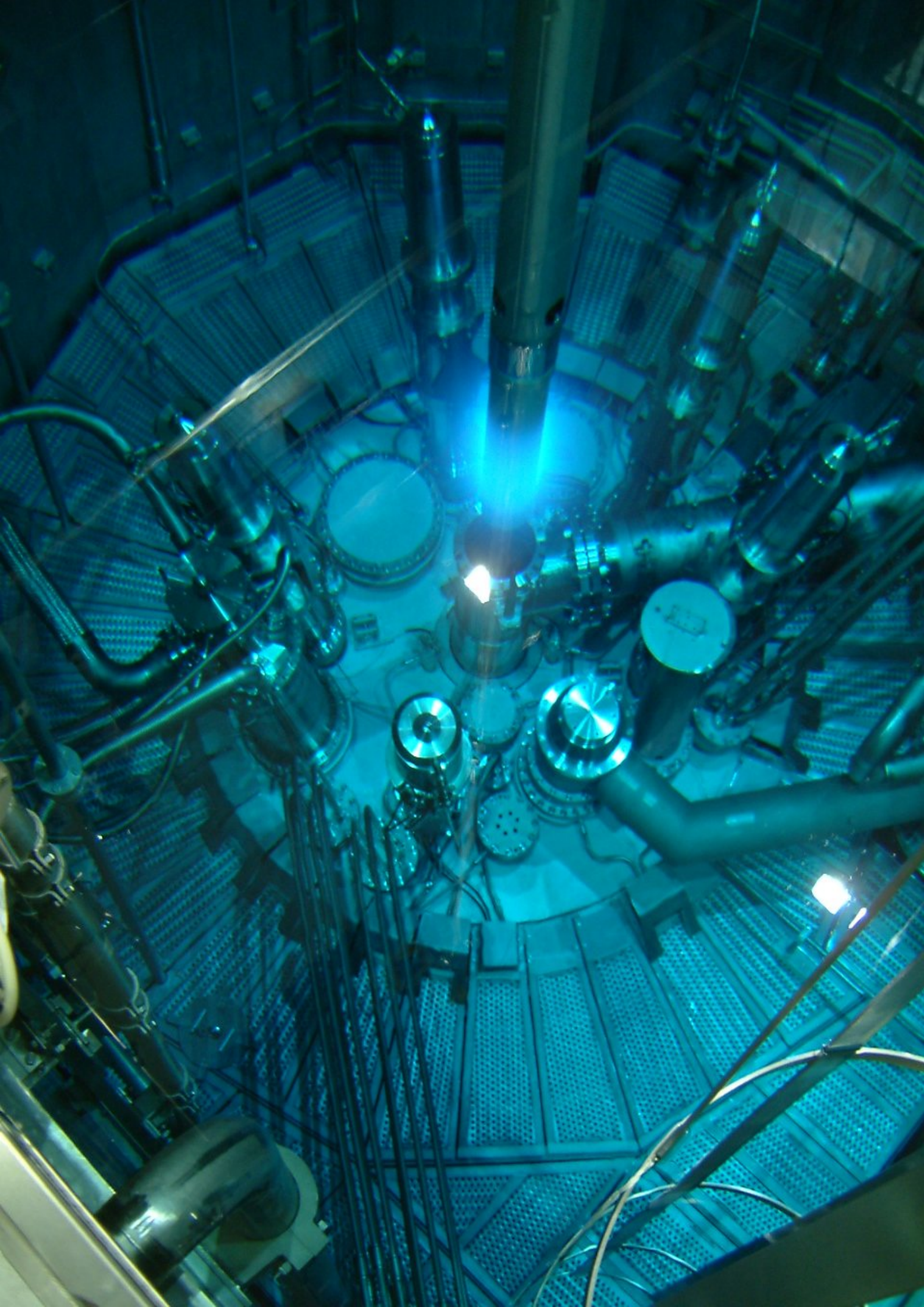Control rod regulates to keep the neutron flux and thermal power constant (1 kW)

cover image: neutron flux during first criticallity
inlet picture: unloading of the first fuel element

Contents

Directors' report

Successful Nuclear Commissioning of the FRM-II

Professor Heinz Maier-Leibnitz is the founder of Neutron Physics in Germany and Western Europe. He had built the Atomic Egg and later on the famous neutron research facility, the Institute Laue Langevin. From now on the TU München honors its famous physics teacher by calling its new neutron source "Forschungs-Neutronenquelle Heinz Maier-Leibnitz". For a while the well known shortcut FRM-II will also stay in use.

The outstanding event of the past year definitely was the success-ful nuclear commissioning of the FRM-II. On 2nd March 2004 at 2:01 pm the FRM-II produced its first neutrons by a self-amplifying nu-clear reaction. During the following months the FRM-II ran on "cook-ing power", i.e. with power lev-els in the order of some 1 - 100 kWatt in order to measure its es-sential nuclear parameters. On 20th March a power level of 2 MWatt was reached. The full power of 20 MWatt showed up on the power meters on 24th August for the first time. Finally on 21st October 2004 the equivalent of 52 full power days was achieved and the nuclear com-missioning was ended successfully on 24th October with the visual in-spection of the used fuel element. Congratulation to both, the staffs of Siemens/Framatome ANP and of FRM-II, who have achieved this suc-cess in close mutual collaboration. Details of the nuclear commission-ing are reported in section 1.1.

Most of the beam hole instru-ments and all irradiation facilities could align their components with the first neutrons. Everywhere the measured neutron fluxes coincided with the calculated ones in remark-able precision. To note some of the most exciting results: the sup-pression of the fast neutron flux in the irradiation positions is in the order of 10^4. The flux of thermal positrons on the experimental plat-form is in the order of 10^8 e$^+$/(cm^{2}s) with a spot being 8 mm in diame-ter, and there is hope for more in the near future. The time-of-flight spectrometer counts 10^{10} n/(cm^{2}s) at its sample position, of course all choppers open. The Cold Neutron Source achieves its promised 20 K with a heat load of almost 5 kWatt and the Hot Source is really hot, namely 2090°C. Numerous details are reported in the following contri-butions.

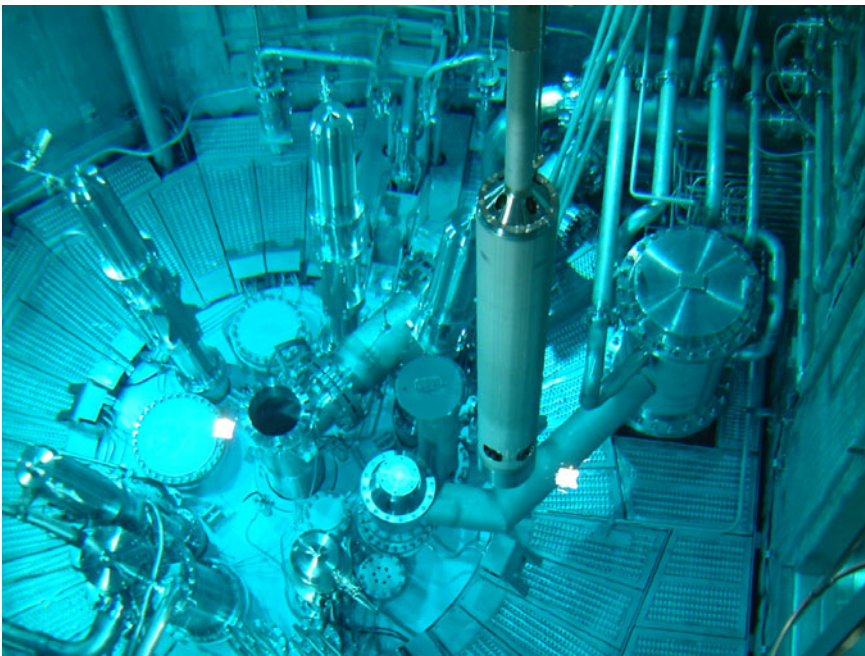According to a Bavarian tradition

Figure 1: Insertion fo the first fuel element into the reactor

important achievements need to be celebrated. On 9th July the President of the Technische Universität Prof. Dr. Wolfgang Herrmann invited Bavarian and German politicians, international neutron scientists and last but not least the colleagues from the Technische Universität München to officially inaugurate the new German neutron source. And thousand guests followed the invitation on a white and blue Bavarian summer day. "Neutrons are Light" was the welcome address by Prof. Wolfgang Herrmann. The Bavarian Minister of Science, Research and Culture Dr. Thomas Goppel opened the ceremony by a review of the stony way to accomplish the FRM-II. The Bavarian Minister President Dr. Edmund Stoiber emphasized the commitment and continuity of the Bavarian Government to invest in science. The Federal Minister of the Interior Dr. Otto Schily confirmed the firm support of the Federal Government for innovative research with neutrons and its importance in an European context. Finally, the Archbishop of Freising and München Friedrich Wetter and the Regional Bishop Mrs. Susanne Breit-Keßler, both of them inaugurated the FRM-II by blessing its staff and reminding them of a responsible use of their knowledge for the sake of humanity.

A few days before the artist Hermann Kleinknecht had finished his light installation at the FRM-II. Interpreting our motto "Neutrons are Light", Kleinknecht shows the visitors the light which leads to the neutrons. Shiny LEDs decorate every 2nd pillar of the fence surrounding the FRM II site. From the main entrance an avenue of cool blue light pillars leads to a huge glass cube illuminated inside by blue and green light bars.

The instrumentation and scientific use of the FRM-II got a big boost on 31st June. That day two important contracts were signed. The commitment of the Federal Ministry for Science (BMBF) to support the instrumentation of FRM-II by 31 Million € spread over the coming ten years and the treaty between the TUM and the Research Centre of Jülich (FZ-Jülich) to open an outstation of the FZ-Jülich on the site of the FRM-II. That outstation will operate at least seven instruments, one of them is currently under commissioning and another six are going to be newly constructed or moved from the DIDO research reactor to FRM-II. The other side of the coin is the closure of the research reactor DIDO at the FZ-Jülich by May 2006. At an yet unprecedented speed the TUM and the Bavarian Government launched a new building east of the reactor to house about 30 persons from Jülich, their laboratories and an experimental hall needed for storage, assembling new instruments and later on for accommodating new neutron guides coming from the reactor. In the course of time that outstation will change to an outstation of the Helmholtz-Gesellschaft that houses all activities from National Laboratories.

Two individuals of outstanding importance for the success of the FRM-II retired on 31st July. Ministerialdirigent Jürgen Großkreutz has passed his office to Ministerialrätin Dr. Ulrike Kirste. He was awarded with the Bavarian Order of Merit for having navigated the FRM-II through so many obstacles. On a voluntary basis Prof. Dr. Klaus Böning, the father of the compact core, keeps on teaching and communicating his knowledge about reactor physics to young students. Earlier on 31st March Dr. Wolfgang Waschkowski retired, very well known for his presentations committed to explaining the use of neutrons to a broader public. Of course he continues guiding visitors through FRM-II.

Figure 2: Prof. Dr. Klaus Böning and Ministerialdirigent Jürgen Großkreutz

Obtaining a significant share of industrial users certainly is an ambitious aim. A workshop organized by one of the members of the Strategierat, Prof. Dr. Heinz Voggenreiter, and held on 23rd June in Garching was aimed at researchers in the industry. The building of the Centre for Industrial Applications located on the premises of the FRM-II has almost been finished. We expect it to be handed over in spring 2005.

The construction of new instruments and amelioration of existing ones is never ending. Learning from the first neutron fluxes the radiological shieldings have been reinforced for the instruments in the experimental hall and for all neutron guides from the tunnel through the casemate up to the instruments. The new neutron guides for the small angle camera SANS-1 and the station for prompt gamma analysis PGA have been fed through the wall separating the neutron guide tunnel and the casemate. At an official ceremony taking place in December the instrument PUMA financed by the BMBF was officially inaugurated in the presence of both, the president of the TUM, Prof. Dr. Wolfgang A. Herrmann, and the president of the University of Göttingen, Prof. Dr. Horst Kern. As an early Christmas gift the He-3 polarizing facility has been successfully taken into operation on 22nd December.

In October 2004 FRM-II asked the international user community to submit proposals for a first "friendly" use of our instruments. 14 beam hole instruments will receive their first users during the two next fuel cycles. Altogether these instruments have been overbooked by a factor of two. The external scientific committee allocated beam time to user groups coming from 7 countries. Access for users from EU, other than Germans, will be supported within the EU framework program 6.

And when does routine operation start? Currently Siemens/Framatome ANP and FRM-II are preparing the FRM-II for the routine operation. This includes the removal of test facilities of the commissioning phase, exchange of one of the plugs for the neutron beam holes and last but not least a lot of paper work which reports on all the experience we have gained during the start up of the FRM-II. We are optimistic and hope for a start of routine operation in April 2005.

Guido Engelke   Winfried Petry   Klaus Schreckenbach
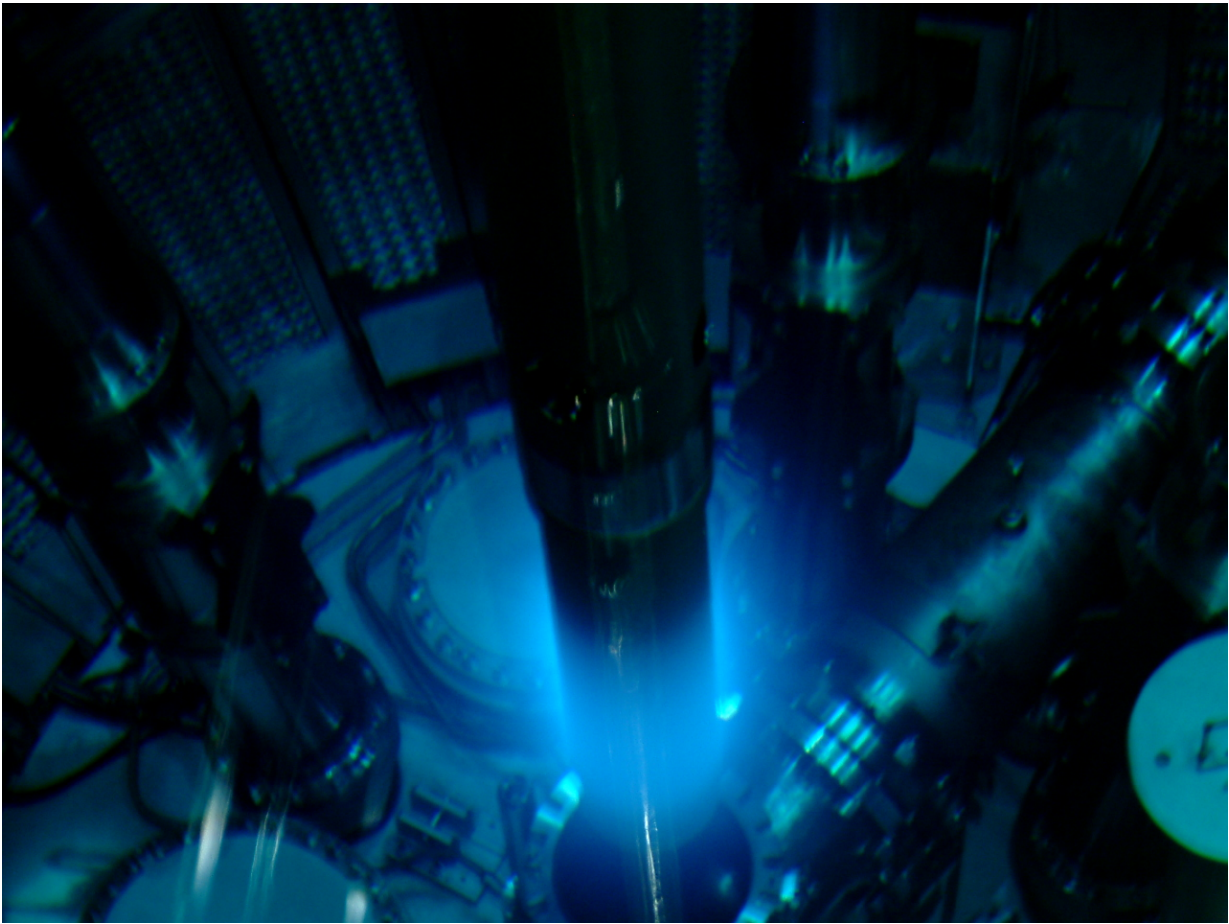
25.10.2004 Unloading of the first fuel element.

The Year in Pictures

Inauguration of the FRM-II on 26.6.2004

26.6.2004 Edmund Stoiber, Bavarian Minister-President, and his wife are welcomed by Prof. Dr. Wolfgang Herrmann on the occasion of the inauguaration of FRM-II.

26.6.2004 Cardinal F. Wetter, MDir. J. Großkreutz, Mrs. K. Stoiber, Minister-President Dr. E. Stoiber and State Minister Dr. T. Goppel in the reactor hall.

26.6.2004 Otto Schily (Federal Minister of the Interior)
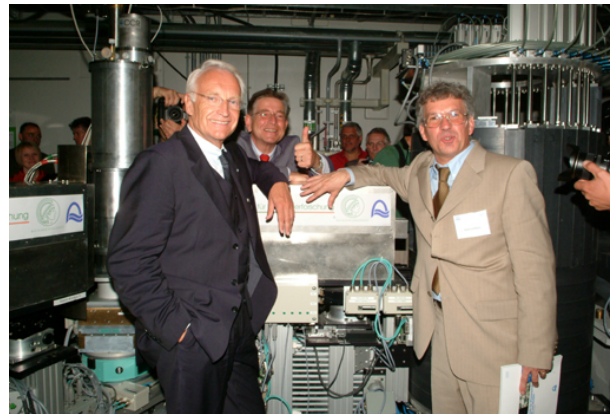
26.6.2004 Minister-President Dr. E. Stoiber, State Minister Dr. T. Goppel and Prof. Dr. W. Petry in the experimental hall at the TRIPS instrument.

30.6.2004 Signing the agreement to establish an outstation of FZ Jülich at the FRM-II: Front row (from left): Fr. Dzwonnek, Vice Chairman of the Board of Directors of FZ Jülich, Prof. Treusch, Chairman of the Board of Directors of FZ Jülich, Hr. Eisenbeiß, represenative of the TUM, standing (from left): MD Dr. Schunk, BMBF, Prof. Petry, scientific director of FRM-II, MDgt. Großkreutz, BStMfWFK.

17.08.04 Dr. Mohammad Al Ali Al Maadid (3rd from left), Ahmed Abdulla Al Mazroei (right) and Prof. Kerstin Wessig visit the FRM-II, accompanied by Prof. Dr. Gradinger(2nd from left) and Dr. R. Burgkart from the Klinik für Orthopädie.

23.7.2004 RDin Claudia Mangels and MRin Dr. Ulrike Kirste from the Bavarian State Ministry of Sciences, Research and the Arts visit the reactor.

23.10.2004 Presentation of th radiation protection group at the day of open doors

Minister-President Dr. E. Stoiber during the summer interview produced by the german television ZDF.

7.11.2004 Federal Chancellery Chief-of-Staff Frank Walter Steinmeier visiting the FRM-II.

1 Central services

1.1 FRM-II at Full Power

K. Schreckenbach[1], **Chr. Morkel**[1]
[1]ZWE FRM-II, TU München

After a long period of delay during 2001-2003 the Bavarian Regulatory Authority granted the third partial licence in May 2003 and finally permitted the nuclear start up of the FRM II at February 13th, 2004. Then, at March 2nd, 2004 the start up team of Framatome-ANP and Technische Universität München (TUM) reached the first criticality of the reactor at 2:01 pm under the eyes of the Regulatory Body and several technical experts. Following the event of the first criticality a series of low power tests at 200 kW was performed till April 12th, 2004. These careful checks included all relevant safety installations, radiological systems and a first power calibration. The phase of low power tests was closed with a first neutronic inspection of the yet fresh -or nearly fresh- fuel element: In perfect accordance with prior MCNP-calculations (Dr. Röhrmoser, Prof. Böning) the anisotropy of the burn up due to tank installations near the reactor core (hot source, cold source) could shown to be small (Fig. 1.1).

At April 20th, 2004 the power tests started at the level of 2 MW followed by 5 steps - 6 MW, 10 MW, 14 MW, 18 MW and full power 20 MW - which was reached at August 24th, 2004 for the first time. As the nuclear start up procedure took only about half of the full reactor cycle (52 days at 20 MW), there were 28 days left for a

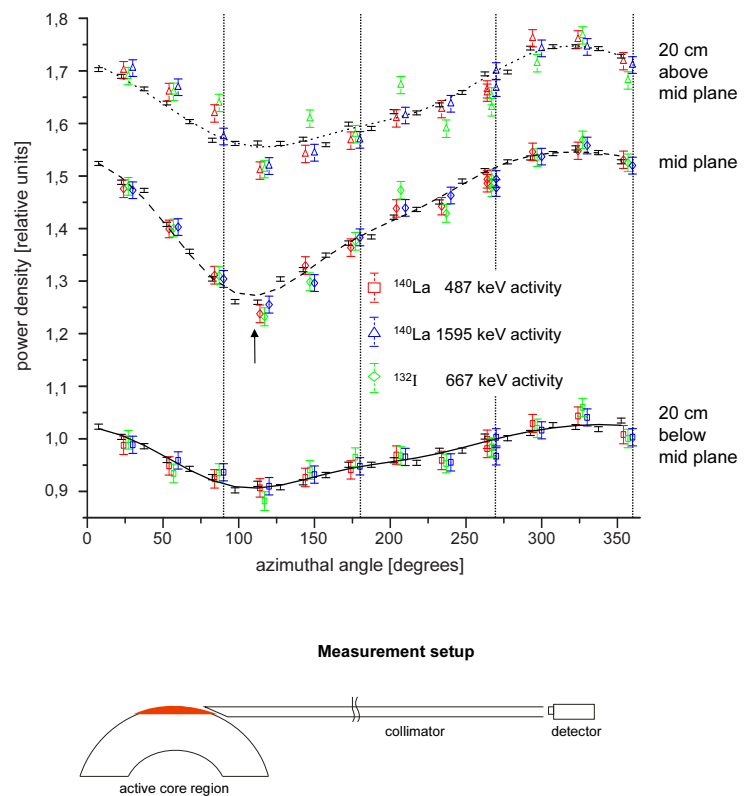Figure 1.1: Comparison of power densities at different heights after 2 days at $P \approx 50$kW, precalculated and by measuring fission product activities some days after operation.
Densities are measured and calculated at an outer segment (thickness 13 mm) as function of the azimuthal angle.
A dip in the power density (arrow) is clearly visible near to the azimuthal position of the cold source (center at 98°).

first permanent full power test operation of the new reactor. During this time, several experimental components such as the hot source, the cold source and some irradiation facilities were carefully tested and adjusted to full power conditions, including the response of these components to a reactor scram. Furthermore neutron scattering test experiments and flux measurements inside the moderator tank were performed. These gold foil activations confirm a perturbed flux of $6.4 \times 10^{14} n/cm^2 s$ at the thermal flux maximum in close agreement with earlier calculations of $8 \times 10^{14} n/cm^2 s$ for the unperturbed flux.

At October 21st, 2004 the maximum permitted burn up of 1040 MWd was reached successfully, and the reactor was shut down according to the authorized schedule. There are promising indications, that there is still some reactivity left in the fuel element at the nominal end of cycle, which would allow for an additional operation of the fuel element for about one week. It will be checked crucially and would need another permit of the Regulatory Authority, whether a cycle of about 60 days is possible. A "problem" to be solved in future. The nuclear start up of FRM II being technically completed, it is time now to finish the involvement of the general contractor Framatome-ANP. Negotiations concerning the transfer of the full responsibility for FRM II from FANP to TUM have begun. Before starting with further power operation, some improvements at beam tubes and neutron guides are foreseen and a detailed report of the nuclear start up has to be submitted to the authority for approval. Then, after a successful straight forward nuclear start up procedure of only 8 month, the final permit of the Bavarian State Ministry of Environment (StMUGV) to routine operation of FRM II is expected early in 2005.

1.2 Sample Environment

J. Peters [1], **H. Kolb** [1], **A. Schmidt** [1], **A. Pscheidt** [1], **J. Wenzlaff** [1]
[1]ZWE FRM-II, TU München

2004 was dedicated to extensive tests of our low and high temperature equipment.

Three sample tube cryostats (CCR) were assembled and tested. Additional three CCR's are now in production to complete the pool. In early 2005, seven cryostats of this type will be available at FRM-II. Tests have been done on new sample sticks providing an exchange gas sample chamber and allowing temperatures from 3.5K up to 350K. First tests of a 3He/4He dilution insert have been successful (co-operation with the Walther Meissner Institute, Garching).

On the Triple Axis Neutron Resonance Spinecho instrument, a CCR stood the test over weeks in a first user experiment.
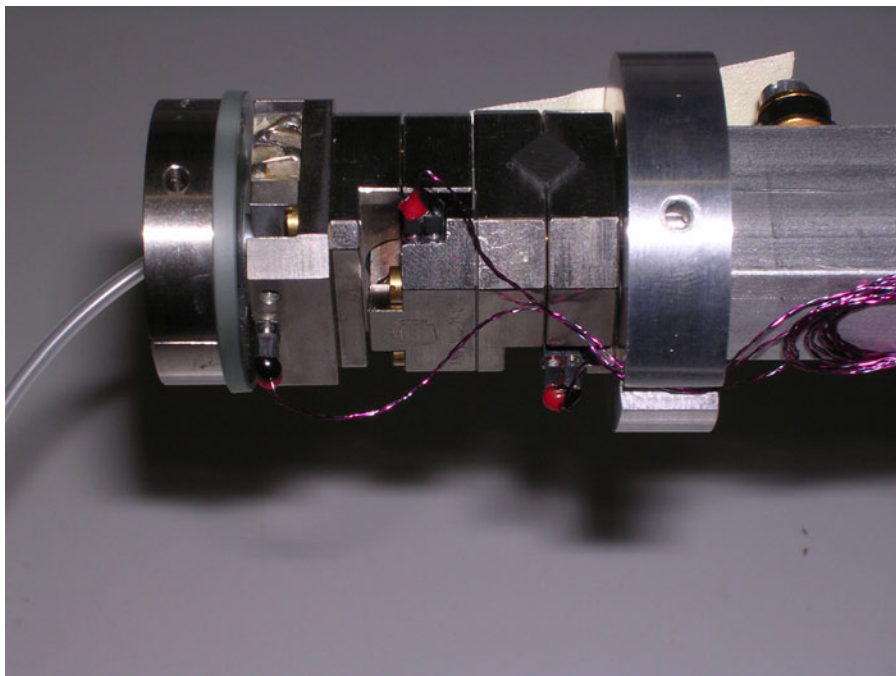

Figure 1.2: Stack of Actuators

A set of ultra small and compact actuators for temperatures down to the mK-range (developed by attocube, Germany) are now available.

Different types of these elements allow e.g. linear travel in the range of millimeters with a resolution in the range of nanometers depending on temperature. A rotator element provides endless rotation providing nm-resolution and optical readout of absolute position. The modular design allows to form a goniometer fitting in the sample tube of a CCR. High vacuum conditions or magnetic fields up to 15 T are applicable.

For the polarised cold neutron three axis spectrometer PANDA, a compact dewar for a Beryllium filter block has been designed and manufactured, based on liquid nitrogen cooling. The filter will suppress neutrons with energies higher than 5 meV.

Regarding our high temperature equipment, tests have been done on the new IR-radiation furnace for small samples (3 x 5 mm). Heating is done via four commercial available reflectors equipped with halogen lamps. The main constraint regarding long term stability of the furnace, overheating of the bulbs , has been overcome by design modifications.

Dedicated to the TOF-TOF spectrometer an adopted high temperature furnace was designed and manufactured including adjustment flanges. Based on melting samples, a calibration procedure has been tested to improve the reliability and reproducibility of the temperature readout of our high temperature furnace HTF.

1.3 Measurement of neutron flux and beam divergence at the neutron guide system at FRM-II

A. Kastenmüller [1], **A. Röhrmoser** [1], **C. Schanzer** [2], **K. Zeitelhack** [1]
[1]ZWE FRM-II, TU München
[2]Physikdepartment E21, TU München

Introduction

A proper performance of the neutron guide system is of crucial importance for the new neutron scattering instruments installed at FRM-II. During the commissioning of the reactor we measured the integral and differential neutron flux as well as the distribution of beam divergence at the exit of some representative cold neutron guides. The experimental results can be compared to extensive simulation calculations based on MCNP and McStas. The main objectives were a quality verification of the present neutron guides and reliable predictions for new guides to be installed in the upgrade or guides not accessible for measurements.

Experimental setup

A versatile fully remote controlled Time-of-Flight spectrometer has been built for the intended measurements. It consists of a Gd-coated single disk chopper (U = 4600 rpm), a flight path in air with length L=1 m, and a square shaped ^{3}He-tube (efficiency $\varepsilon = 0.66$ at $\lambda = 1.8\,\text{Å}$) for neutron detection. The wavelength dependence of ^{3}He-efficiency and beam attenuation in air and detector wall are taken into account in the data analysis. The wavelength resolution varies from $\Delta\lambda/\lambda \approx 0{,}01$ to ≈ 0.06 for $\lambda = 10\,\text{Å}$ and $\lambda = 1.8\,\text{Å}$ respectively.

The angular resolution of $\Delta\alpha \approx 0.1°$ is defined by the chopper entrance aperture ($\varnothing = 1\,mm$) and a slit ($1 \times 100\,mm^2$) in front of the ^{3}He-detector. Readout and data acquisition were performed with the FRM-II detector lab standard ToF-electronics [1].

Due to radiation protection reasons we had to restrict the investigation to three representative guides where existing monochromator or chopper shieldings enabled access during the commissioning of FRM-II.

Characteristic parameters and integrated neutron flux extrapolated to the nominal reactor power (20 MW) of these n-guides are listed in Table 1.1.

	NL1	NL2b	NL6a
cross section [mm^2]	60×120	170×12	60×120
λ_{crit} [Å]	1,8	2,8	2,9
coating	m=2/m=2,5	^{58}Ni/m=2	^{58}Ni/m=2/m=2,2
length [m]	32	54	49
specialty		twisted	
Φ_{int} [1/cm^2/s]	$9,8 \cdot 10^9$	$1,8 \cdot 10^9$	$4,9 \cdot 10^9$

Table 1.1: Characteristic parameters of the neutron guides investigated with the ToF-spectrometer

Results

Fig. 1.3 shows the differential neutron flux $d\Phi/d\lambda$ at the exit of neutron guide NL1 measured with the ToF-spectrometer at reactor power 9,5 MW. The resulting integral flux $\Phi_{int} = 2,7 \cdot 10^9 n/cm^2/s$ is consistent with independent gold foil activation measurements. During this phase of the commissioning the cold source was operated with only 10,6l filling of liquid D_2 deviating from nominal conditions (≈ 14l LD_2). Taking into account real conditions of the cold source simulation calculations based on MCNP and McStas show good agreement to the data. Assuming the cold source being operated at nominal conditions at reactor power 20 MW an integral flux $\Phi_{int} = 9,8 \cdot 10^9 n/cm^2/s$ is deduced from the simulation calculation.

Fig. 1.4 shows the vertical beam divergence at the exit of ^{58}Ni coated neutron guide NL6a for different wavelengths ($\Delta\lambda/\lambda = \pm 5\%$) measured at reactor power 190 kW. The widths of the distributions correspond well to the critical angle of reflection Θ_{crit} of ^{58}Ni-coating. The wavelength independent oscillatory structure observed is due to a spacial inhomogeneity of the cold source not being operated in nominal conditions at reactor power 190 kW. Though not shown here the results of simulation calculations which take into account the spacial inhomogeneity of the cold source are in agreement with the measured data.

The study of the twisted n-guide NL2b was of special interest. According the measured data there is evidence that the aimed 90°-turn in the divergence phase space is feasible. However, it is difficult to draw final conclusions from the data, as no McStas calculations are available for NL2b at present.

Summary

The differential neutron flux and beam divergence have been studied at representative cold neutron guides. The measured distributions can be well explained by simulation calculations. This should allow reliable predictions for the cold guides not accessible or yet to be installed. In addition, the guides investigated reveal good quality with respect to reflective coating and installation.

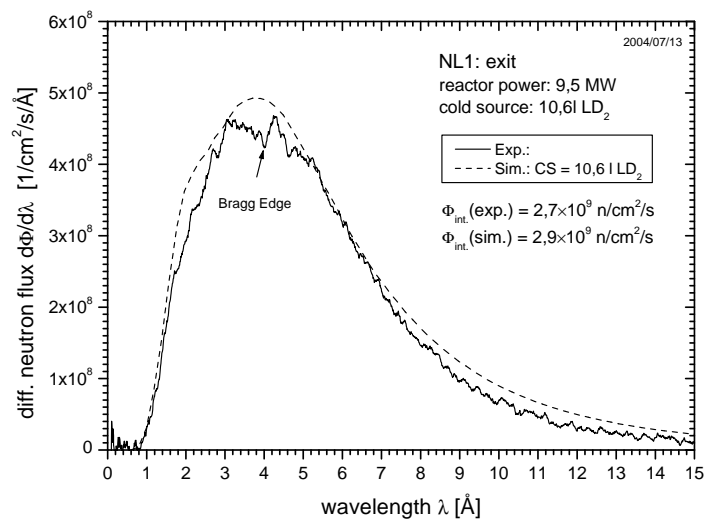[1] Zeitelhack, K., Kastenmüller, A., Maier, D., Panradl, M. FRM-II annual report (**2003**).

Figure 1.3: Measured and calculated differential neutron flux at the exit of the cold neutron guide NL1
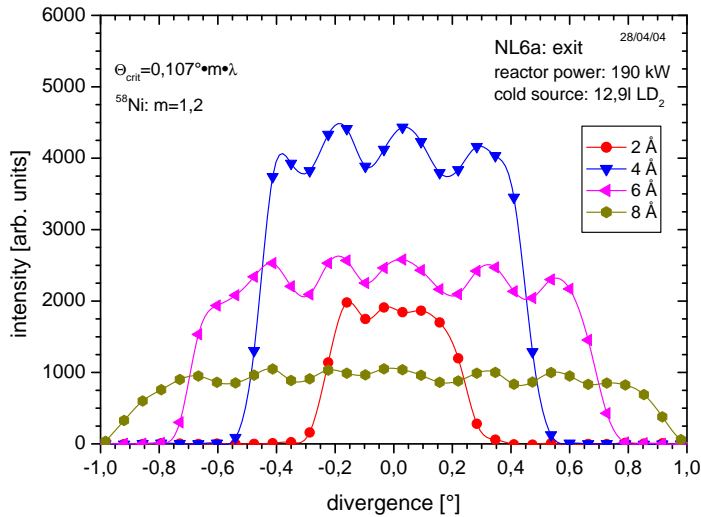
Figure 1.4: Vertical beam divergence at the exit of ^{58}Ni-coated neutron guide NL6a

1.4 Progress Report on the Neutron Guides of FRM II

Ch. Breunig[1], **E. Kahle**[1], **H. Hofmann**[1], **G. L. Borchert**[1], **D. Hohl**[2], **S. Semecky**[3]
[1]ZWE FRM-II, TU München
[2]Technische Dienstleistungen, München
[3]Kommunikationstechnik, München

In the course of 2004 the FRM II delivered for the first time neutrons to the experiments beginning with low intensities and gradually increasing to the duty value. This provided the opportunity especially concerning the neutron guides (NG) to gain experience, to check the performance and to detect deficiencies. As a consequence, the neutron optics group was engaged in two major projects:

Improvement in the shielding of the NG

Systematic measurements of the radiation around the NG showed that the envisaged radiation level of 3μSv/h was surpassed. The following deficiencies of the shielding were revealed:

- Generally the NG's lead shielding of 7cm thickness in the NG hall is not sufficient.
- The assumption, that the neutrons are completely absorbed in the boron glass plates of the NG is not correct. Due to scattering an essential part of the neutrons can leave the NG producing a rather high background level.
- The Gd layer of the polarizing NG NL5 creates high energy gamma radiation.
- A pronounced radiation level was detected in the surroundings of the adjustment frames of the NG and other construction units which caused a reduction of the lead shielding.
- In the casemate area the NG are not provided with any shielding. It turned out, that the walls of the casemate are not sufficient to reduce the radiation level to the envisaged value.

Consequently the following measures were taken:

- All NG except the twisted NG NL 2b were equipped with an improved shielding. The glass bodies of the NG were jacketed by 5mm thick boron epoxy plates. They were

enclosed in lead plates, the thickness of which was tailored according to the measured local radiation level, see figure 1.5.

- This led for the polarizing NG NL5 at its entrance to the NG hall to a lead shielding of about 15 cm thickness.
- The NG NL 2b was enwrapped in 5mm thick borated foam sheets and at the tube junctions reinforced with lead plates, see figure 1.6.
- In the casemate all NG, except NL 2b and NL 5 have been jacketed by 100 mm boron PE and 50 mm lead, see figures 1.7 and 1.8. NL 5 has been enclosed by 50 mm boron PE and 100 mm lead, NL 2b is

Figure 1.5: View of the NG NL 5, NL 6a and NL 6b in the NG hall. After having introduced the boron epoxy layers directly around the glass elements, the lead shield of originally 7cm thickness has been reinforced by several layers of lead plates, each 25 mm thick.

Figure 1.6: View of the NG NL 2a and NL 2b in the NG hall. The NG NL 2b (left) is in the state of being enwrapped with boron foam sheets. The NG NL 2a (right) is being equipped with additional lead plates.

already equipped with a lead shield.

Replacement of the NG 4

The old NG 4 was constructed to take only a third of the available neutron flux. Facing the request of an efficient use of the neutron flux and the necessity to host and serve more instruments, it was decided to rebuild the NG 4. The replacement will consist of two separate NG: NL 4a and NL 4b, which will share the complete available neutron flux. NL 4a will take the upper part of the neutron beam. It is composed of a novel vertical S-shaped structure and a straight section separated by a selector unit. It will serve a state-of-the-art SANS facility SANS1. The lower part of the neutron beam exhibits a radius of curvature of 390 m and leads to a PGA station. As the distance of the two new NG is rather small in the tunnel area they are housed there in a common vacuum tube, see figure 1.9. Close to the tunnel wall the mutual distance of NL4a and NL 4b is large enough so that they can be enclosed in separate vacuum tubes. To avoid an activation of Co, which is usually component of steel, the vacuum tubes were made of aluminium. The construction of NL 4a and NL 4b has been completed up to the high speed shutters close to the casemate wall. It is planned to accomplish the construction in the first half of 2005.

Figure 1.7: Looking at the shielding structure of the NG in the casemate during the assembling period. The glass body of the NG is enclosed by two layers of boron treated PE (blue). They are covered with lead plates (grey).

Figure 1.8: View of the NG NL 1, NL 2a and NL 2b in the casemate after accomplishment of the rather massive sandwich shielding.

Figure 1.9: View of the NG in the tunnel area. The more bright colour of vacuum housing of NL 4a,b indicates the aluminium material.

1.5 HELIOS – a facility to produce a polarized ^{3}He gas at FRM-II

S. Masalovich [1], **G. Borchert** [1], **W. Petry** [1,2], **O. Lykhvar** [1]
[1]ZWE FRM-II, TU München
[2]E13, Physik-Department, TU München

The progress achieved in a production of a dense spin-polarized ^{3}He gas is of significant importance for many research areas where a polarized gas is considered as a subject or a tool for investigations. In particular, it makes a great impact on the instrumentation for neutron polarization and polarization analysis.

With the aim of large-scale production of a polarized ^{3}He gas for neutron spin filters, the special nonmagnetic (iron-free) laboratory with the total area of about 60m^2 was built at the FRM-II site. The MEOP (Metastability Exchange Optical Pumping) station was installed in this laboratory (Fig. 1.10) and the final check-up has been done in December 2004.

The station exhibits the following features:

- Steady-state gas polarization: 78%

- Production rate: 27 bar·litre/day (@ 72%)
- Maximum gas pressure in the target cell: 5.3 bar

Polarized gas may be collected in a detachable cell with the pressure of a few bars and then transported to a neutron instrument. Clearly, for long-running neutron measurements it is very desirable to have a neutron spin filter that would be capable to keep a high gas polarization for a long time. For a given cell this time depends on the parameter called a ${}^3He$ spin polarization relaxation time. The latter is mostly affected by the purity of the walls and the purity of the material the cell is made of. Therefore a great care has to be taken in order to get a cell with a proper relaxation time. At the FRM-II site a special laboratory was built and equipped for cell preparation. Currently two quartz cells are
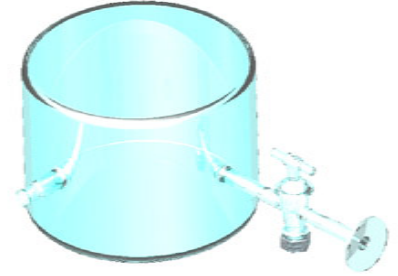

Figure 1.11: Quartz cell for polarized ^{3}He gas

available. The cell is shaped as a short cylinder (Fig. 1.11) with the diameter 120mm and 80mm high and may be filled with polarized gas compressed up to 3 bars. The transmission of the empty cell measured with 1.5Å neutrons was found to be 0.84.

The quality of the neutron spin filter (@ 70% ^{3}He polarization) based on such cell may be derived from Fig. 1.12 for desirable neutron wavelength. In this figure the contour map of the quality factor Q is plotted as a function of the gas pressure (p), the neutron path length in the cell (L) and the neutron wavelength (λ). The quality factor is defined as $Q = P \cdot \sqrt{T}$ [1], where T is the transmission of the neutron spin filter and P the polarization of the neutron beam after passing a spin filter cell.

From Fig. 1.12 one can see, for example, that for neutrons with the wavelength 1.8Å and for the cell of 80mm high the maximum quality factor may be obtained with the gas pressure about 1.75 bar.

To bring the polarized gas to a neutron experiment without losing a polarization, a special transporta-
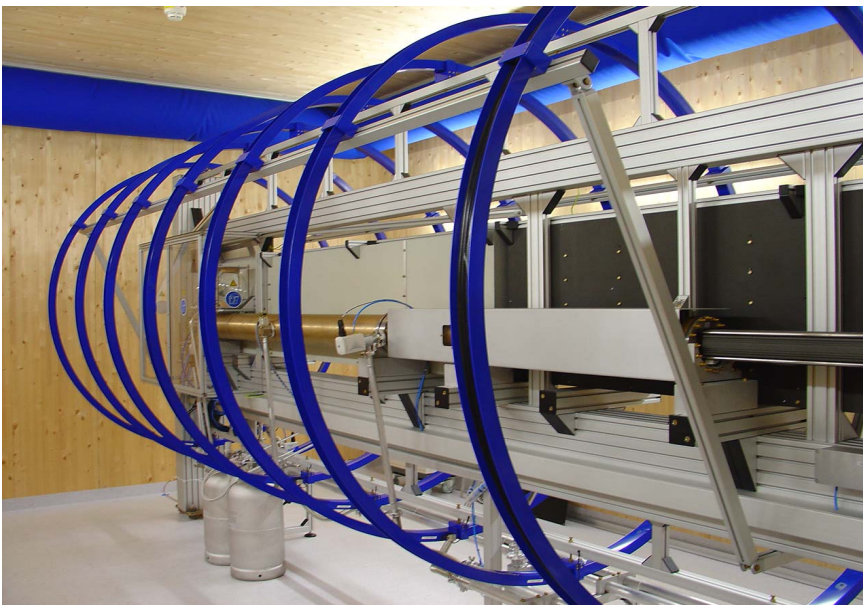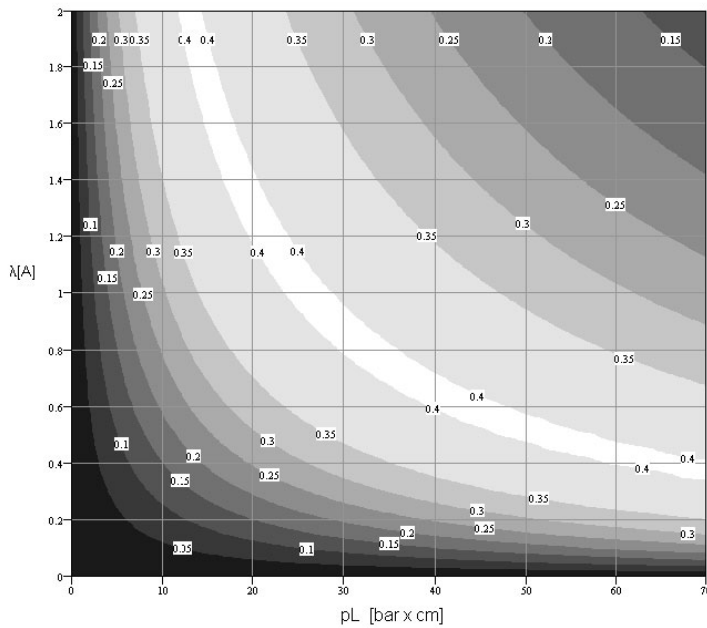

Figure 1.10: HELIOS at FRM-II

Figure 1.12: Quality factor of a neutron spin filter with 70% gas polarization

tion box with homogeneous magnetic field has to be built. This box has also to ensure a good shielding against any external magnetic fields, which may happen on the way to a neutron instrument. Such a transportation box suitable for our cells has been designed and the components have been ordered. The calculated homogeneity of the magnetic field over the cell volume is better than 10^{-3} 1/cm and thus does not limit the lifetime of the gas polarization in the cell. The test of this transportation system will be done in January 2005.

We expect the first neutron spin filters for neutron polarization at FRM-II to be available in February - March 2005.

[1] Tasset, F., Ressouche, E. *NIM A*, 359, (1995), 537–541.

1.6 IT Services

Jörg Pulz[1], **Jörn Beckmann**[1], **Joachim Dettbarn**[1], **Josef Ertl**[1], **Stefan Galinski**[1], **Hartmut Gilde**[1], **Christoph Herbster**[1], **Jens Krüger**[1], **Jakob Mittermaier**[1], **Roman Müller**[1], **Sebastian Roth**[1], **Manuel Stowasser**[1], **Harald Wenninger**[1], **Birgitta Wildmoser**[1], **Felix Zöbisch**[1]
[1]ZWE FRM-II, TU München

Overview

In 2004 the Network Group mainly continued the work from the last years, as reported in the 2002 and 2003 Annual report. Due to the reactor start-up and the regular operation further instrument networks had to be realized. To reduce the risk of service outages, different possible solutions were considered, tested and integrated. Major efforts and achievements of this year were:

- Extended redundancy for the user account database and the Windows Domain
- New mail server for increasing requirements
- Synchronizing the FRM-II computers clocks
- Instrument networks and independent servers
- Redundant DHCP service - an attempt
- TACO-box enhancements
- NeXuS integration in NICOS

User account database and Windows Domain

As mentioned in the 2003 Annual report, the FRM-II User Management system was completely migrated to an LDAP based system. The LDAP implementation of choice was OpenLDAP [1].

To accomplish the highest availability of the LDAP system, we decided to place an replication server in nearly every building. Each replication server is additionally featured with Samba [2]. Samba is configured to work like a Windows Primary Domain Controller (PDC) on the LDAP master server. All replication servers are configured as Backup Domain Controllers (BDC). Clients are configured to use the nearest server first. In case this server is not reachable the clients can use the other servers too.

This way offers fast access and equal availability of Unix and Win-

dows based systems and reduces service outages to a very minimum.

Improved mail handling

In 2003, a mail server with spam detection and virus protection capabilities was introduced. To comply with the FRM-II corporate identity regulations special mail address rewrite rules had to be implemented.

For every outgoing mail the system has to check the sender address against the LDAP user database. If the address did not match the style as laid down in the FRM-II regulations, it has to be rewritten. After detailed investigation and several configuration attempts it has resulted that the Postfix [3] mail handler did not match our requirements. To remedy this deficiency, the whole mail handling system was rebuilt utilizing Sendmail [4] instead of Postfix. Sendmail offers the ability of very fine grained configuration using the *m4* macro language. Sending encrypted mail by means of TLS and user authentication against the LDAP system along with recipient verification using LDAP is also possible.

Precise time synchronization

At the FRM-II, the home directories for all users are accessible by means of NFS and Samba. Additionally, access to measured data is provided by the same mechanisms. To gain reliable concurrent access to the data, all client workstations and servers must have the same notion of time. To accomplish this, the computers clocks have to be synchronized.

We decided to use the official reference implementation of NTP [5] for network based time synchronization. The protocol versions NTPv3 and NTPv4 (SNTP) are described in RFC 1305 and RFC 2030. Different types of hardware clocks can be used as accurate time source for NTP. We are using two hardware clocks developed by Meinberg Funkuhren [6]. The first clock is DCF77 based and utilizes the transmitted frequencies and signals derived from the atomic clocks of the Physikalisch-Technische Bundesanstalt (PTB) [7] in Braunschweig. The second hardware clock is based on the public available Standard Positioning Service (SPS) provided by the Global Positioning System (GPS) satellites´ on-board atomic clocks.

All computers inside the FRM-II network are able to access the NTP servers to synchronize the local clock. The use of these hardware clocks together with NTP offers the necessary accuracy for the reliable use of network based filesystems.

Independent instrument servers and networks

In 2003, two instrument network installations at the instruments PANDA and PUMA were put into operation. Together with the use of an independent instrument server the concept has proved itself a success. The idea behind instrument networks and servers was already described in the 2003 Annual report.

To realize independence for further instruments, the structured cabling for STRESS-SPEC, NEPOMUC, HEIDI, RESI and TOFTOF has been done. Instrument servers for STRESS-SPEC, HEIDI, MIRA and MATSCI-R were installed and put into operation. Preparations for the remaining instruments were made so that these can be finalized in early 2005.

Failover for the DHCP service

For easy IP address assignment and host configuration, we have configured nearly all hosts to request this type of information from a central DHCP server.

The initial definition of the DHCP protocol was designed for only one server without failover mechanisms. Later this definition has been extended to support redundant operation using two independent servers. Current versions of the ISC-DHCP server [8] support these techniques. Additional patches provide the ability to store the host configuration in an LDAP database.

To reduce the risk of DHCP service outages extensive failover testing was done. The testbed consists of two DHCP servers in conjunction with an LDAP backend for the host configurations. Several clients with different operating systems were tested. All tests turned out that the DHCP failover mechanisms work flawlessly and provide a very reliable service operation. The integration in the real FRM-II network is planned for early 2005.

"TACO-Box"

The TACO-Box Linux distribution is an operating system for embedded system control devices. It was entirely rebuilt from scratch. Unlike the previous versions, the new system is not based on an existing distribution, but resembles a "Linux from scratch" system [9]. Therefore TACO-Box is well adapted for the small control devices used at FRM-II.

The main goal was to create a small and up to date Linux by using a 2.4.28 kernel, glibc 2.3.3 and software designed for usage on em-

bedded systems. Most tasks are handled by BusyBox [10]. Busy-Box combines tiny versions of many common UNIX utilities into a single small executable. Remote system access is provided by the Dropbear SSH server [11]. The install system fits on two floppy disks, the base system's size is about 4 MB.

TACO software can be installed with the help of scripts. TACO is then started automatically by an init similar to SysV.

NeXuS in NICOS

The relevance of using the international standardized NeXuS format for the storage of the neutron measurement data at FRM-II has been decided years before. However, in the beginning of 2004 support for NeXuS[12] was quite scarce and there was little more available than the basic NeXuS class definitions and the essential C API. As the most popular language used by the instrument responsible's at FRM-II is the powerful and yet easy-to-use Python[13] language, the need of making the NAPI available to Python was one of our basic tasks.

A one-to-one correspondence of the C NAPI functions and the Python NAPI functions was achieved by using SWIG[14] and making extensive use of the SWIG typemaps. This way no modifications to the original NAPI core library were necessary and the user had not to be confronted with the annoying and dangerous task of creating and handling opaque C pointers. In order to make life even more simple, the idea of using the object oriented features of Python and providing an oo-like layer on top of the Python SWIG layer to interface the underlying NAPI was self-evident. The context-dependent

state-machine of NeXuS inherited from the underlying HDF had to be wrapped into some kind of oo-structure. Finally a package was implemented that is closely related to the principles of the XML DOM API mechanisms featuring validation against the basic NeXuS structure and translation of XML-templates into NeXuS-structures.

Consequently, the Python modules in the instrument specific NICOS [15] environment used to dynamically store the data in ASCII format during a continuous scan have been supplemented with an additional module capable of continuously storing the data in NeXuS format. Being able to write and read NeXuS content from the programming language wasn't sufficient yet.

A means to get a quick and deep view to the NeXuS file and being able to visualize significant measurement data by browsing the content and doing plots was essential for the NeXuS format to be established. As the few and very basic NeXuS viewers available at this point of time didn't suit our requirements, a NeXuS viewer was written on the base of Qt and the module management system OpenDaVE formerly developed in our house. The well-defined and modularized plugin architecture of OpenDaVE makes it possible to use the ready-built modules either as plugins or as standalone applications. The existing NeXuS structures and the existing basic modules of OpenDaVE have been extended and, together with a bunch of newly created modules, have been used to build a stand-alone application capable of visualizing nexus content in a tree-view like manner and being able to plot the NXdata using diverse plotting packages (qwt[16], qwtplot3d [17], gnuplot[18]).

[1] Zeilenga, K., Chu, H., Masarati, P. OpenLDAP. http://www.openldap.org/.

[2] Tridgell, A., et. al. The Samba Project. http://www.samba.org/.

[3] Venema, W. Postfix. http://www.postfix.org/.

[4] Allman, E., et. al. Sendmail. http://www.sendmail.org/.

[5] Mills, D. L., et. al. The NTP Project. http://www.ntp.org/.

[6] Meinberg Funkuhren. http://www.meinberg.de/.

[7] Physikalisch-Technische Bundesanstalt. http://www.ptb.de/.

[8] Consortium, I. S. Dynamic Host Configuration Protocol Distribution. http://www.isc.org/sw/dhcp/.

[9] Linux From Scratch. http://www.linuxfromscratch.org/.

[10] BusyBox: The Swiss Army Knife of Embedded Linux. http://www.busybox.net/.

[11] Dropbear - SSH server and client. http://matt.ucc.asn.au/dropbear/dropbear.html.

[12] Neutron & X-ray Data Format. http://www.nexus.anl.gov/.

[13] Python Programming Language. http://www.python.org/.

[14] SWIG - Simplified Wrapper and Interface Generator. http://www.swig.org/.

[15] NICOS. http://nicos.sf.net/.

[16] Qwt - Qt Widgets for Technical Applications. http://qwt.sf.net/.

[17] QwtPlot3D. http://qwtplot3d.sf.net/.

[18] Gnuplot. http://www.gnuplot.info/.

1.7 User office at the FRM-II

J. Neuhaus[1], **S. Galinski**[1], **J. Dettbarn**[1]
[1]ZWE FRM-II, TU München

The FRM-II as a user facility for experiments with neutrons and positrons will welcome a large number of external scientists each year. Access to the instruments is provided via a proposal system where scientist can apply for beam time every 6 months. For the interaction with the users and to organize the scientific experiments a management software has been developed. An Internet browser has been chosen as user front end to provide easy access to the system from any place in the world. Based on in house experience a system using the scripting language PHP has been designed. In order not to start from scratch a public available user portal system was selected as backend. We have chosen PHP-Nuke for reasons of modularity, multi-lingual features and good documentation. In view of the expected international users the supported languages were limited to the most prominent European languages as English, Spanish, French and Italian.

From the user point of view several tasks can be organized that way, using a personalized account to the system. The scientific proposal can be submitted in form of a two page pdf-file accompanied with additional informations on the proposed experiment. The user can keep track of all his proposals and gets feedback from the allocation of beam time and schedule of the experiment. Furthermore he can organize the stay for the experiment via the user office system. After completion of the experiment reports and a list of publications can be submitted.

On the other hand quite a number of special accounts exist in the system having access to different kind of informations and applications. Instrument scientists can comment on technical feasibility of the proposed experiments. Referees can view the submitted proposals and vote on the scientific merit. The decision of the allocation of beam time is fed into the system by the scientific secretaries. The experiments are approved by the security departments at the FRM-II as radiation protection and working security. Instrument scientists or group leaders organize the schedule of the experiments including necessary equipment like cryostats, furnaces or high field magnets. The visitor service organizes the access to the site and computing infrastructure at the FRM-II. Finally the system provides informations on the planed experiments for the scientists (local contacts) on site.

In addition to the organization of the experiments the user office provides statistical informations about the use of instruments or equipment. It distributes informations for the users in form of announcements and news letters.

A first call for proposals has been managed successfully in November 2004 by the user office system. Additional modules for the organization of the experiments are under development.
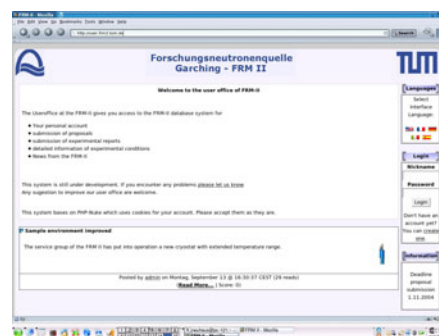

Figure 1.13: Screenshot of the user office testing system.

1.8 New high density fuel for the FRM-II

A. Röhrmoser[1], **W. Petry**[1], **K. Böning**[1], **N. Wieschalla**[1]
[1]ZWE FRM-II, TU München

In 1998 the new "red-green"-Federal Government expressed its wish to take the FRM-II into operation with a fuel element with reduced enrichment - so far the scientific quality of the neutron source is maintained. Hearings with experts about the feasibility of the conversion have been organized by the Federal Ministry of Science and Education. In October 2001 an "Agreement between the Federal Repub-

lic of Germany and the Free State of Bavaria on the conversion of FRM-II" has been written down and finally signed after granting the final license in May 2003. The compromise settled in this agreement has become part of the final nuclear license,i.e. development of a new medium enriched (MEU, with not more than 50% U-235) fuel element until the end of the year 2010.

It is understood that the conversion should neither reduce the reactor safety nor degrade the neutron flux and reactor cycle time more than marginally.

Actual Schedule

Already in November 2001 TUM had established an international working group to study the possibility of a new fuel with up to now not qualified densities and reduced enrichment. The group consisted of representatives of the TUM (FRM-II), the fuel element manufacturer CERCA and the constructor of FRM-II, Framatome-ANP. In its kick-off meeting in July 2003 the group declared to accept the technological challenge of the development of a fuel with densities in the order of 8 g/cm^3 within the very short time limit of $7\frac{1}{2}$ years.

The project was broken down into three phases of $2\frac{1}{2}$ years duration each:

1. search for the fuel type, test irradiations
2. further test irradiations, final decision on the fuel type and design of the fuel element
3. fabrication of the fuel element and licensing

MEU Conversion FRM-II, Phase I

In program phase I the high density fuel shall be chosen or at least done a preselection. This first $2\frac{1}{2}$ years phase spreads from 7.2003 till 12.2005 and the following tasks are assigned to phase I:

1. calculations for the high density fuel(s) for FRM-II geometry
2. irradiations of MEU full size fuel plates
3. participation in international research programs

Calculations with UMo dispersion fuel, first results

Any scenario to convert the FRM-II has to keep the reactor power constant at 20 MW. Without changing the whole D$_2$O moderator tank with all its installations and its shutdown rods the core geometry must remain unchanged. This is necessary not only to avoid a complete new licensing procedure but also a reactor shutdown period of many years and costs of more than 150 million Euros as stated by a sharp estimation.

For an enrichment of 50% an advanced fuel with very high density is required when maintaining the dimensions of the HEU compact core fuel element of the FRM-II. The new uranium-molybdenum dispersion fuel (UMo-Al) presently under research worldwide promises realistic uranium densities of up to 8.0 g/cm^3. TUM did actual neutronics calculations for this fuel with the same procedures that led to the HEU design of FRM-II (criticality, burn up …). The result was now that the density in the fuel must be at least 7.75 g/cm^3 with an enrichment of 50% U-235. When taking into account other aspects like the

less fortunate power density distribution with UMo, the minium density can hardly be below 8.0 g/cm^3. The core contains then 10.8 kg U-235 instead of 7.5 in the actual HEU case. The total U mass is 22 kg instead of 8 kg now. Necessary efforts to flatten the power distribution will reduce criticality.

One key point is the maximum of the fission density (FD) in the fuel plates. Because of the very inhomogeneous power and fission density in the plates maxima are reached only in very small areas of the plate. This is different from irradiation tests where the plates are much more homogeneously irradiated. The relevant maximum values in FRM-II must be assigned to the inner part of the plate and possibly to the plate ends. A result of these preliminary calculations is that the maximum of fission density in the meat is up to $2.0 \cdot 10^{21}$ cm^{-3} in a narrow area at the inner and outer border of the high density region. Test irradiations have to show whether the new fuel withstands the mentioned fission densities under full power conditions. Still the thermal flux is depressed by about 8.0% when compared to the actual HEU fuel, i.e. the aim of only marginal consequences for the scientific use is not yet met.

Actual Irradiation Program

For Phase I it was decided to plan an irradiation of four test plates of full size: For this, six plates are already produced by CERCA with UMo/Al dispersion fuel (8% wt. Mo) and wait to be irradiated.

The uranium densities are 8.0 g/cm^3 for 4 plates and 7 .0 g/cm^3 for the two other plates. Two of the 8.0 g/cm^3 plates contain the additive of a possible considerable "dif-

fusion blocker". Those blockers are presently object of research and development worldwide. We used 2% of silicon additive in the Al matrix. Including a safety margin a FD of $2.3 \cdot 10^{21}$ cm^{-3} shall be reached by the test irradiations. According to calculations of CEA this will be reached in a remarkable area of the plates within four cycles of the MTR reactor OSIRIS at CEA-Saclay.

In case any of the 8.0 g/cm^3 plates will fail during the irradiation, it can be replaced by the two 7.0 g/cm^3 plates in the test facility.

1.9 Cold Neutron Source

E. Gutsmiedl [1], **D. Päthe** [1], **K. Zeitelhack** [1], **F. Grünauer** [1], **A. Schölderle** [2]

[1]ZWE FRM-II, TU München
[2]LINDE, Höllriegelskreuth

Commisioning of the Cold Source at the FRM-II

During the year 2004 the new research reactor FRM-II of the Technical University of Munich was successfully tested in regards of cold and hot commissioning.

One major FRM-II component for producing cold neutrons for many different experiments is the cold neutron source (cns) [1].

The cns of the FRM-II is a liquid deuterium source, which is favorable to feed many neutron guides for cold neutron experiments. The liquid deuterium ($\approx$ 2.4 kg) is kept on the boiling point at full reactor power. Thermal neutrons are moderated to lower energies by the cold boiling liquid. In 2003 and early 2004 all auxiliary systems (cooling machine, metal hydride deuterium storage system, vacuum system) have been tested successfully during the cold commissioning phase.

From March 2004 to October 2004, the cns was tested together with the FRM-II reactor at different nuclear power steps (0 - 20 MW).

The control logic of the cooling machine (max. cooling power 5 kW at 25 K) was optimized to follow every power transients of the FRM-II reactor (power changes and fast shut down).

In Autumn 2004 the cns performance of producing cold neutrons was determined by measuring the spectral cold neutron flux of the cns through the beam channel SR4. The measured cold neutron flux of the

Figure 1.14: In-Pool assembly of cold neutron source

cns agrees quite well with the results
of Monte Carlo calculations of the
cns.

[1] Gobrecht, K., Gutsmiedl, E.,
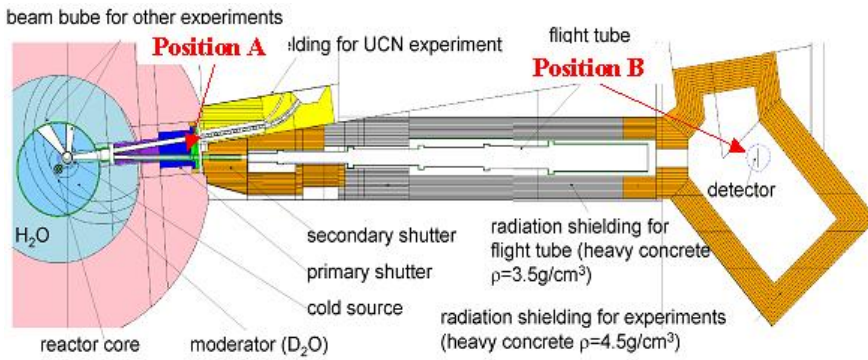Scheuer, A. *Physica B*, 311, (2002),
148 – 151.

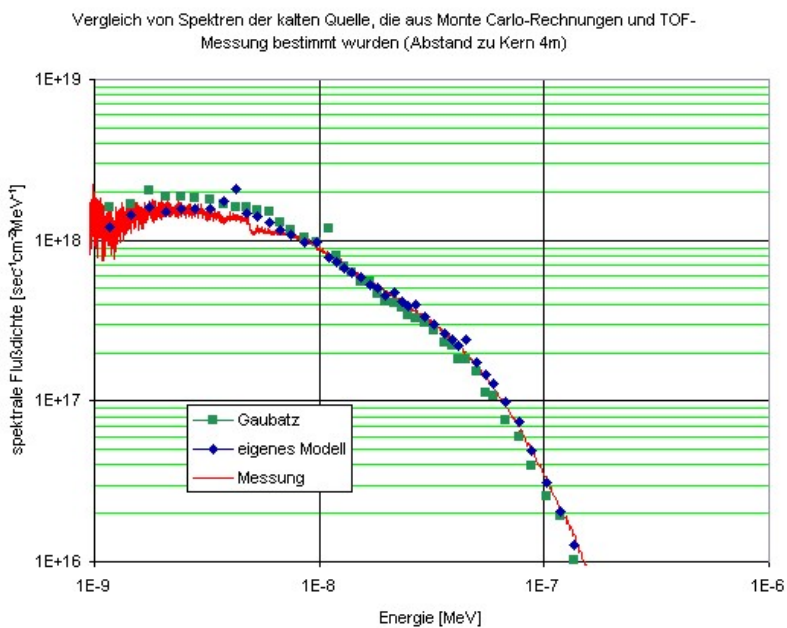Figure 1.15: Setup of spectral cold neutron flux measurement

Figure 1.16: Spectral cold neutron flux; measurement and MCNP calculation

1.10 Hot Neutron Source

E. Gutsmiedl [1], **C. Müller** [1], **A. Scheuer** [2]
[1]ZWE FRM-II, TU München
[2]TÜV Rheinland, Köln

Commisioning of the Hot Source at the FRM-II

During the year 2004 the new research reactor FRM-II of the Technical University of Munich was successfully tested in regards of cold an hot commisioning.

One secondary neutron source at the FRM-II for producing hot neutrons for the beam tube SR9 is the hot neutron source (hns)[1].

The hot neutron source is a graphite block, insulated by graphite wool and protected by a inertial gas (neon). The graphite block is heated up over 2000 °C by the gamma radiation of the FRM-II reactor fuel element.

The thermal neutrons are accelerated to energies between 0.1 eV an 1 eV by the hot graphite.

In 2003 and early 2004 all auxiliary systems (gas system, control system, vacuum system)have been tested successfully during the cold commisioning phase.

From March 2004 to October 2004, the hot neutron source was tested together with the FRM-II reactor at different nuclear power steps (0 - 20 MWatt).

The temperature of the graphite block was measured with a in situe noise thermometer, which measure the temperature via the electrical thermal noise of a resistor.

The graphite temperature at full reactor power (20 MWatt) is over 2000 °C, which correspond to theoretical calculations of the temperature profile in the hot neutron source.

[1] Müller, C., Gutsmiedl, E. *Jahresbericht FRM-II 2002.*

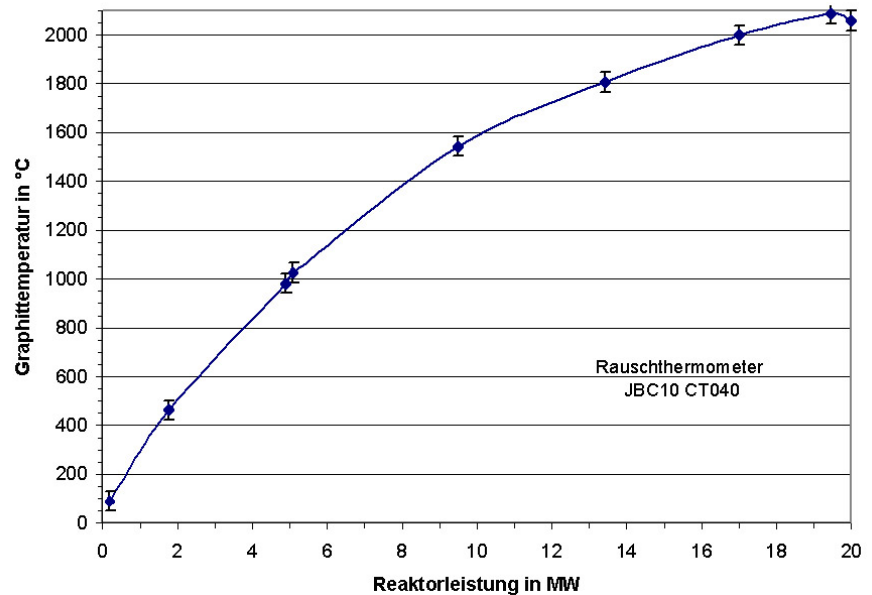Figure 1.17: In-Pool assembly of the hot neutron source

Figure 1.18: Graphite temperature of hot neutron source, measured with a noise thermometer

2 Diffractometers

2.1 STRESS-SPEC – Materials Science Diffractometer

M. Hofmann [1], **G.A. Seidl** [1], **R. Schneider** [2], **J. Rebelo-Kornmeier** [1], **A. Mantwill** [1]
[1]ZWE FRM-II, TU München
[2]BENSC, Hahn-Meitner-Insitut, Berlin

Introduction

After last year's extensive test phase at the HMI [1] the Materials Science diffractometer STRESS-SPEC was moved back to the FRM-II in January 2004. The instrument was reinstalled at beamport SR3 (figure 2.1) and several test experiments have been performed during the first reactor cycle. In the next reactor cycle commissioning will continue and first user experiments can be run.

New components

In course of the test phase some parts of the equipment were modified due to the experience gained using the diffractometer in real life conditions. For instance new primary and secondary slit systems have been installed with regard to reproducibility of the geometrical alignment and sturdiness. Both slit systems are linked to the sample table and the detector in such a way that the center of the beam remains the same under all conditions. Therefore a new alignment will not be necessary even in case the wavelength or the slit to sample position has been changed.

The new high capacity Eulerian cradle has been delivered and tested and is now available for routine operation. It has a   load capacity
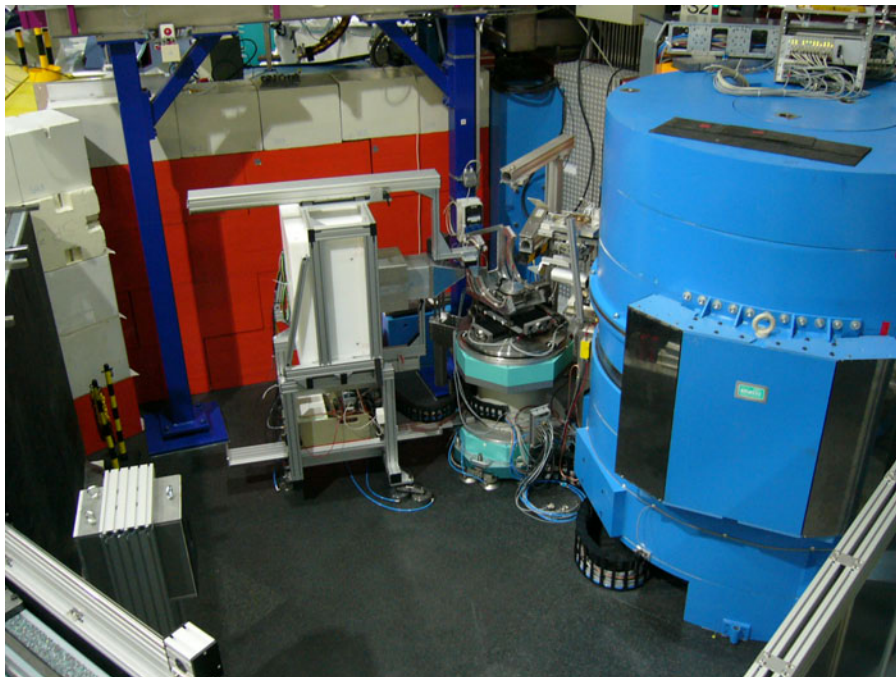

Figure 2.1: The diffractometer STRESS-SPEC equipped with high capacity Eulerain cradle

of about 50 kg and will allow to measure all strain directions without the need to remount the sample. Further main components comprise a secondary shuttersystem, new primary collimators with iron foils (they will replace the original primary collimators with high performance thermoplastic foils at the earliest possible date in 2005) and shielding of the experimental area including an interlock system to restrict access while the neutron beam is on.

First tests using neutrons

In course of the first reactor cycle we started to commission the diffractometer. The tests included flux measurements at the monochromator position using gold foils. The measured flux was $1*10^{10}$ n/cm^2/s which agrees well with MC calculations.

The first experiments were all carried out using the (511) reflection of the Ge-monochromator. An iron pin alignement sample was used to

measure the resolution function of the instrument (figure 2.2), which is in excellent agreement with model predictions. It was also shown that the focussing option of the Ge-monochromator works within specifications and the alignment procedures for setting up the gauge volume defining slits can be performed within reasonable time for real stress measurements. A first prelimanry user experiment was carried out on a prototype rocket nuzzle with the results being comparable to previous measurements using other neutron strain scanners.

[1] Hofmann, M., Seidl, G., Schneider, R. Ann. Report. Technical report, FRM II (**2003**).
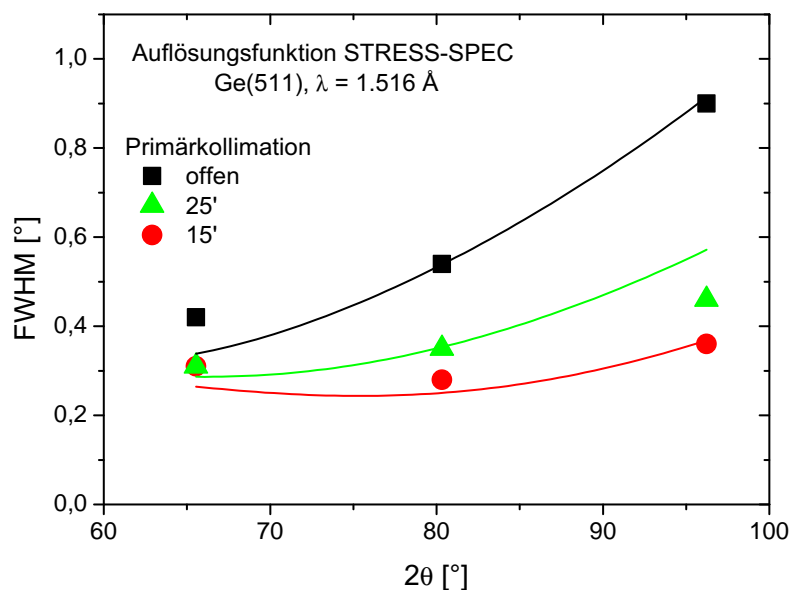

Figure 2.2: Resolution function of STRESS-SPEC using different primary collimation. Symbols are measured peak width and lines are calculated resolution functions

2.2 MatSci-R – The Materials Science Neutron/X-Ray Reflectometer at FRM-II

A. Rühm [1], **U. Wildgruber** [1], **J. Franke** [1], **J. Major** [1], **H. Dosch** [1]
[1]Max-Planck-Institut für Metallforschung, Stuttgart

The Materials Science Neutron/X-Ray Reflectometer MatSci-R (Fig. 2.3) is built and will be operated by the Max-Planck-Institut für Metallforschung, Stuttgart, as part of the joint MPG initiative for research with neutrons at the new research reactor FRM-II. It is a monochromatic continuous beam instrument at the neutron guide NL-1 which utilizes neutrons in the wavelength range 2-6 Å from the cold source.

The MatSci-R instrument can be operated as both a horizontal and a vertical reflectometer. At the moment only the standard liquid mode is being implemented in which a
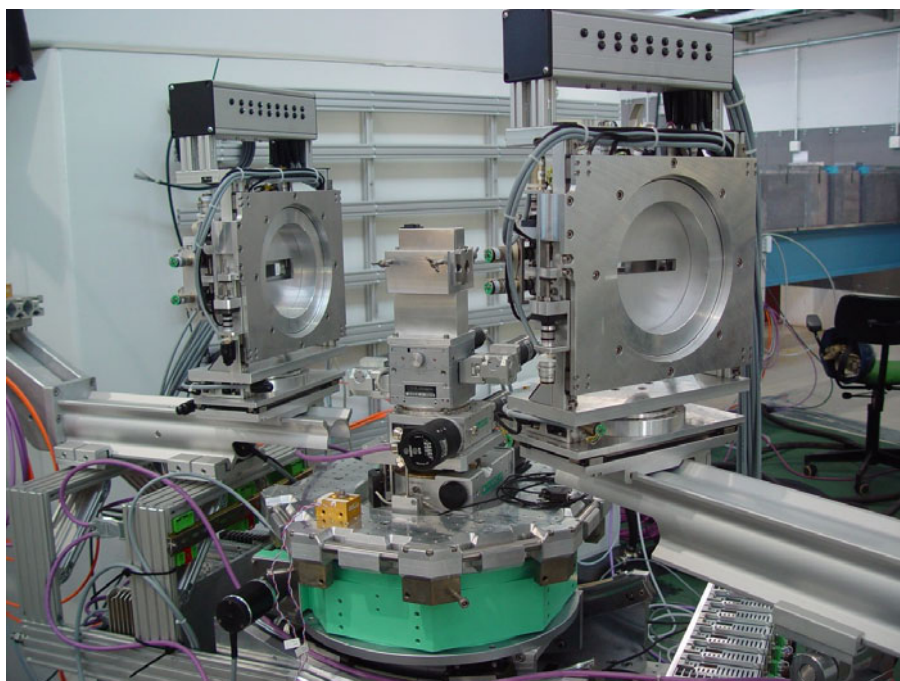

Figure 2.3: The MatSci-R instrument in its current state. Shown is the sample table with alignment laser mounted and two slit systems next to it. The neutron beam is entering from the direction of the monochromator shielding on the left.

portion of 6 cm (H) x 1 cm (V) of the white beam is used. In this horizontal mode, the monochromatic beam can be tilted towards the floor by moving the sample table down and tilting the monochromator so that free surfaces of liquid samples can also be investigated. The range of incidence angles in this mode is 0-5°, the range of exit angles 0-20°. The instrument can also be used for grazing incidence diffraction (GID). In-plane scattering angles can then exceed ±135° depending on the experimental configuration. For the unpolarized monochromatic beam we expect a neutron intensity of up to $3 \cdot 10^6 \mathrm{cm}^{-1}\mathrm{s}^{-1}$ (for 2% bandwidth) at the sample position at the nominal reactor power of 20 MW. Further instrument parameters are summarized in Tab. 2.1.

In the final configuration, the instrument will encompass the following components: HOPG monochromator, cooled graphite or beryllium filter, shutter, entrance slit system 1, alternative beam conditioning components (multilayer polarizer, SERGIS coils), slit system 2, sample, X-ray reflectometer, slit system 3, alternative beam conditioning components (^{3}He analyzer, SERGIS coils), slit system 4, detector.

Monochromator

The monochromator consists of 33 highly oriented pyrolitic graphite (HOPG) crystals which are arranged in eleven stacks of three crystals each (Fig. 2.4). The monochromator and the movable shield wall are designed for the selection of neutrons in the wavelength range from 2 to 6 Å out of the white beam. At the moment we have eleven single crystals mounted for first monochromator tests (Fig. 2.4).
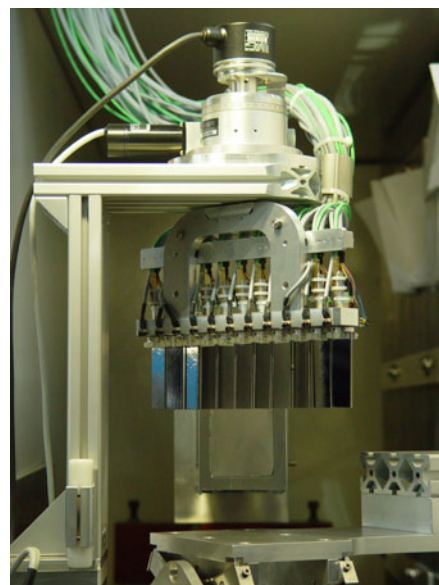

Figure 2.4: The monochromator stage for eleven stacks of three HOPG crystals each, currently with eleven single crystals mounted. The Al exit window of the neutron guide NL-1 is visible in the back.

SERGIS / NSE equipment

A spin-echo resolved grazing incidence (SERGIS [1, 2]) setup is currently being implemented and tested at the EVA reflectometer at ILL, Grenoble. In summer 2005 this equipment will be transfered to and become part of the MatSci-R instrument.

Sample stage

The sample stage is designed to support sample environments and other equipment (like magnets) of up to 400 kg. It encompasses an active vibration damping (Halcyonics) for the study of liquid surfaces. Sample ovens and cryostats as well as magnets will be added subsequently according to the users' demands.

Neutron wavelength range	2 - 6 Å
Neutron guide cross section	6 cm (horiz.) × 12 cm (vert.)
Beam cross section accepted by the monochromator	6 cm (horiz.) × 1 cm (vert.)
Monochromator	11 × 3 HOPG crystals, horizontally focussing (mosaicity 0.32° - 0.65°)
Energy resolution	2%
Max. incidence angle	5°
Max. exit angle	20°
Max. out-of-plane momentum transfer (specular)	$0.55 \, \text{Å}^{-1}$
Max. total momentum transfer (within reflection plane)	$1.35 \, \text{Å}^{-1}$
Max. in-plane momentum transfer (grazing angle diffraction)	$> 5.4 \, \text{Å}^{-1}$
Total neutron flux at monochromator	$4 \cdot 10^9$ neutrons $\mathrm{cm}^{-2} \, \mathrm{s}^{-1}$
Peak neutron flux at monochromator	$4 \cdot 10^8$ neutrons $\mathrm{cm}^{-2} \, \mathrm{s}^{-1} \, \text{Å}^{-1}$ (at 4 Å)
Monochromatic neutron flux for reflectometery at sample	$3 \cdot 10^6$ neutrons $\mathrm{cm}^{-2} \, \mathrm{s}^{-1}$ (estimated)

Table 2.1: MatSci-R instrument parameters (for liquid mode).

Add-on X-ray reflectometer

The MatSci-R reflectometer is a combined neutron/X-ray reflectometer. The X-rays are provided by a sealed tube source (at the moment 3kW CuKα, 1.541 Å, options are MoKα, 0.709 Å, and CoKα, 1.789 Å) which is rotated around the sample in a vertical plane together with the X-ray detector. Neutron and X-ray beams cross each other at a 90° angle. Neutron and X-ray experiments can be performed simultaneously or independently of each other. The X-ray option encompasses two precisely controlled linear motions for adjusting the incidence angle, a multilayer mirror which collimates the beam in the vertical (acceptance angle 0.75°, rest divergence 0.034°), and an optional channel cut monochromator (rest divergence 0.001°). The X-ray incidence angle can be varied between -1°and +11°. As an X-ray detector we have a scintillator detector available. At a later stage it is planned to also make a 1D position-sensitive detector available for off-specular measurements.

Detector

Currently we are testing a 2D position sensitive He wire detector manufactured at ESRF, Grenoble. Electonics and software were purchased from GKSS, Geesthacht. The detector has an active area of 190 mm x 190 mm and will be mainly used for the recording of off-specular scattering intensities. As an alternative detector for extending the dynamic range of the neutron detection a standard 1" neutron detector tube (spatially integrating) will be available.

Software

The MatSci-R instrument is controlled by a custom-made software (*rcontrol*) based on LabView and the LuaView scripting language. Basic operation of the instrument is already possible at the present stage of the software development.

Status

In the course of the year 2004 the sample table with the vibration damping stage (Halcyonics) was manufactured, installed and tested. Three tilt sensors for variable use at the instrument were tested successfully. The basic assembly of the instrument, including monochromator stage, optical benches, sample table and detector tower, is finished. The assembly is based on ITEM- and X95-profiles as well as custom-made parts. Both sample stage and detector tower can be moved on airpads under computer control. The monochromator stage has been carefully aligned with a mechanical probe head in the design position. Two of the three slit systems are completely wired and ready for use. The manufacturing of the boron-epoxy blades is in progress (Lehrstuhl für Leichtbau, TUM) and a complete set of blades willl be available in February 2005. The wiring of all motors, limit switches, position sensors and encoders is practically completed. The support for all motor controllers (Monopack, Sixpack, Bautz) is implemented in the control software. LuaView scripting capabilities (scans, macros) have also been implemented in the control software. Eleven HOPG crystals are mounted on the monochromator stage and are ready for first tests and alignment in the neutron beam. The position sensitive neutron detector is currently being tested in connection with the readout electronics (N110, ESRF) and the control software (GKSS). A scintillator detector for X-ray experiments has been purchased and tested.

Currently we focus on finishing the installation and test of all components which are enclosed in the monochromator shielding hutch (beam stop, shielding, wiring, beam shutter, laser target on the exit window of the neutron guide, web cam for remote monitoring). This will allow us to close the hutch, open the shutter and start with the monochromator alignment when the next reactor cycle starts in early 2005.

[1] Felcher, G. P., te Velthuis, S. G. E., Major, J., Dosch, H., Anderson, C., Habicht, K., Keller, T. In Anderson, I. S., Guérard, B., editors, *Advances in Neutron Scattering Instrumentation, Proceedings of SPIE*, volume 4785, 164 (SPIE Optical Engineering Press, Bellingham, WA, USA, **2002**).

[2] Major, J. ., Dosch, H., Felcher, G. P., Habicht, K., Keller, T., te Velthuis, S. G. E., Vorobiev, A., Wahl, M. *Physica B*, 336, (2003), 8.

2.3 MIRA – Very cold neutrons for new methods

R. Georgii[1], **N. Arend**[2], **P. Böni**[2], **H. Fußsettter**[1], **D. Lamago**[1], **S. Mühlbauer**[1], **H. Wagensonner**[1], **C. Schanzer**[2], **V.R. Shah**[2], **S. Mühlbauer**[1], **P. Böni**[2], **T. Keller**[3]

[1]ZWE FRM-II, TU München
[2]E21, Physik-Department, TU München
[3]Max-Planck-Institute for Solid State Research, Stuttgart

Introduction

The construction of MIRA in its basic configuration has been finished early in the year. We also tested the position sensitive detector, having an active area of 18x18 cm^2 with a resolution of 1.5 to 1.8 mm, and integrated it in the instrument successfully. The instrument control software was also brought to working level. Thus the instrument was ready for neutrons:

On March, 2 2004 the FRM-II became critical for the first time at a thermal power of 1kW. On March, 8 the first neutrons have been measured at MIRA at a power of 50 kW and despite the low neutron intensity first tests of the monochromator were already possible.

In August the final power of 20MW was reached and then kept constant for 4 weeks. This gave us the possibility to perform several demonstration experiments showing the performance of MIRA, already using different options of the instrument including different sample environments as low temperature and magnetic field (see Figure 2.5). Such the performance of the whole instrument was successfully tested under realistic conditions.

Current improvements of the instrument are setting up a neutron spin-echo option (N. Arend, see below) and building an improved water-cooled electromagnet up to 0.25 T (S. Mühlbauer).

Experiments

In the following the demonstration experiments performed are described.

The helical ferromagnet MnSi (D. Lamago, see 6.2): A MnSi single crystal at 10 K was measured in SANS geometry. Four scattering peaks were found indicating with their relative intensities the existence of the helical ferromagnetic phase.

The flux line lattice of Nb (S. Mühlbauer, see 6.3): A Nb sample cooled down to 6 K was measured in SANS geometry. Around the central beam a six-fold symmetry of the scattered neutron intensity could be observed. This is the footprint of the flux line lattice in the Shubnikov-phase of a type II superconductor.

Reflectivity measurements on a magnetic multilayer (Ch. Schanzer, see below): Unpolarisied neutron reflectivity measurements on a Ti/FeCoV/NiO/FeVoV/Ti magnetic multilayer have been performed partly in order to prepare later planned magnetic experiments and partly to improve the chemical lateral structure determination of the sample obtained with X-ray reflectometry.

Multi-MIEZE and NRSE options at MIRA

The instrument MIRA is currently being equipped with a multi-MIEZE

Figure 2.5: MIRA in the polarised reflectometer option equipped with a magnet and a closed cycle cooling machine.

(Modulation of IntEnsity with Zero Effort [1]) and NRSE (Neutron Resonance Spin Echo) option. A crucial part of every NRSE based instrument are the NRSE coils. The FRM-II hosts two other instruments with Neutron Resonance Spin Echo (NRSE) capabilities, NRSE-TAS and RESEDA. Although not identical and optimised for the respective wave lengths, the NRSE coils installed at both instruments share a common basic design.

The DC coils are wound of an 8 mm by 0.5 mm aluminum band, coated with an Al_2O_3 layer to ensure electrical insulation. This coating is known to have two properties not ideal for application in neutron science (e.g. Small Angle Neutron Scattering (SANS)), especially with cold neutrons being utilised: The insulation layer is grown using a electro-chemical technique (anodising) and therefore features homogenously distributed pikes on its surface, forming a scattering grid-like structure. Furthermore it contains significant amounts of crystal water, which is intrinsic to the manufacturing process. The aluminum band must be specially treated before using it for coil winding, namely exposition to a D_2O atmosphere at high temperature ($> 120°C$) in order to exchange H_20 by D_20, which has a significantly lower scattering cross section. Furthermore, since the winding density is relatively low, high currents ($\approx 100\,A$) must be used to achieve the nominal DC field of 0.03 T.

The decision to develop a new NRSE coil design for MIRA was driven by the following goals:

- improvement of the neutron scattering/absorption properties at long neutron wave lengths
- since the construction of the RESEDA/NRSE-TAS coils requires some technical experience (especially with the winding process), a simpler and better reproducible design was desired, using standardised industrial materials and production engineering.
- decrease the required current to achieve the same nominal field strength

Fig. 2.7 and 2.8 show the current design, it is based on both an approach developed at the Max-Planck-Institute for Metal Research in Stuttgart [2] and the RESEDA/NRSE-TAS layout [3].

The idea is to form the DC coil by stacking single windings (Fig. 2.7) made out of 2 mm aluminum sheets. The contacting is done by pointwise welding and each layer is isolated against the next. The body of the DC coil, formed by the single Al sheets, does contain water cooling channels that will also serve as an alignment aid during assembly. Fig. 2.8 depicts a sketch of a partially assembled MIRA NRSE coil, including the radio frequency coils, whose layout is an enhanced version of the RESEDA coils.

The window, where neutrons will penetrate the coil, is indicated in the center. Fig. 2.6 shows a test assembly of the DC coil, on which investigations of electrical and thermal properties can be performed.
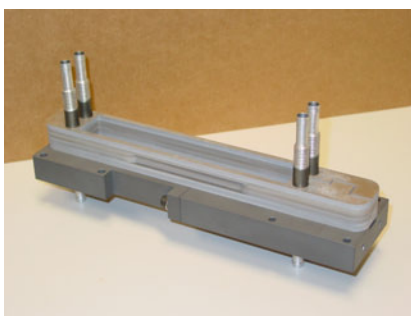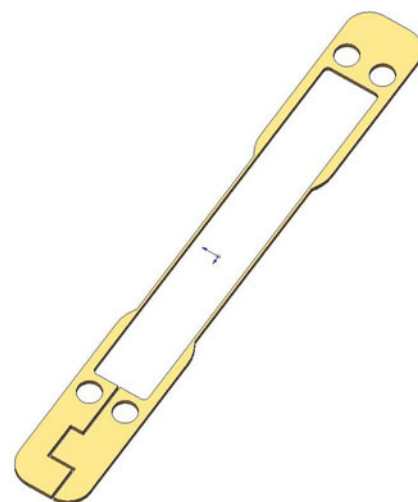

Figure 2.6: DC coil test assembly.

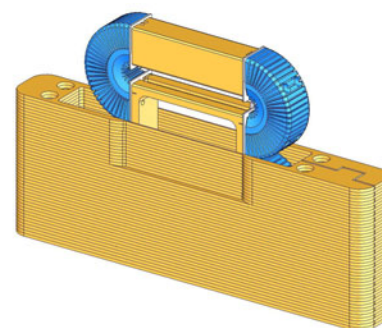Figure 2.7: Winding geometry of the MIRA DC coils.

Figure 2.8: Assembled MIRA NRSE coil.

First neutron reflectometry results from the new instrument MIRA at FRM-II

Neutron reflectometry is a powerful tool to probe the depth profile of thin films and multilayers. In additon, using polarised neutrons the magnetic depth profile of ferromagnetic nanostructures can be unraveled. Here, we report the first reflectivity experiments performed at the new instrument MIRA at the new high flux neutron source FRM-II. MIRA is designed as a versatile instrument to provide various options for different types of experiments. One option of MIRA is as a reflectometer using a monochromatic
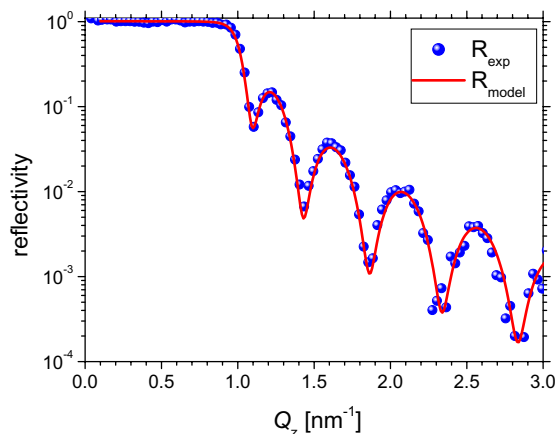
Figure 2.9: Neutron reflectivity of Ni single film (t_{Ni} = 52.55 nm). The symbols represent the experimental data whereas the solid line shows the computed reflectivity.

since the magnetic field environment was not ready at the time of the experiments and therefore the magnetic state of the samples could not be defined absolutely. Nevertheless these first results obtained from MIRA confirm our structural layer model, which is the basis for the analysis of polarised neutron reflectivity measurements performed at the AMOR reflectometer at PSI [4, 5]. In addition to the successful test of the layer profile of our samples we could establish the reflectometry option of MIRA. It is a promising instrument especially once polarised neutrons are available allowing to investigate magnetic structures in detail.
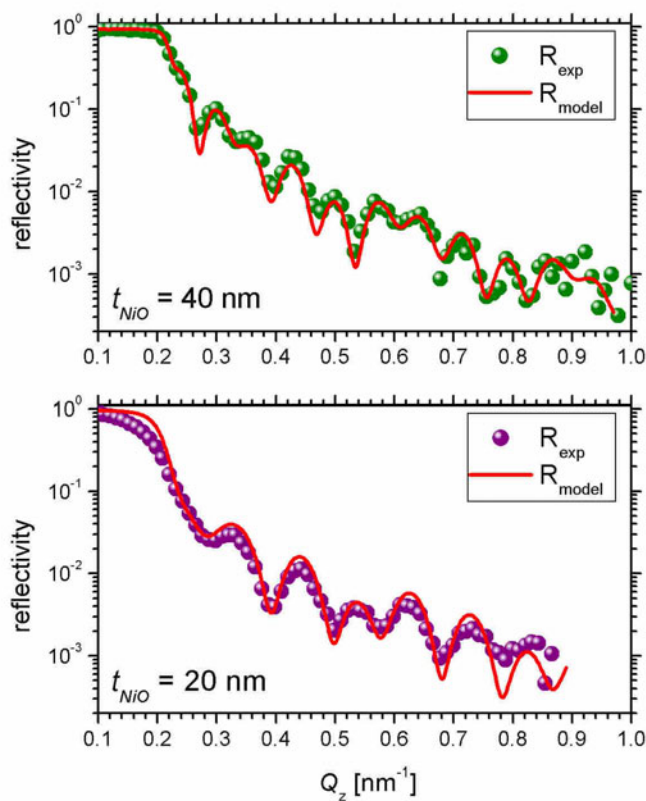
beam from a mica crystal. At present, MIRA is ready for unpolarised neutron reflectivity measurements, which is used the first time to measure reflectivity on a Ni single film and on FeCoV (20 nm)/NiO (t_{NiO})/FeCoV (20 nm) trilayers in order to test the structural layer model as obtained from X-ray reflectivity (XRR).

Prior to the reflectivity experiments the instrument including the sample stage was aligned. In particular, the design of the sample stage allows to change samples without the necessity of a new alignment. From neutron reflectivity on a Ni single film (fig. 2.9) we obtained the characteristics of the neutron beam: λ = 0.98 nm, $\Delta\lambda$ = 0.02 nm, $\Delta\theta$ = 0.06°.

Fig. 2.10 shows the neutron reflectivities of FeCoV/NiO/FeCoV trilayers. The agreement of experimental and computed reflectivities is satisfactory. Some discrepancies are remaining as the model reflectivities include only a contribution from an average magnetisation of the ferromagnetic FeCoV layers. This may not be completely real

Figure 2.10: Neutron reflectivity of FeCoV (20 nm)/NiO (t_{NiO})/FeCoV (20 nm) trilayers. The structural parameters, as obtained from the refinement of the X-ray reflectivity, are directly used to calculate the nuclear SLD profile of the trilayers for neutrons. From the combination of nuclear and magnetic contributions to the scattering length the model reflectivities are calculated.

[1] Keller, T., Golub, R., Gähler, R. In Pike, R., Sabatier, P., editors, *Scattering and Inverse Scattering in Pure and Applied Science*, 1264–86 (Academic Press, San Diego, CA, **2002**).

[2] Wahl, M. Master's thesis, Max-Planck-Institut für Met-

allforschung, Stuttgart, Germany/Institut für Theoretische und Angewandte Physik, Universität Stuttgart, Germany (**2003**).

[3] Gähler, R., Golub, R. *J. Physique*, 49, (1988), 1195.

[4] Shah, V., Schanzer, C., Böni, P., Braun, H. B. *J. Magn. Magn. Mater.* In press.

[5] Schanzer, C., Shah, V., Gutberlet, T., Gupta, M., Böni, P., Braun, H. B. *Physica B.* In press.

2.4 Status of the Horizontal Reflectometer REFSANS at FRM-II

R. Kampmann[1], **M. Haese-Seiller**[1], **V. Kudryashov**[1], **C. Daniel**[2], **B. Nickel**[3], **J. Rädler**[3], **A. Schreyer**[1], **E. Sackmann**[2]

[1]GKSS Forschungszentrum, Institut für Werkstofforschung, Geesthacht, Germany
[2] Physik Department E22, TU München, Garching, Germany
[3]Ludwig-Maximilians-Universität München, Germany

The horizontal reflectometer REFSANS is dedicated to the comprehensive analysis of the air/water interface by means of specular and off-specular reflectivity as well as GISANS measurements [1, 2, 3]. In parts, novel components concerning the chopper system, the neutron optics, the detector and the data acquisition system have been developed to meet the requirements of the different operation modi. An overview of the status of REFSANS as achieved in 2004 is presented in this report.

In the chopper chamber the slave chopper (SC) can be positioned in neutron guide gaps at distances between $\approx 5\,\text{cm}$ and $2.1\,\text{m}$ from the master chopper (MC) for setting the wavelength resolution in the broad range of $0.25\,\% < \Delta\lambda/\lambda < 15\,\%$ (Fig. 2.11). Double disc choppers allow adjusting the transmission window between 0°and 120°(Fig. 2.11 and 2.12) in accordance with the wavelength resolution.

GISANS geometry is achieved by means of collimating the beam horizontally and vertically. In this geometry the intensity is increased by more than one order of magnitude by means of focussing 13 partial beams in the detector plane at a distance of $\sim 10\,\text{m}$ from the sample. The latter is performed by means of pre-collimating the beams in

Figure 2.11: View of neutron optics, master chopper (MC) and slave chopper (SC) without disks in the chopper chamber (NL-2b: end of neutron guide NL-2b at the entrance of the chopper housing; NG-1, NG-2, NG-3, and NG-4: neutron guide elements.
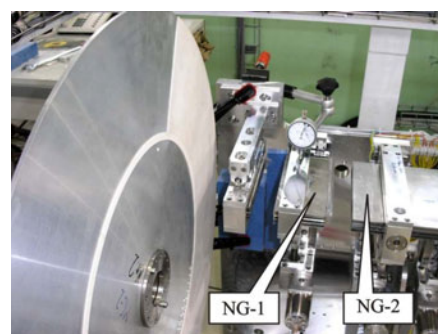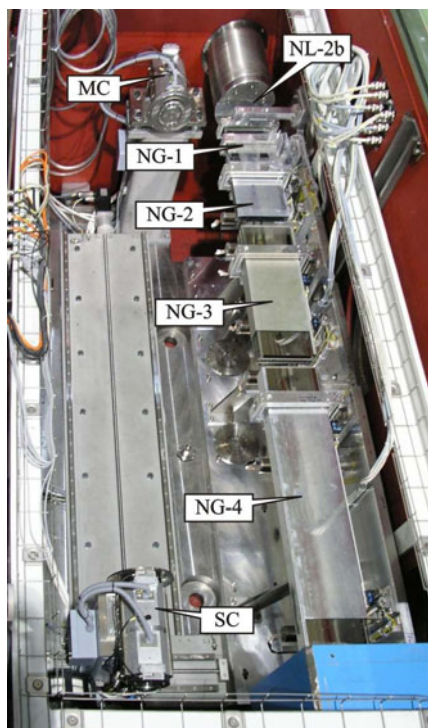

Figure 2.12: Master chopper with one disc and neutron guide elements NG-1 and NG-2 mounted in the chopper chamber.

Figure 2.13: View of neutron guide element 3 with its upper channel used for continuing NL-2b (height: 12 mm; width: 170 mm) and its lower channel designed as a radial pre-collimator.

radially collimating neutron guide channels in the chopper chamber (Fig. 2.13) and by comb-like aper-

tures in the beam guide chamber (between neutron optical bodies; Fig. 2.14) preventing mixing of neutrons in different partial beams [1, 3, 4].

The sample environment (Fig. 2.15) is designed for experiments at the air/water interface as well as at the air/solid and liquid/solid interface. In all cases one can make use of a microscope in upright or inverted position either for preparation purposes or as a complementary measuring option (e.g. fluorescence techniques). The further equipment consists of a damping table, a temperature controlled film balance and a set of translational tables (x, y, z) together with a three-axis goniometer (χ, ϕ, Ω).

Figure 2.14: View of a neutron optical body of the beam guide chamber with the mechanics for vertically aligning a NGE. The NGE consists of an upper channel (uc) for continuing NL-2b (height: 12 mm; width: 170 mm) and a lower channel (lc) designed for vertically collimating and keeping the large horizontal beam divergence.
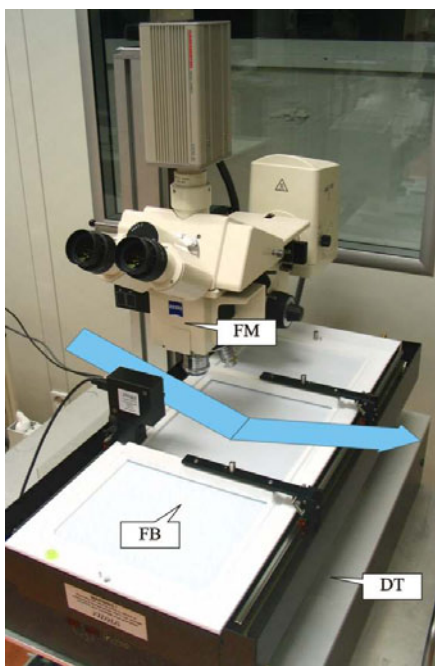

Figure 2.15: Setup for air-water experiments including damping table (DT), film balance (FB) and fluorescence microscope (FM). The path of the neutron beam is indicated by the arrows.

In the scattering tube the 2D-detector with an active area of 500 mm × 500 mm (Fig. 2.16) and a position resolution of ≈ 2 mm × 3 mm can be positioned at distances between ≈ 2 m and ≈ 12 m from the sample. With its high quantum efficiency for neutrons (≈ 80 % for $\lambda \sim$ 0.8 nm) (Fig. 2.17) and a very low one for gammas ($< 10^{-6}$ for E ∼ 660 keV) the detector meets all requirements for measuring low reflectivity and weak GISANS contributions [5].
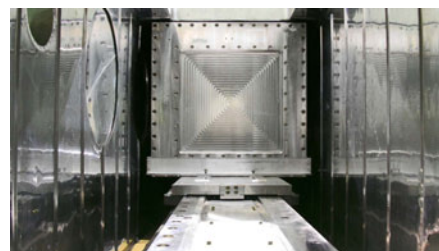

Figure 2.16: REFSANS detector mounted on the 12 m long translation table in the scattering tube.

The main components of REFSANS (chopper system, neutron optics, sample environment, 2D-detector, shielding, scattering tube with lifting system and data acquisition system) have successfully been tested and are being put into operation. First measurements will be performed at REFSANS early in 2005.

Acknowledgements
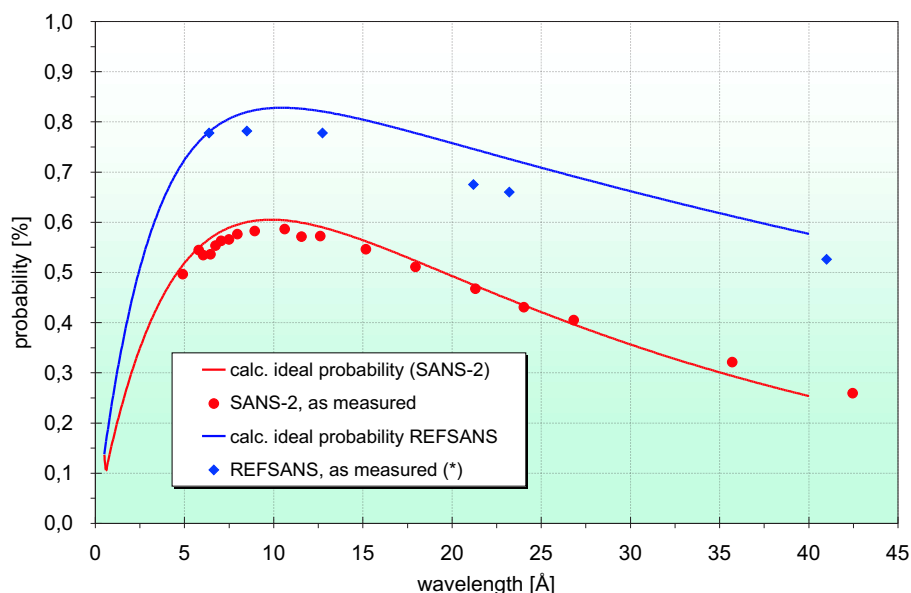
Figure 2.17: Neutron detection probability of the REFSANS detector and its prototype (SANS-2).

rokov, A., Frisius, F., Tristl, M., Sackmann, E. *Applied Physics A*, 74, (2002), 249–251.

[2] Kampmann, R., Haese-Seiller, M., Kudryashov, V., Deriglazov, V., Syromiatnikov, V., Tristl, M., Toperverg, B., Okorokov, A., Schreyer, A., Sackmann, E. *Physica B*, 335, (2003), 274–277.

[3] Kampmann, R., Haese-Seiller, M., Kudryashov, V., Deriglazov, V., Tristl, M., Schreyer, A., Sackmann, E. *Nuclear Instruments and Methods A*. To be submitted.

[4] Kampmann, R., Haese-Seiller, M., Kudryashov, V., Daniel, C., Deriglazov, V., Toperverg, B., Schreyer, A., Sackmann, E. *Annual Report FRM-II, (2003)*, 30–32.

[5] Kampmann, R., Marmotti, M., Haese-Seiller, M., Kudryashov, V. *Nuclear Instruments and Methods A Nuclear Instruments and Methods A*, 529, (2004), 342–347.

[1] Kampmann, R., Haese-Seiller, M., Marmotti, M., Burmester, J., Deriglazov, V., Syromiatnikov, V., Oko-

2.5 RESI – The Single Crystal Diffractometer

B. Pedersen[1], **G. Seidl**[1], **W. Scherer**[2], **F. Frey**[3]
[1]ZWE FRM-II, TU München
[2]Inst. f. Physik, Universität Augsburg
[3]Sektion Kristallographie, GeoDepartment, LMU München

During the last year the commissioning of the thermal single diffractometer RESI has been started. Following the startup of the reactor in May we were able to use the first neutrons to start the adjustment of the focusing Cu-422 monochromator and the focusing Ge-511 monochromator. During the first full power time in October, the Cu-422 monochromator has been fine-tuned and and detailed tests of the instrument have been carried out. These included assessment of the properties of the image plate system, the software and the hardware.
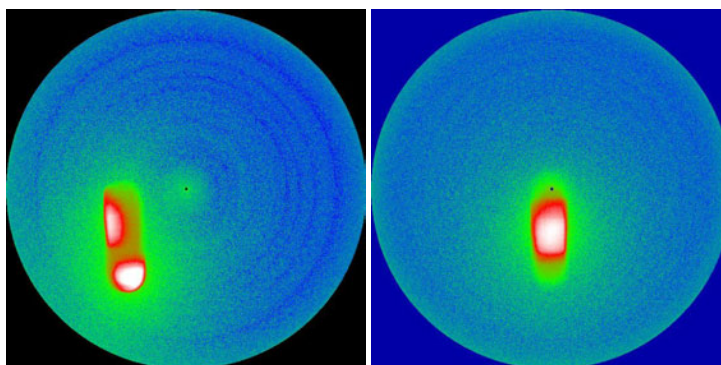

Figure 2.18: Images of the monochromatic beam: left) prior to focusing, right) focused beam (Cu-422 monochromator, $\lambda = 1.0$Å)

Results

The highly sophisticated monochromator mechanics, which allows adjustment of the individual crystals in three degrees of freedom has proven to be very useful. Using the image plate as a "camera" for neutrons, we were able to focus the monochromatic beam on an area of about 20×30 mm, thereby increasing the flux density on the sample position by approx. a factor of 5.

Different test crystals were used to align the goniometer and to test the integration of Bragg intensities. A typical diffraction image of a sodium gallium phosphate is shown in Figure 2.19.
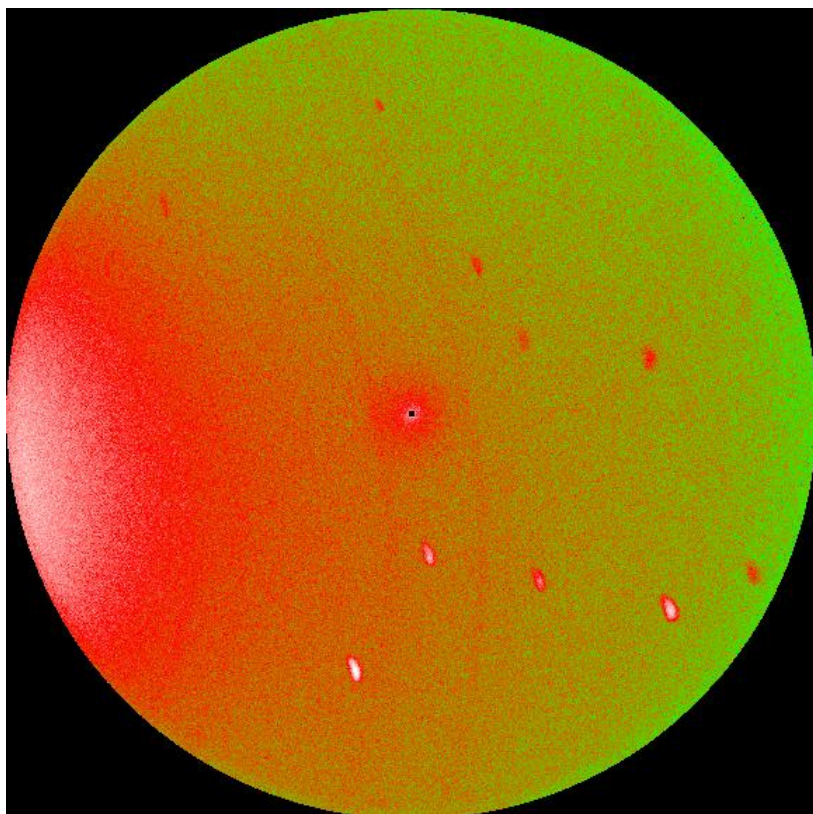
Due to the limited beam time, we did not collect complete datasets, so refinement results are not yet available.

The gamma sensitivity of the imaging plate, which has been a major concern during the design phase, has proven to be neglegible. This can be attributed to the very low background at the detector position due to highly effective shielding of the neutron guide and the monochromator. With closed secondary shutter, we observe almost no increase of the radiation level above the values recorded before reactor startup.

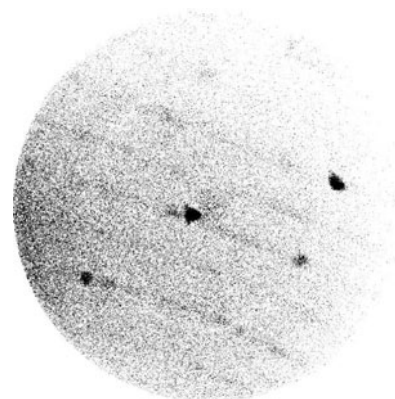Further tests were carried out to assess the ability to collect diffuse

Figure 2.20: Diffraction image (AlNiCo quasi crystal). Both Bragg and diffuse scattering can be seen.

scattering data. Here, we used a rather large AlNiCo quasicrystal. As shown in figure 2.20, diffuse scattering can be observed up to high diffraction angles, even in the presence of strong Bragg reflections. Here the large dynamic range of the imaging plate system proves to be a significant advantage.

These tests also indicated some possible improvements of the beam shaping. A boron carbide nozzle (10mm diameter) directly in front of the sample has been designed to reduce the background due to air scattering.

Outlook

The next steps in the commissioning of the instrument will comprise the setup of the heavy goniometer with tilting option or Eulerian cradle and the analyzer option. Parallel to this work, instrument RESI is available for first user experiments. 52 days of the cycles 2 and 3 have been assigned to external users.

Figure 2.19: Diffraction image (sodium gallium phosphate, $2 \times 3 \times 1.5$ mm^3, 1500sec/degree, sample-detector distance 250mm). Some powder rings from the Al sample holder can be seen.

2.6 First test measurements at the new structure powder diffractometer (SPODI) at the FRM-II

M. Schlapp[2,1], **M. Hölzel**[2,1], **R. Gilles**[2], **F. Elf**[3], **B. Krimmer**[2], **H. von Boysen**[4], **H. Fuess**[1]

[1]Fachbereich Materialwissenschaft, Technische Universität Darmstadt
[2]ZWE FRM-II, TU München
[3]Mineralogisch-Petrologisches Institut und Museum der Universität Bonn
[4]Ludwig-Maximilians-Universität, Depart. für Geo- und Umweltwissenschaften, München

Figure 2.21: Set-up of the Structure Powder Diffractometer SPODI at the FRM-II.

Introduction

The design and status of the new Structure POwder DIffractometer (SPODI) (figure 2.21) is reviewed. To solve complicated structures reliably by powder diffraction, not only high resolution and intensity are essential, but, in particular, also good peak profiles that can be described as perfect as possible. For strongly overlapping reflections, uncertainties in the exact shape can lead to a wrong distribution of the intensities. Moreover, such knowledge virtually increases the resolution of the instrument far beyond that given by the widths of the peaks. Similar arguments hold for a good peak to background ratio which can

be achieved not only by a low background, but also by narrow tails of the peaks. Finally, such good peak shapes should be maintained up to large scattering angles 2θ. Based on these considerations, computer simulations have been used to optimize both the single components and their interaction along the instrument. The resulting concept together with test measurements of single components at neutron sources have been described in reference [1, 2, 3, 4, 5, 6]. The high flux at the sample position with neutrons of very low vertical divergence because of the 5m distance to the monochromator allows the unique possibility to integrate a small-angle scattering apparatus in the whole system [7].

Results and Discussion

Using the first adjustment of the focusing monochromator the beam was deposed to the sample position on which a corundum sample was mounted. As one of the first patterns figure 2.22 shows the diffraction pattern of a measurement without sample collimator and preliminary adjustment of the detector electronics. Rietveld fitting procedure results in identification of the expected peaks with broad FWHM's. The pattern includes no correction of the umbrella effect which means the intensity was added up in vertical direction not using the position sensitivity. A single peak analysis of the {116} reflection with different integration of detector height displays the shifts of the determined position of the peak ($\Delta 2\theta$ up to 0.11°) and increasing asymmetry in the peak profiles for higher detector heights (figure 2.23). The fitting parameter η which describes the Lorentzian contribution in the Voigt function (the value $\eta = 0$ stands for Gaussian function and $\eta = 1$ for Lorentzian function, respectively) resulted in values $\eta = 0.1$ for the different detector heights and confirmed the nearly perfect Gaussian profile.

This effect of peak shift and peak asymmetry will increase dramatically with decreasing scattering angle towards $2\theta = 0°$ or with increasing scattering angle towards $2\theta = 180°$. The peak profile will not be
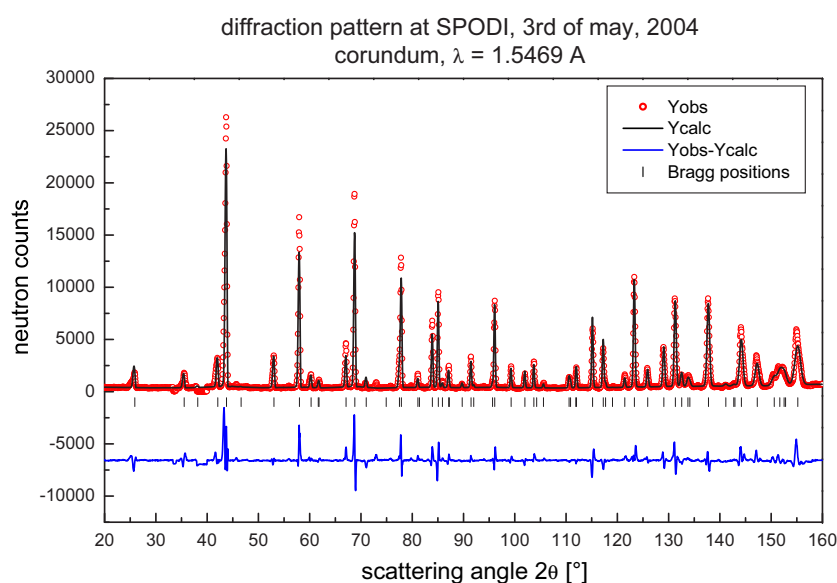
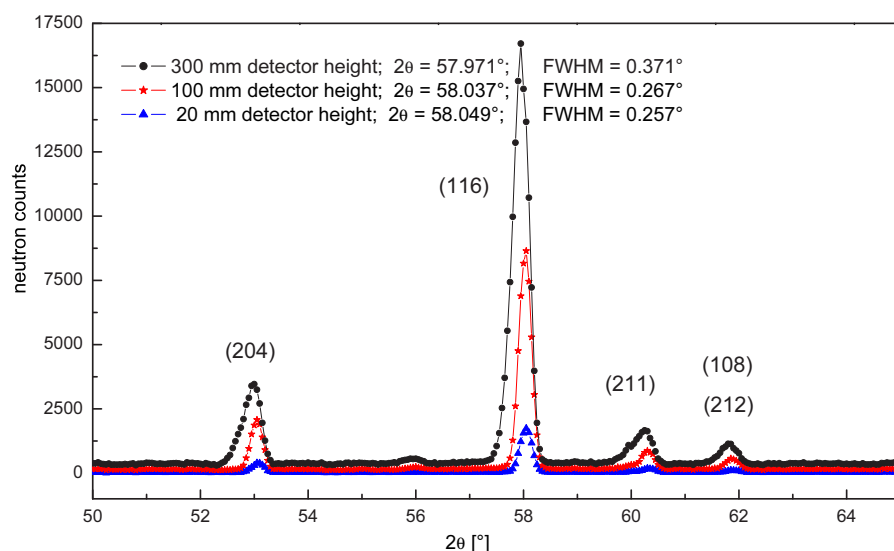Figure 2.22: Diffraction pattern of corundum measured at SPODI

Figure 2.23: Corundum diffraction pattern with evaluation of different detector heights displaying the position shift of peaks and asymmetry of the profiles.

an one-dimensional diffraction pattern for further processing by Rietveld programs. The only way to avoid peak shift and peak asymmetry and to conserve all information inherent in the diffraction experiment is to integrate along Debye-Scherrer rings. The detector matrix can be interpreted as rectangular grid, whereas theoretical Debye-Scherrer rings form a curvilinear grid. In general, these two grids do not coincide. Therefore it is necessary to calculate the intensity at points of the Debye-Scherrer grid due to surrounding matrix grid points. This is performed by bilinear (horizontal and vertical) interpolation in dependency on distance. At last the intensities have to be normalized in relation to the arc length of the lines recorded by the detector. The result of this computer time consuming procedure is shown as solid line in figure 2.24. In comparison to the integration of a detector tube there are now no peak position shifts, no asymmetrie of the peak profile shape and, more important, the FWHM is reduced and the resolution is enhanced. This simulation does not include the smearing caused by neutron optics and sample dimensions.

Conclusion

First measurements at the new structure powder diffractometer SPODI have shown the great potentials of the instrument. It was the first instrument at FRM-II to lead a monochromatic beam on a sample for a diffraction pattern.

The first alignment of the monochromator under the help of McStas simulations for the choice of tilting angle and focusing geometry revealed high intensity at the sample position. The quasi

constant over the whole range of 2θ. The reason will be clear by remembering the Debye-Scherrer diffraction geometry: The powder sample is centered at the intersection point of primary beam and cylinder axis, which are perpendicular. The sample position is the starting point of the Laue cones. The cone axes coincide with the primary beam and are perpendicular to the cylinder axis. The Debye-Scherrer rings resp. ring sectors are intersection lines of the cylindrical detector and these cones. The two-dimensional detector matrix has to be transformed to
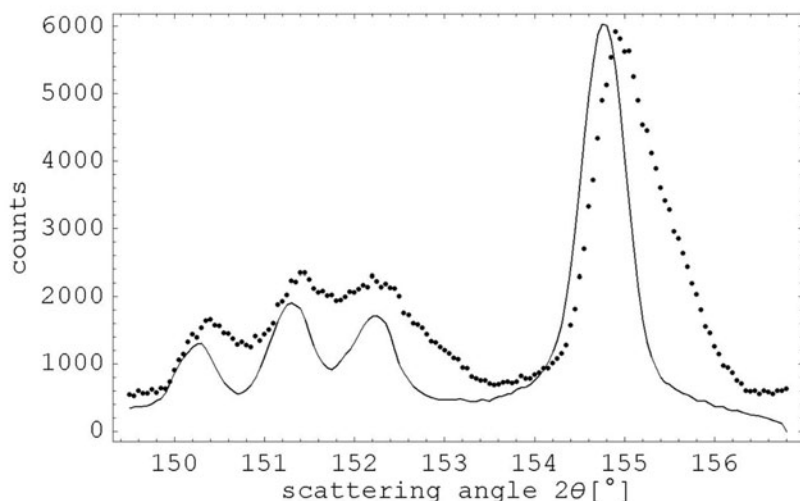
Figure 2.24: Comparison of transformation methods: vertical summation (dotted) and summation along Debye-Scherrer rings (solid)

two-dimensional detector allows enhancements in the resolution and more accurately determination of peak position as arised in the corundum measurement.

Acknowledgement The support of this study by the German BMBF under grant FKZ03-FU5FRM is gratefully acknowledged.

A more detailed version of this text was submitted by R. Gilles et al.

to Z. f. Kristallographie for publication.

[1] Gilles, R., Artus, G., Saroun, J., Boysen, H., Fuess, H. *Physica B*, 276-278, (2000), 87.

[2] Gilles, R., Saroun, J., Boysen, H., Fuess, H. In *Proc. HERCULES X Euro Conference*, 282 (**2000**).

[3] Gilles, R., Krimmer, B., Saroun, J., Boysen, H., Fuess, H. *Mat. Sci. For.*, 378-381, (2001), 282.

[4] Gilles, R., Krimmer, B., Boysen, H., Fuess, H. *Appl. Phys. A 74 (Suppl.)*, 74, (2002), S148.

[5] Hoelzel, M., Gilles, R., Schlapp, M., Boysen, H., Fuess, H. *Physica B*, 350, (2004), e671.

[6] Gilles, R. Habilitation, TU Darmstadt (**2004**).

[7] Schlapp, M., Hoelzel, M., Gilles, R., Ioffe, A., Brueckel, T., Fuess, H., von Seggern, H. *Physica B*, 350, (2004), e861.

2.7 HEiDi – Single Crystal Diffractometer with Hot Neutrons

M. Meven[1], **V. Hutanu**[2], **G. Heger**[2]
[1]ZWE FRM-II, TU München
[2]Institut für Kristallographie, RWTH Aachen

Figure 2.25: Detector unit at the $\Theta_{mono} = 20^o$ position

Scientific design

HEiDi is a project of the RWTH Aachen and the TU München. The instrument was build up in front of beam tube SR-9B to use the hot source of the FRM-II. At the hot source the spectrum of the thermal neutron flux becomes shifted to shorter wavelengths. Therefore, following Braggs Law $2d \sin \Theta = \lambda$ HEiDi can observe a very large range – defined as $|\vec{Q}| = \sin \Theta_{max}/\lambda$ – of the reciprocal space. This favorizes the instrument for crystallographic studies on single crystal samples for which details of the atomic or magnetic structure are of special interest. Examples are investigations of mean square displacements near structural phase transitions (observation of anharmonicities), of disorder in molecular crystals, of hydrogen bonds and of magnetic ordering. Other applications are structure analyses on rare earth (e.g. Gd, Sm) compounds. They can only be studied by neutron diffraction at short wavelengths because at larger wavelengths their absorption cross section becomes too big.

In 2004 the instrument was com-

pleted in order to begin the first tests and adjustments of HEiDi with neutrons together with the nuclear commissioning of the FRM-II. Details of the instrument and its applications were presented at the ECM22 in Budapest and at the DNS2004 in Dresden. In the following the actual status of HEiDi and the results from the tests of some of HEiDis components during the first reactor period are presented:

Current status

Biological Shielding

The efficiency of the biological shielding in front of the instrument and its two experiment shutters (in front and behind the monochromator unit) were tested at the maximum thermal power of 20 MW of the reactor. In the accessible area around the instrument not more than about 1 μSv/h at any position was detected if the beam exit to the diffractometer unit was closed.

A beam stop and a second biological shielding were mounted to absorb radiation from the monochromatized primary beam and scattered neutrons from the sample environment behind the instrument. Both perform very well which means that there is no significant increase of gamma or neutron radiation during operation of the instrument outside this second barrier.

Collimators

Three collimators with Gd coated metal foils were manufactured at the HMI in Berlin and mounted into the main beam shutter of SR-9. Homogenity and transmission were tested in 2002/2003 at the SV28 neutron diffractometer at the FZ Jülich yielding completely satisfying re-

sults with an intensity ratio of 1:2:4 for the 15', 30' and 60' collimator of SR-9B. Gold foil activation analysis of the white beam at the monochromator position and measurements at 20MW with monochromatized beams of 0.87 Å and 0.55 Å at the monitor position near the sample yield an intensity ratio of 1:2.0:3.2 for the 15', 30' and 60' collimators. While the agreement with the theory is perfect for the 15' and 30' collimator there is a surprising loss of intensity for the 60' collimator. An ex-

planation for this result has not been found yet; a significant missalignment of the 60' collimator is very unlikely.

Monochromator Unit

There are four axes/directions to define the orientation of the monochromator unit with respect to the "white" beam from the reactor and the outgoing channel to the experiment. These are the Θ_{mono}-axis, an x-table and a tilting
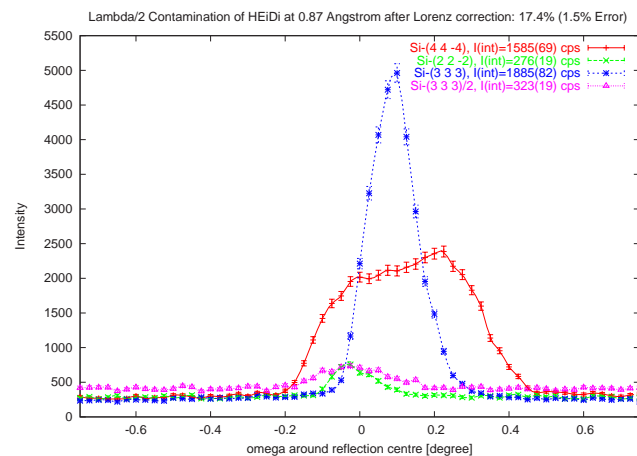

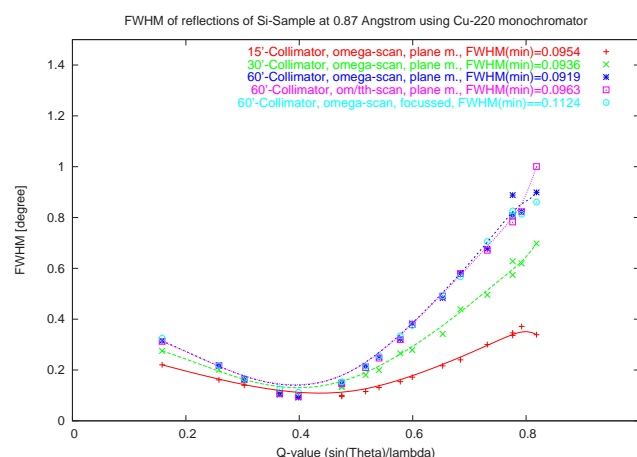Figure 2.26: $\lambda/2$ contamination

Figure 2.27: Resolution function

goniometer moving perpendicular to $\Theta_{Monochromator}$ and a selector-axis to switch between different available monochromator crystals. All axes where optimized for the $\Theta_{mono} = 20^0$ exit using the Cu-(220) and the Cu-(420) monochromator crystal and a Si cube of about 5 mm length per edge as sample. The ratio between the flux at 0.87 Å and the flux at 0.55 Å was found to be 3:1. This is in good agreement with former Monte-Carlo (MC) calculations of the flux distribution performed at the FRM-II.

To increase the neutron flux at the sample position all monochromator crystals can be focussed vertically. MC simulations of the beam path yield a gain factor of 2.5. The experimental results were found to be in very close agreement to this with a gain factor of 2.4 for both wavelengths.

Profiles of Bragg reflections taken from the sample show only a minor broadening between no focussing and full focussing for the Cu-(220) monochromator with a rocking scan width of $\Delta\omega \approx 0.9^0$ (FWHM). For the Cu-(420) monochromator we got another picture. In the non focussing mode the FWHMs of the reflections correspond to the results of the Cu-(220) monochromator. An increase of the focussing angle yields a peak broadening of the width ending up with a double peak structure and a doubling of the FWHMs at the maximum focussing position. The small width of the double peak still allows an accurate measurement of integrated intensities. Nevertheless we will perform a 2D image of the monochromatized outgoing beam in order to identify

Figure 2.28: normalized integrated intensities

and correct one or more missaligned Cu-(420) crystals as soon as there are neutrons available again.

Filter Unit

For λ = 0.87 Å(Cu-(220)) and λ = 0.55 Å(Cu-(420)) there exists the problem of the so called $\lambda/2$ contamination. If there is a given crystal lattice and a given Bragg angle due to Braggs Law not only neutrons of a certain wavelength λ but also those of higher order like $\lambda/2$, $\lambda/3$ and so on can pass. Reflectivity drops significantly with shorter wavelengths. Therefore, only the $\lambda/2$ radiation has to be taken care of to get a really monochromatized beam. To avoid $\lambda/2$ contaminations, filters can be used which consist of thin foils of elements which have a resonance (and therefore strong absorption cross section) at or near to $\lambda/2$. Measurements of allowed and forbidden Si reflections at 0.87 Å showed a $\lambda/2$ contamination of 17.4%, see figure 2.26. This

is much higher than a tolerable ratio of less than 1% which is suitable for structure analyses using Bragg data of integrated intensities. From these results and the neutron flux distribution at the exit of SR-9 the thicknesses of all necessary filters (about six for three different Θ_{mono} and two different Cu monochromators) were derived in order to get suitable foils for the filter unit.

Resolution function

The resolution function of HEiDi wsa determined with a Si sample crystal. The mosaicity of this perfect crystal is well below those of the monochromator crystals. Therefore the FWHMs of the Bragg peaks of the Si sample give directly the instrumental resolution for different $|\vec{Q}|$ values ($|\vec{Q}| = \sin\Theta/\lambda$). The results for 0.87 Å using three different collimations (15', 30', 60') and focussing and non-focussing modes are shown in figure 2.27.
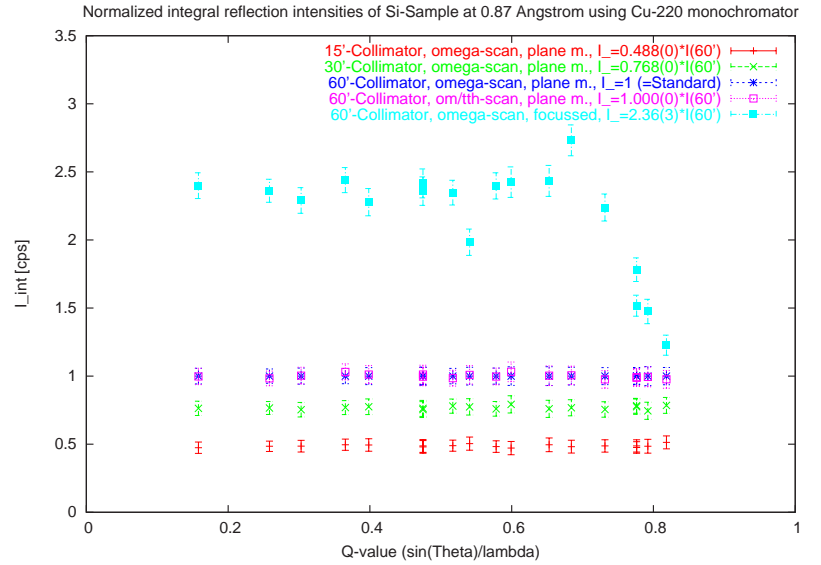
Reflection profiles are well de-

fined for all three collimations. If the Bragg angle Θ gets close to Θ_{mono} the FWHMs become very narrow with values below 0.1^0. It is obvious that the divergence ratio of four between the 15' and the 60' collimator does not yield a corresponding increase of FWHMs or integrated intensities, see fig. 2.28. Only a factor of two was found for the ratio of integrated intensities over the complete Q range. This makes it very likely that the integrated reflection intensities are limited by the small mosaicities of the monochromator crystals. Furthermore, it was found that there is no significant difference between the focussing and the non focussing mode exept of the gain factor of 2.4, see fig. 2.27.

Software

The measurement program for this instrument was written originally for an x-ray diffractometer at the RWTH Aachen using ANSI-C. Only minor changes were necessary to control HEiDi with this software using hardware specific drivers (e.g. Taco) to support the different components. The software controls all relevant components of the instrument and collects data of Bragg reflections using crystallographic informations about the sample. Though all basic functions of the instrument work, full hardware support by the drivers has not been reached yet, e.g. synchronous movements of all axes. This will be one of the major tasks in the near future to increase the efficiency of the instrument significantly.

An interesting feature of this program is its capability to be controlled remotely. That means that the user can not only observe the progress of the data collection from

his office but also perform modifications to the running measurement.

Outlook

Instrumental Design

The first tests on HEiDi have proven its capability to collect Bragg data sets. The next steps are:

The issues found during the first reactor period have to be corrected. The adjustment of the instrument will be continued for the untested wavelengths using the $\Theta_{mono} = 10^o$ and the $\Theta_{mono} = 25^o$ positions.

At the beginning of 2005 two additional components will be delivered. One component is the Ge-(311) monochromator crystal. It will be checked and adjusted in its focussing unit as a sample mounted on the diffractometer during the next reactor period. After this, it will be mounted on the free place of the selector in the monochromator unit. The other component is the small $(200*200mm^2)$ 2D ^{3}He detector for which the electronical part has already been assembled.

Polarized Neutrons

On Juli 2004 the Institut für Kristallographie at the RWTH Aachen was granted financial support from the BMBF for the project "Polarisierte Neutronen für die Spindichtebestimmung an magnetischen Strukturen". On December 2004 Dr. Vladimir Hutanu became the responsible scientist for this project and started his work doing some calculations to find a suitable size and design for the ^{3}He spin filter cells and suitable magnetic cavities.

The efficiency of ^{3}He NSF (Neutron Spin Filter) used as a polariser or analyser is usually described with quality factor Q, $Q = P_n^2 T_n$ where T_n transmission and P_n polarisation are depending in a different way from the cell's "opacity" which is the effective absorption coefficient of polarised ^{3}He and neutrons with antiparallel oriented spin. In fig. 2.29 are presented neutron's polarisation, transmission and quality factor Q of 10 and 15 cm long cells filled with 3 bars of ^{3}He polarised at 70% as function of the neutron wave-
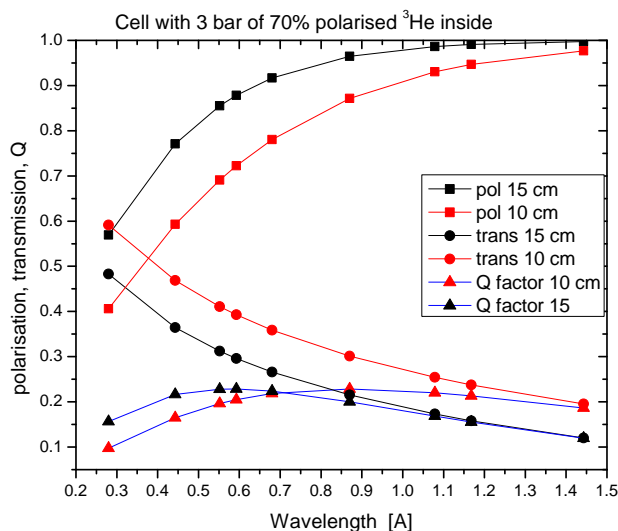

Figure 2.29: Cell optimization

lengths accessible at HEIDI. Optimising the cell parameters for the wavelength of 0.68 Å and 0.87 Å the first NSF cells specifications were elaborated. Cells with 13 cm length, 6 cm in diameter and working pressure up to 3 bar seems to be optimal for our application. Not the last role in the practical application play also relaxation characteristics of the polarised ^{3}He containers. The values of 200 hours for characteristic relaxation $T1$ at 1 bar would be preferable, but 100 hours as a lower threshold is reasonably desirable. Next steps will be the final definition and construction of the spin filter cells as well as the magnetic environment and the construction of an amagnetic base for the diffractometer.

3 Spectrometers

3.1 PANDA – The cold neutron three-axes spectrometer

P. Link[1], **D. Etzdorf**[1], **A. Schneiderwind**[2], **R. Schedler**[2], **R. Sprungk**[2], **E. Kaiser**[2], **C. Wetzig**[2], **M. Dörr**[2], **S. Sahling**[2], **M. Loewenhaupt**[2]
[1]ZWE FRM II, TU München
[2]Inst. f. Festkörperphysikphysik, TU Dresden

Personal

Early 2004 Dr. M. Rotter left the PANDA project and the TU Dresden for a position at TU Vienna in Austria. Since 1st of November Dr. Astrid Schneidewind has joined the team as instrument co-responsible.

Project status and progress

The year 2004 has been governed by two aspects, on one hand the completion and assembly of instrument components and on the other hand the installation of peripheral equipment.

Following the neutron flight path we start with the new optional sapphire filter component in the neutron guide channel, which has been added in November. The remote controlled unit drives a 70mm thick sapphire single crystal into the white beam. We expect that this filter reduces thermal and epithermal background considerably.

The primary spectrometer has been completed including the secondary shutter inside the monochromator shielding. A first test has been performed with neutrons. It showed that the primary shielding needs only minor improvement. We used the opportunity also to measure the white beam neutron flux at the monochromator

Figure 3.1: The experimental area of PANDA

position. The result $3.5 \cdot 10^9$ n/cm^2/s corresponds to the expected value from Monte-Carlo simulation. We note both PG002 and Heusler alloy crystals mounted on the corresponding monochromator and analyser mechanics ready to use.

Concerning the secondary spectrometer we finally have all components assembled and wiring for all electro-mechanics has been completed. The components are now integrated into the remote control software and ready to use.

The experimental area has been surrounded by shielding elements made of PE, lead, and stainless steel for radiation protection. This special design has been preferred because of space and weight limitations at the PANDA site. On top of the monochromator shielding we mounted a platform, which allows us there to install sample environment equipment in a comfortable way and moreover without restricting spectrometer movements on the ground. This will be most important

for the use of the 15T cryo-magnet system.

Outlook

During the year 2005, all neutron optical alignment should be done and PANDA may enter routine operation for first user experiments.
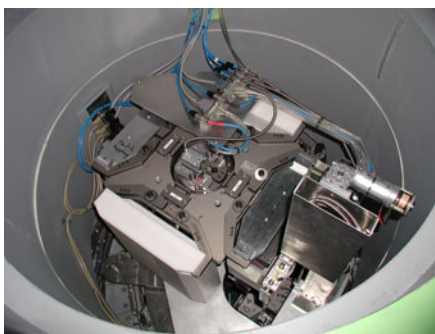

Figure 3.2: View inside the monochromator shielding with the remote controlled crystal changer

3.2 PUMA – The Thermal Three Axes Spektrometer at SR7

K. Hradil[2], **H. Schneider**[2], **G. Eckold**[2], **P. Link**[1], **J. Neuhaus**[1]
[1]ZWE FRM-II, TU München
[2]Institute of Pysical Chemistry, University of Göttingen

The three axes spectrometer PUMA is situated at the thermal beam tube SR7 within the experimental hall of FRM-II. It is built up and operated within a cooperation of the Institute of Physical Chemistry (University of Göttingen) and the Department of Physics E13 (TU München). Its main characteristics have been described within the report 2003 and can be found at http://www.frm2.tum.de/puma.

Fig. 3.3 shows a view of the instrument PUMA in its actual state. Concerning the single detector option of PUMA all necessary components for the commissioning phase of the instrument are in place and operational. The main activities during 2004 were performing tests of the components within the interaction of the whole spectrometer and the continuously improvement of the control program.

Problems with the absolute encoders of the main axes demanded a complete exchange of the devices including those of the monochromator-unit. Consequently, a complete realignment of all spectrometer components was necessary.

First measurements testing the primary shielding of PUMA with neutrons showed that a considerable flux of epithermal neutrons outside the monochromator drum
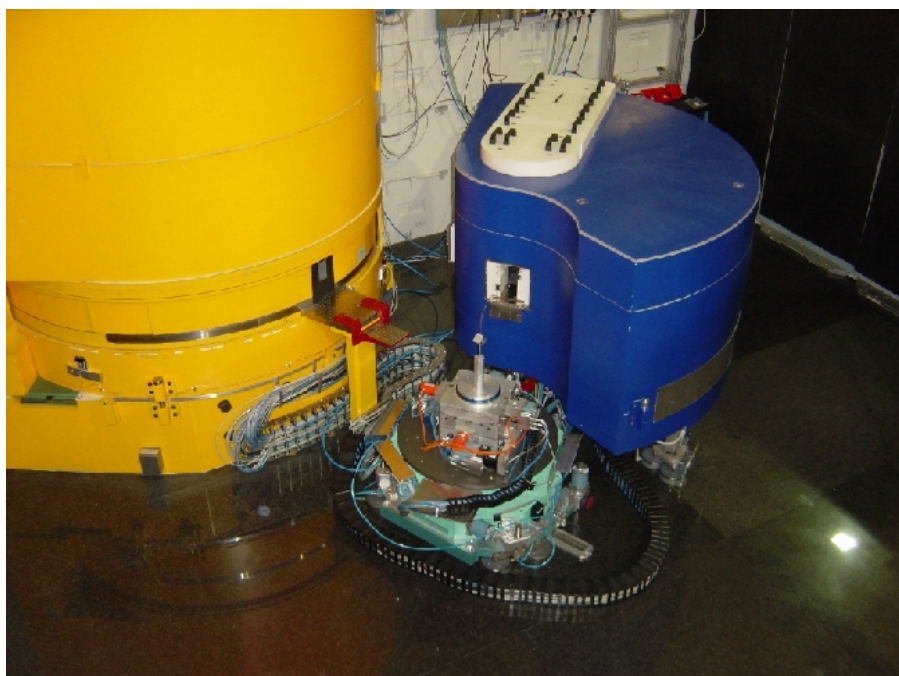

Figure 3.3: View on the instrument PUMA

and, hence, major improvements of the shielding became necessary. Presently, construction and fabrication of additional parts are under way. An efficient shielding of the experimental area made from a composite structure of iron, B_4C in vulcanized rubber, PE and lead allows for a sufficient radioprotection of the surrounding accessible area.

The doubly focusing PG(002)-monochromator device has been tested mechanically in Göttingen yielding an excellent mechanical accuracy that allows a very precise adjustment of vertical and horizontal curvature. Meanwhile, the PG(002) monochromator was transferred to FRM-II and installed within the monochomator change unit (Fig. 3.4). First provisional tests with neutrons showed that the flux at the sample position agrees well with the results of McStas simulations. In particular, on optimal focusing gain factor in intensity of 9 (flat/focussed) was determined just as expected from the simulations.

The bent mechanics of the Si(311) monochromator as provided by Swiss Neutronics had to be improved due to mechanical inaccuracies. These problems have now been solved so that the device will be installed in the monochromator changer in the near future.

The mechanical design of the multianalyser component was enhanced during the year and a first test unit could be placed on the analyser table. After some improvements of details the unit of 11 analyser blades will be manufactured and mechanically tested. The design concept for the two detector options is finished. We will use an array of 11 individual detectors for the dispersive arrangement, each corresponding to one of the analyser blades, and 7 position dependent detector tubes for the focusing arrangement. Both units will be built during 2005.The detector electronics is available. Due to the total number of 18 detectors we decided to use the compact system of Mesytec company providing a central unit and compact units for the preamplifiers which can be placed within the shielding of the detectors thus allowing for short distances of wiring . At the moment in cooperation with Mesytec a control program is developed to implement it within the TACO control system of FRM-II.

First tests of devices of the instrument sample environment were performed. The closed cycle cryo-stat was successful tested within a temperature range from 3.5 K to 300 K. A second close cycle cryostat with a high temperature option (up to 800 K) is delivered. Moreover, the furnace for the Eulerian cradle (up to 1000 °C) is already available.

Even if adjustment and characterization of the individual components of the spectrometer still needs some beam time, PUMA is principally ready for operation in its basic version. Hence, it was already considered in the first proposal round for "friendly users".
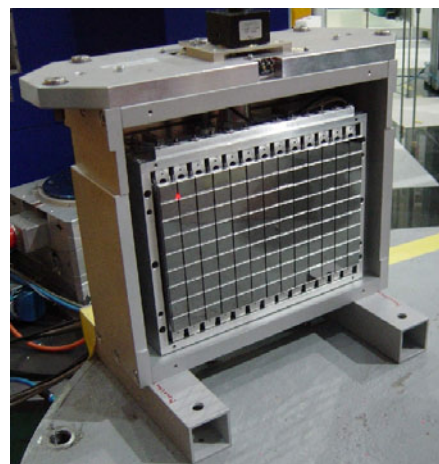

Figure 3.4: Bent mechanics of the monochromator with 117 PG(0 0 2) crystals

3.3 RESEDA – the Neutron Resonance Spin Echo Spectrometer

W. Häußler[1], **P. Boeni**[1], **B. Gohla-Neudecker**[1], **Heinz Wagensonner**[2]
[1]E21, Physik-Department, TU München
[2]ZWE FRM-II, TU München

RESEDA, the quasielastic Neutron Resonance Spin Echo (NRSE)-spectrometer at the FRM-II is located in the neutron guide hall. The neutron guide NL 5b leading to the instrument is bended, in order to provide a sufficient number of reflections, and to prevent direct sight to the neutron source. Thanks to its length (65 m), the bending radius of NL 5b can be relatively large ($r = 1640$ m), providing a broad neutron wavelength band ($\lambda = 2.5 - 15$ Å) with polarization being presumably better than 96%.

One part of the activities in 2004 at RESEDA was concentrated on the radiation shielding of NL 5b. Due to the results of first measurements of the radiation background performed just after the reactor start in May 2004, both guide and shielding were changed. The first part of the polarizing guide (8 m) was

Figure 3.5: The velocity selector and the neutron guide leading towards RESEDA.

moved into the casemate, the lead shielding along the other part of the guide was doubled and a neutron shielding was mounted. New magnetic components needed for the polarizing guide, were installed, and the magnetic field was properly adjusted along the whole neutron guide.

Another major part of the activities was concentrated on the construction of the selector housing (s. Fig. 3.5). Base plate, aluminum support, rotary table and neutron shielding were built. The housing was modified in order to close openings in the shielding, and cable channels were added. At the same time, the beam shutter in front of the selector was planned and con-structed. In order to have enough space for the shutter, the neutron guide between selector housing and RESEDA was moved by 10 cm. The magnetic guide field inside the selector housing was modeled, and the components needed therefore were produced. The selector vacuum system was purchased and installed. In December, all components of the selector were mounted and tested. Finally, the three-dimensional model of the selector housing and all installations was actualized, because in the previous model, both several dimensions were wrong, and main components were missing.

At RESEDA, several mechanical parts were reengineered. For ex-ample, the drive mechanics was modified, because the long (4 m) and heavy secondary spectrometer arms did not move. Both motors and encoders were substituted by a friction wheel drive and an absolute encoder. From the extensive work on the electronics, we mention only the most important part: the RF-circuits were put into operation. Both the existing RF coils were modified, in order to eliminate short circuits, and new RF coils were constructed. For the first time, the RF coils were connected to the amplifiers by RF transformers. The circuits were tested, the resonance frequencies, resistances and currents were determined. The RF transformers were adapted to the measured resistances. Bugs in the capacitor switches were eliminated. Two complete sets of coils and electronic components were chosen, which have identical resonance frequencies. Finally, due to problems with the RF amplifier supplier, new amplifiers were ordered from a different company.

Another major part of the activities was concentrated on the development of a new instrument-control-program. It was decided to skip the non-functioning fragments of the existing code, and to start the development of TACO servers being the FRM-II standard, also for RESEDA. These activities are still going on and will hopefully be finished before the first measurements.

3.4 RSSM – The Backscattering Spectrometer

P. Rottländer [1], **W. Bünten** [1], **T. Kozielewski** [1], **M. Prager** [1], **D. Richter** [1]
[1]Institut für Festkörperforschung, Forschungszentrum Jülich

The backscattering spectrometer RSSM is situated at the end position of neutron guide 6a. It is designed to optimize neutron flux while retaining the high energy resolution of backscattering spectrometers. Also, it offers a high degree of flexibility by providing different sets of crystals and a diffractometer option.

In 2004, most major components were finished and assembly of everything has begun. A neutron velocity selector filters neutrons which have no chance to be used by the instrument. It was ordered last year, and has been tested and delivered in august.

The phase-space transformation chopper is one of the most advanced parts of the instrument's design. It transforms a parallel neutron beam into one which is much better monochromatized but more diverging. This is achieved by means of graphite crystals moving at a speed of 300 m/s. Therefore, it has high requirements to the materials and technology. To avoid regular unmounting and rebalancing of the wheel, it was decided to use a maintenance-free magnetic bearing. But it proved to be a very hard task to find a working point for the magnetic bearing. When trying to find a working point for the bearing, several technical problems occured, the major of which was the breakdown of the motors, probably due to manufacturing faults. Due to the continuing problems, we decided not only to go on with the present design but also to develop a conventional drive based on hybrid bearings. We expect the drive with magnetic bearings to be ready for a long-term test in march, the one with hybrid bearings to be finished in may. In order to make best use of the time, we decided to conduct some more calculations and material tests in order to ensure safe operation of the chopper wheel.

The final monochromatisation is performed by crystals where a perpendicular neutron incidence assures a high energy resolution. To achieve an energy variation, the monochromator crystals are mounted on a support which performs an oscillatory movement. The drive was developed and delivered in the previous years by Aerolas. In 2004, it was subject to a six-week test
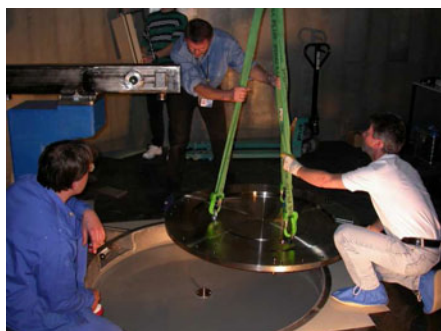

Figure 3.6: The central disc is used to align the main components of the instrument with high precision

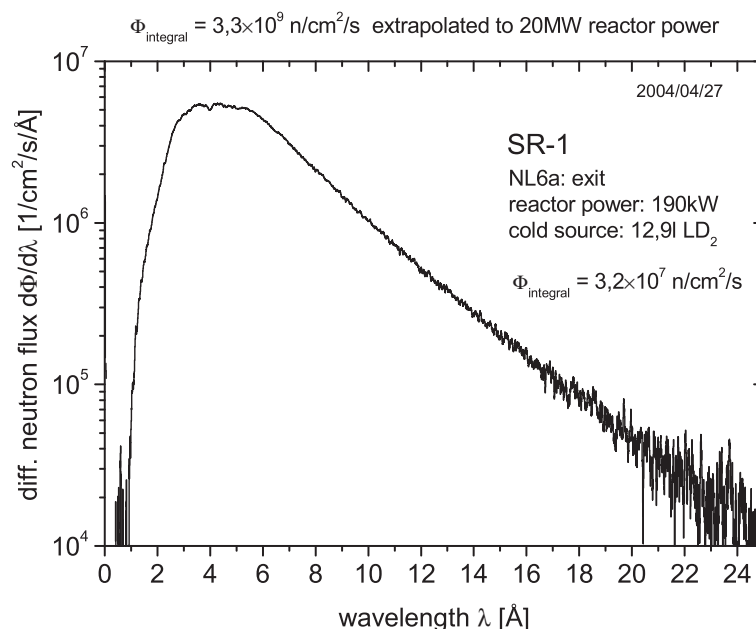Figure 3.7: Installing the large-angle reflectors

Figure 3.8: Measured neutron spectrum at the end of the primary neutron guide

run where several minor problems have been found and fixed.

The remaining polished Si(111) crystals have been glued to their analyser shells, and also the mounting of the Si(311) crystals to the analyser shells and rings is nearly completed.

To reduce neutron loss and experimental noise, the instrument is situated in a chamber which can be filled with argon as a protective gas. The gas-tight instrument chamber was assembled in february and subsequently leak tested. It proved to be necessary to carefully seal the screed floor to avoid having argon leak through it. By now, we have reached a leak rate well below the one that was specified ($2 - 3$ l/min). As a protection against neutrons entering or leaving the chamber, the walls were fitted with a layer of polyethylene as moderator and cadmium foil as neutron absorber.

In summer, the last of the super-mirrors of the neutron guide were fabricated and tested by S-DH and subsequently the neutron guide was installed in the neutron guide hall in Garching and optically aligned.

In order to adjust the instrument to different monochromator crystals, the instrument has to be rotated around the base point of the PST chopper. Therefore, a rotating frame has been installed in the instrument chamber, and the Doppler, and the unpolished Si(111) analysers were mounted to it. In the meantime, also the installation of supplies for argon and pressurised air has begun. Fig. 3.7 shows the present view of the interior of the instrument chamber.

The detector bank now has been assembled and wired, and some tests will be made early 2005. At the same time, the read-out electronics of the Doppler drive position and speed has been assembled and tested by the electronics institute in Jülich (ZEL), and is now being integrated with the detector electronics. The electronics racks for the mechanical degrees of freedom and the TACO servers will also be finished early next year.

As a first measurement to characterise the instrument, the neutron flux at the end of the facility-supplied neutron guide has been determined by K. Zeitelhack and others. The measurement is shown in Fig. 3.8 and shows a good agreement with the simulations; the intensity compares quite well to earlier simulations.

3.5 First commissioning steps at the time–of–flight spectrometer TOFTOF at FRM–II

T. Unruh[1], **J. Ringe**[1], **A. Gaspar**[1], **J. Neuhaus**[1], **W. Petry**[1,2]
[1]ZWE FRM-II, TU München
[2]Physik Department E13, TU München

On 9th of march 2004, already 7 days after the startup of the FRM-II reactor, some of the basic functional elements of the time–of–flight spectrometer TOFTOF could be tested at a reactor power of 15 kW. With these first neutrons we could demonstrate that the efficiency of the shielding of the spectrometer is in full agreement with our expectations. All of the 605 detectors counted for the first time neutrons generated by the reactor.

Some more beam time was necessary to adjust and optimize the hard– and software of the chopper system; but finally the neutrons
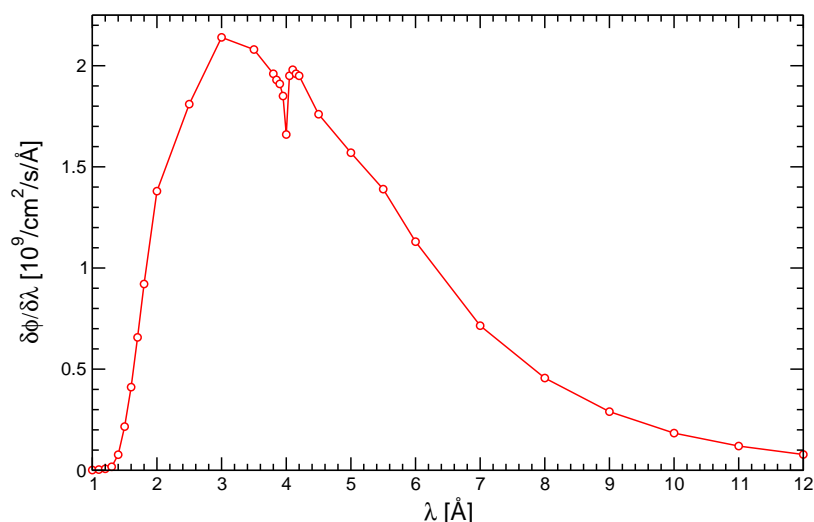

Figure 3.9: Differential neutron flux at sample position of the TOFTOF spectrometer (beam cross section: 23 mm × 46 mm, integrated flux: $1 \cdot 10^{10}$ n/cm^2/s)

found their way through the numerous slits of the 7 chopper discs, and the start signal for the time–of–flight electronics is now reliably generated. For the first commissioning steps roughly 4 days at 15 kW, 2 days at 200 kW, 0.5 days at 300 kW, 2 days at 19 MW and 17 days at (full) 20 MW reactor power could be used.

In Figure 3.9 the spectrum of the white neutron flux at the sample position of the TOFTOF spectrometer is illustrated. The measurement was performed using the TOFTOF primary spectrometer. Each wavelength was selected using the chopper system. The maximum peak flux, measured with a calibrated monitor (fission chamber) was used to calculate the distinct data points. The integrated flux (with respect to the neutron energy) agrees well with the results of gold foil activation measurements, which yielded $1.16 \cdot 10^{10}$ n/cm^2/s. The activation measurements were performed at the sample position at 300 kW reactor power and linearly extrapolated to a reactor power of 20 MW. According to the good alignment of the whole neutron guide not only the high neutron flux but also a very homogeneous beam profile could be achieved as it is displayed in Figure 3.10.

The sample chamber has been prepared to integrate standard sample environments as e.g. a cryostat and an oven. An xyz-table in combination with horizontal rotation and two partial Euler cradles are available to position miscellaneous sample environments in the beam. This sample goniometer was used in conjunction with a laser distometer to determine the sample–detector distances for each detector, which is necessary for the final alignment of the detectors. This distance measurement is fully automated and integrated into the overall TOFTOF instrument control system NICOS. Also most of the components of the spectrometer are now integrated into this software including the chopper system, safety system (shutter control), complete detector electronics and all motor drives.

Before the comissioning of the spectrometer can be continued in 2005, some of the Cd–shieldings between the detectors and the large Al–foil of the flight chamber must be installed. Subsequently all components of the spectrometer are ready for use and first measurements with the completed instrument will be performed.
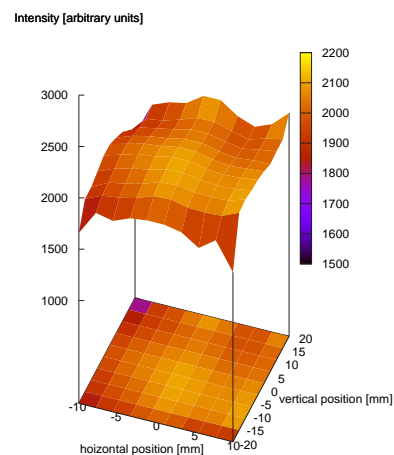

Figure 3.10: Profile of the primary beam of the TOFTOF Spectrometer at the end of the neutron guide for 1.8Å neutrons.

3.6 First Results from the TRISP Spectrometer –
Magnon Linewidths in MnF_2

S. Bayrakci[1], **K. Buchner**[1,2], **K. Habicht**[3], **T. Keller**[1,2], **B. Keimer**[1], **M. Ohl**[1]
[1]Max-Planck-Institute for Solid State Research, Stuttgart, Germany
[2]ZWE FRM-II, TU München, Germany
[3]BENSC, Hahn-Meitner-Institute, Berlin, Germany

Figure 3.11: The TRISP spectrometer [1] at the FRM-II is operational. In a first study, of magnon linewidths in the antiferromagnet MnF_2, an energy resolution as low as $1 \mu eV$ was obtained. The polarized neutron flux of $4 \times 10^7 \mathrm{cm}^{-2}\mathrm{s}^{-1}$ at the sample (at $k_i = 3 Å^{-1}$) is competitive with the best polarized TAS instruments [2]. The background is very low (1 count per 10 min).

An extensive theoretical literature developed over several decades [3] treats the energy renormalization and lifetime of spin waves in Heisenberg antiferromagnets. However, outside narrow regions of temperature and wavevector, such results have remained untestable by any technique. In the case of conventional inelastic neutron scattering (INS) experiments, the restriction results from limitations of the instrumental resolution.

In MnF_2, one of the most intensively studied antiferromagnets, the magnon linewidth Γ has been investigated in the critical region: therein is the linewidth sufficiently broad that INS measurements are

not resolution-limited. An INS study [4] of the low-temperature damping in the nearly isotropic antiferromagnet $RbMnF_3$ found partial agreement with theory [3]. However, the extracted linewidths were in many cases significantly smaller than the instrumental resolution.

In this experiment, we used the NRSE-TAS technique to measure the magnon linewidth in MnF_2 over a broad range of temperatures. The TRIPS spectrometer incorporates both the triple-axis (TAS) and the neutron resonance spin echo (NRSE) components. The associated method of *spin echo phonon focusing* [5] exploits the excellent resolution of the spin echo technique over the entire Brillouin zone, thus

permitting accurate measurement of the linewidths of narrow dispersive excitations. NRSE-TAS instruments are uniquely suited to such investigations.

During the construction phase of the FRM-II, a first experiment was conducted using the NRSE option on the TAS V2 at the HMI, Berlin. As this spectrometer is located on a cold neutron guide, the experiment was limited to small magnon energies and wavevectors ($q \le 0.2$ r.l.u.). After the startup of the FRM-II, we repeated the experiment on TRISP, using the same crystal and a comparable spectrometer configuration.

Our sample was a half-cylindrical crystal $8.5 \mathrm{cm}^3$ in volume, mounted in the *ac*-plane. We investigated magnons with $|q|$ ranging from $0 - 0.5$ r.l.u., at temperatures between 4 and $60 K$ ($0.06 - 0.9 T_N$). We focused on magnons propagating along q_c in the antiferromagnetic Brillouin zone centered at (100), as no losses of beam polarisation due to spin-flip processes during scattering occur in this configuration.

Precise measurements of the magnon dispersion are needed in order to set the tilt angles and the frequencies of the radio-frequency (RF) coils in the NRSE spectrometer arms for proper *focusing* of the magnon. The magnon energies could be measured conveniently during the experiment, as the TRIPS instrument can also be used in TAS mode while the NRSE portion of the
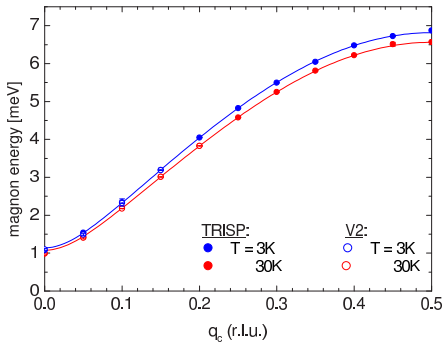
Figure 3.12: Magnon dispersion in MnF_2 along (00l) at 3K and 30K, measured at (100). Data from both TRISP (solid circles) and V2-NRSE (open circles) is shown. The solid lines are fits of the TRISP data to the spin-wave theory cited in the text. The V2 data is limited to $q \le 0.2$ r.l.u.

spectrometer is in place, with the RF coils switched off. Magnon dispersion data taken on TRISP is shown in Fig. 3.12. Counting times were as low as 17 seconds per point in the triple-axis scans, for $k_f = 1.7\text{Å}^{-1}$. For comparison, dispersion data taken on V2-NRSE is also shown; there is good agreement between the two data sets. The data was fitted to an analytical expression for the dispersion from spin-wave theory [6]. Since this expression fits the data well, the slope of the dispersion at a given point could be calculated analytically. The corresponding coil tilt angles in the first and second spectrometer arms
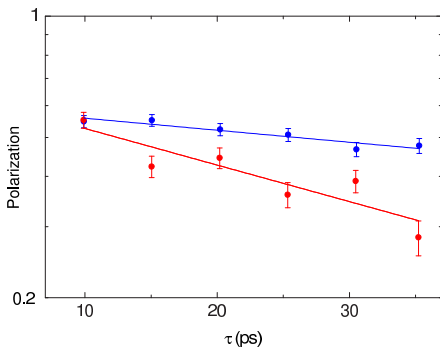
were as large as ($\theta_1 = -29.3°$, $\theta_2 = +9.85°$, for $q_c = 0.2$r.l.u.).

In the NRSE-TAS technique, the polarization of the scattered neutrons is measured as a function of the spin-echo time τ [7]. This polarization is the Fourier transform of the spectral lineshape. The observed polarizations decay as $P(\tau) = \exp(-\Gamma \cdot \tau)$, which corresponds to a *Lorentzian* lineshape. From a fit to such a polarization, we obtain the linewidth Γ. Sample data taken at TRISP is shown in Fig. 3.13.

Selected raw linewidth data is shown in Fig. 3.14. For a given value of q, the data exhibits an monotonic increase in linewidth with increasing temperature. Also included in the Figure is earlier data taken on the V2-NRSE. Agreement between corresponding points in the two data sets is good. At low temperature and small q, we observe instrumental broadening of the linewidths, which arises from the curvature of the dispersion and the finite momentum resolution. These instrumental effects were corrected using an analytical resolution function [8]. The corrected TRISP data are shown in Fig. 3.15. A continuation experiment is planned for the purpose of detailed comparison of a denser data set with available theoretical results.
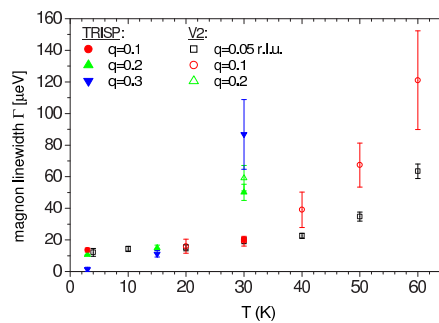

Figure 3.15: Magnon linewidths along (00l) in MnF_2 as a function of q, at various temperatures. The data have been corrected for the instrumental resolution. All of the data were taken on TRISP.

[1] "TRIple axis SPin echo", renamed from "NRSE-TAS".

[2] The ILL Yellow Book.

[3] Harris, A., Kumar, D., Halperin, B., Hohenberg, P. *Phys. Rev. B*, 3, (1971), 961.

[4] Windsor, C., Saunderson, D., Schedler, E. *Phys. Rev. Lett.*, 37, (1976), 855.

[5] Mezei, F. *Inelastic Neutron Scattering* (IAEA, **1978**).

[6] Okazaki, A., Turberfield, K., Stevenson, R. *Phys. Lett.*, 8, (1964), 9.

[7] Habicht, K., Golub, R., Mezei, F., Keimer, B., Keller, T. *Phys. Rev. B*, 69, (2004), 104301.

[8] Habicht, K., Keller, T., Golub, R. *J. Appl. Cryst.*, 36, (2003), 1307.

Figure 3.13: Raw polarization data taken on TRISP with $q = 0.3$r.l.u., at $T = 3K$ (blue) and 15K (red), as a function of the spin-echo time τ. The corresponding difference in linewidth is 9μeV.

Figure 3.14: Experimentally determined magnon linewidths in MnF_2 along (00l) at various values of q, as a function of temperature. Raw data from both TRISP (solid circles) and V2-NRSE (open circles) are shown.
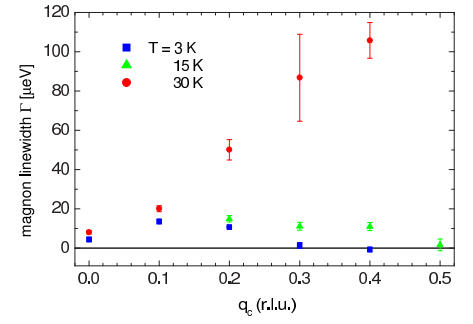
4 Fundamental Physics

4.1 MAFF — Munich Accelerator for Fission Fragments

D. Habs[1,3], **R. Krücken**[2,3], **M. Groß**[1,3], **W. Assmann**[1,3], **L. Beck**[1,3], **T. Faestermann**[2,3], **R. Großmann**[1,3], **S. Heinz**[1,3], **Ph. Jüttner**[4], **O. Kester**[1,3], **H.-J. Maier**[1,3], **P. Maier-Komor**[2,3], **F. Nebel**[2,3], **M. Schumann**[1,3], **J. Szerypo**[1,3], **P. G. Thirolf**[1,3], **F.-L. Tralmer**[4], **E. Zech**[2,3]

[1]Ludwig-Maximilians-Universität, Garching
[2]E12, Physik-Department, TU München
[3]Maier-Leibnitz-Labor f. Kern- und Teilchenphysik, Garching
[4]ZWE FRM-II, TU München

The **M**unich **A**ccelerator for **F**ission **F**ragments (MAFF) is a reactor-based Radioactive Ion Beam (RIB) facility which is being planned and set-up at the FRM-II mainly by the group for experimental nuclear physics (Prof. Habs, LMU) and the physics department E12 (Prof. Krücken, TUM).

The goal of this installation is the production of very intense beams of neutron-rich isotopes that will be available for a broad range of nuclear physics experiments as well as applied physics and nuclear medicine [1, 2, 3]. In a first step the beam will have an energy of 30 keV (low-energy beam). In a second step also a high-energy beamline will be set up where the ions are post-accelerated to energies adjustable in the range 3.7–5.9 MeV/u.

Authorisation procedure

A first tender has been filed by the TÜV Süd for the MAFF authorisation procedure that required further negotiations which are finally coming to an end now. A crucial issue concerning the cost of this procedure and of the MAFF system is the distribution of radioactivity within the system which has therefore been evaluated by two different methods:

Distribution of radioactivity in the MAFF system

Time-independent method

The target/ion source unit of MAFF releases the great majority (98 %) of radioactive nuclides in a non-ionised state. About 30 % are emitted in gaseous form (mostly noble gases) the rest non-gaseous. The gas particles undergoing multiple reflections from the beamline walls, have an opportunity to spread along the MAFF beamline much further than the others which will usually stick to the beamline surface at a point where they make first contact after having been emitted. The distribution of the non-ionised radioactivity along the beamline is important from both experimental and radiation safety points of view. In order to get a good estimate, Monte Carlo computer simulations were performed with the help of the commercial code MOVAK3D[4]. The calculated fraction of non-ionised gaseous radioactivity close to the experimental area is at the level of $\sim 10^{-7}$ of the activity produced in the target. The non-gaseous activity remains within the reactor beamtube.

Time-dependent radioactivity distribution

Also for the time-dependent calculation a Monte-Carlo approach is used to predict the surface coating of the beam line for all radionuclides. Here the surface areas are used as measure for the probability that they are hit by a particle. The program is completely time-dependent to implement radioactive decay. As a result the surface coating for all radionuclides within the beamline is obtained.

For a test geometry without time-evolution both codes produced the same results within a factor of two.

Ions are transported electrostatically towards the mass-separator, with a complex slit system in the focal plane. All unwanted ions are stopped at the slits, resulting in a high level of radioactive contamination. Material corrosion caused by sputtering will release previously implanted radionuclides. To reduce this effect, the slit geometry can be modified. So far a flat structure has been compared to a wedge shaped structure, both of them enclosed in

a box with a small opening to reduce the solid angle. The wedge structure leads to a 14 % reduction in sputter yield resulting in a total sputter yield of 0.1 for beam particles.

The vacuum system of MAFF

The vacuum system encloses the extremely radioactive target/ion source with a fission product activity of several 10^{14} Bq after one reactor cycle of 52 days. Approximately 20 % of the load of 1 g highly enriched ^{235}U are burnt in one cycle. If all emitted fission products were solid material, about 35 g would be deposited on all walls of the vacuum system during the design lifetime of 30 years. This will not pose a storage problem to the high-vacuum system, and since the vapour pressure of solid material is too low to transport the solid fission products into the vacuum pumps, they will remain at the walls of first deposition if the vacuum is better than 10^{-3} Pa. Even volatile elements like iodine or bromine would be trapped in the condensed film due to chemosorption because a fission product is always a single ion or an atom.

18 refrigerator cryopumps will be installed as high-vacuum pumps, only 9 of them required, the second set is for redundancy. They are a slightly modified model COOLVAC 800 (CF) from Leybold. As all-metal gate valves and metal seals will be used, the radiation hardness of 10^7 Gy is not spoiled by destruction of elastomeric sealings and no leakage due to age-hardening of the gaskets may occur.

About 30 % of the created fission products are noble gases. If they were stable and would not decay to low-vapour pressure elements after short half-lives, about 4500 Pa·l

gas must be pumped mainly by the two cryopanels. A smaller amount and the rest of the released gas from the cryopanels during their regeneration is pumped by the refrigerator cryopumps. The part of gases which did not decay is then transported into decay tanks during warm-up and regeneration of the cryopumps.

15 dry roughing pumps (some for redundancy) are applied for roughing and regeneration purposes. The ACP 28 from adixen (Alcatel subsidiary) has been chosen due to its small leak rate of $5 \cdot 10^{-5}$ Pa·l·s^{-1} and the capability to work below atmospheric pressure. This is a must to prevent radioactivity from escaping into the experimental hall in case of leaks.

The radioactive gases from the decay tanks can be released into the FRM-II exhaust gas system, but even small amounts of aerosols must be avoided. Therefore the gases from the decay tank will be transferred into a second tank via a slow diffusion filter which is under development. Aerosols should not pass this type of filter.

It would be very expensive to design all components of the vacuum system for over-pressure situations which might occur if one of the cryopanels or a cold finger from a cryopump leaks. Therefore the volume of the beam tube unit will be enlarged by adding a 1000 l ballast tank.

Development of components

The in-pile ion source

A prototype of the in-pile ion source of MAFF is currently developed and constructed (see fig. 4.1). An ion source for surface ionisation mode is designed and being built. The surface ionisation source provides ion-
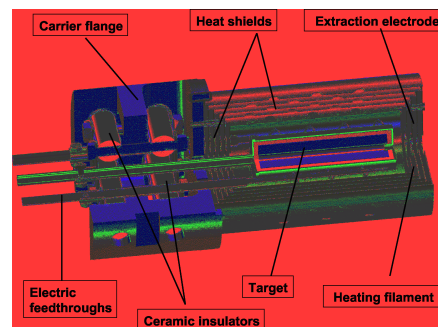

Figure 4.1: Construction of the MAFF target/ion source.

isation efficiencies of nearly 100 % for alkaline metals. This prototype will consist of reactor suitable materials. The MAFF target/ion source has to withstand a maximum thermal neutron flux of $1.5 \cdot 10^{14}$ n/(cm^2 s) and is located at ~ 50 cm distance to the reactor core inside the through-going zircaloy beam tube. The ion extraction system has been redesigned with the computer code IGUN using one electrode formed by the heat shield. The first prototype of the target/ion source [5] has used a two-electrode extraction system. That prototype has shown that a new construction is required in order to protect the ceramic insulators from metal and carbon vapour from the target and the heat shields.

Much effort was spent on the development of appropriate UC$_x$ targets. The target will be externally heated with a tungsten filament by electron bombardment and thus kept at a temperature of about 2400° C, which provides rapid effusion of the fission products into the target channel. The target is veiled with a cylinder of vitreous carbon and a protecting rhenium container at which outlet the surface ionisation takes place. Re has been chosen because it is most inert against C and U at high temperatures, has a high melting point (3180° C) and

can best withstand the high neutron flux.

Several heat shields are supposed to confine the high temperature in the center of the source. Although Re has the disadvantage of a rather high neutron capture cross section it will be used for the two inner-most heat shields due to its thermal strength and short half-life of acti-vation. The other heat shields and the screws will consist of Mo while the ceramic insulators will be made of BeO, which can withstand higher temperatures than Al_2O_3. All parts of the ion source have been ordered and the assembly and operation of the source on the test bench is fore-seen in 2005.

Lens trolley prototype development

The design of the lens trolley and the support structure has progressed and construction of the prototype has started. It will consist of the source trolley's main body, the ad-justment mechanics, drives and the support frame. During design and construction common TÜV require-ments were kept in mind so that some parts of the prototype might be used also for MAFF.

The aim of the prototype is test-ing of certain crucial issues like the adjustment and movement of the trolley and the functionality of the drives.

Commissioning of the cryopanel prototype

Close to the fission source on ei-ther side of the MAFF beamtube, a cryopanel will prevent the migration and spreading of unwanted volatile radioactivity in the beamline system by localising gaseous radioactivity on surfaces cooled down to about 12 K. Being the central element of the radioprotection and safety sys-tem for MAFF, an extensive test pro-gramme is needed to verify the de-sign specifications and to charac-terise the performance of the cry-opanel. Therefore a prototype has been built, consisting of a double-walled tube where cold Helium gas (inlet temperature 12 K) will flow through. It has been mounted in the MAFF test beamline at the MLL which reflects the exact geometrical properties of the innermost part of the MAFF beamtube at the FRM-II.

The cryopanel was connected to a helium refrigerator with a cooling power of 150 W at 4 K, which for the cryopanel tests will be operated at a temperature of 12 K. Therefore a 10 m long vacuum-isolated transfer line for in- and outlet of the cold gas was installed between the refrigera-tor and the test beamline.

In a first commissioning test the cryopanel was cooled down to 12 K. Successful operation could be demonstrated by the improvement of the vacuum pressure from ini-tially $4 \cdot 10^{-7}$ mbar to $2 \cdot 10^{-8}$ mbar in cold state.

The next step will be the installa-tion of temperature sensors to study the thermal profile along the cry-opanel as well as measurements of the pumping capacity and retention capabilities for gaseous elements.

MLL-Trap

A Penning trap system similar to REXTRAP at ISOLDE (CERN) or JYFLTRAP at Jyväskylä is being set up at the MLL to measure nu-clear masses with high precision and/or to do nuclear spectroscopy at trapped ions. The superconduct-ing magnet has been delivered and shimmed to an inhomogeneity of $\Delta B/B \leq 0.3$ ppm. The trap system will first be used at the MLL and can later be moved to MAFF.

[1] Habs, D., *et al.* MAFF — Physics Case and Technical Descrip-tion. http://www.ha.physik.uni-muenchen.de/maff/.

[2] Habs, D., *et al. Proc. EMIS-14, Nucl. Instr. Meth. B*, 204, (2003), 739–745.

[3] Faestermann, T., *et al. Nucl. Phys. A*, 746, (2004), 22c–26c.

[4] Class, G. Report 4292. Techni-cal report, Inst. IRS, KFZ Karlsruhe GmbH (**1987**).

[5] Ospald, F. *Aufbau und Test eines Ionenquellen-Prototypen für den Münchner Spaltfragmentbeschleu-niger (MAFF)*. Master's thesis, LMU München (**January 2003**).
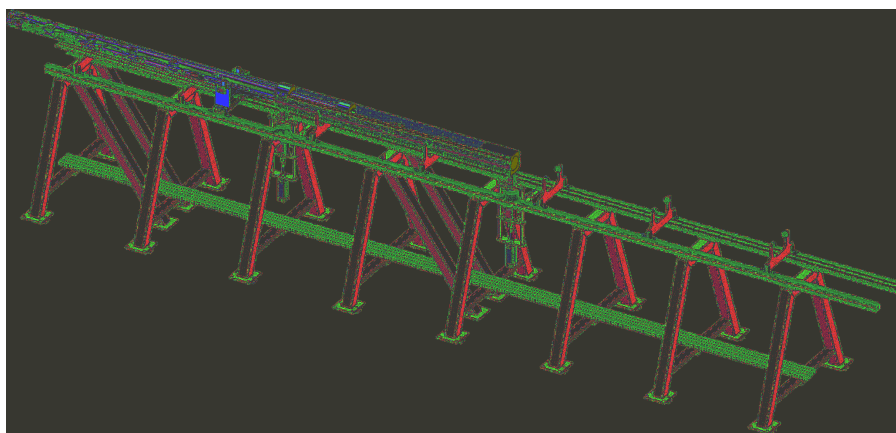
Figure 4.2: The lens trolley test setup.

4.2 The Positron Beam Facility NEPOMUC and its Instrumentation

Christoph Hugenschmidt[1,2], **Reinhard Repper**[2], **Benno Straßer**[2], **Martin Stadlbauer**[1], **Klaus Schreckenbach**[1,2]
[1]E21, Physik-Department, TU München
[2]ZWE FRM-II, TU München

In summer 2004 the in-pile positron source NEPOMUC of the new Munich research reactor FRM II was set into operation at the nominal reactor power of 20 MW. The largest section of the positron beam facility was completed and extended by an additional beam switch in order to connect two spectrometers for positron experiments: positron annihilation induced Auger electron spectroscopy (PAES) [1] and coincident Doppler-broadening spectroscopy (CDB) [2].

NEPOMUC – Neutron Induced Positron Source Munich and the beam facility

The moderated positrons are accelerated to an energy between a few eV and 1 keV by electrical lenses. In the beam tube SR 11 the positron beam is magnetically guided in a solenoid field of typically 7 mT to the experimental platform. An overview of the positron beam facility is given in figure 4.3. The beam line consists of stainless steel vacuum tubes, computer controlled valves and pumping units as well as magnetic field coils. Straight sections are μ-metal shielded and correction coils are mounted at the bent parts of the beam line in order to adjust the positron beam and to minimize transport loss.

NEPOMUC's Instrumentation

In the present arrangement of NEPOMUC's instrumentation the monoenergetic positron beam is magnetically guided to a CDB facility and to a PAES analysis chamber. These facilities were constructed in the lab of E21 and transferred to the reactor in 2004. It is planned to use an additional open beam port for fundamental research with the high intense positron beam. In 2005 it is planned to install an apparatus for the production of the negatively charged positronium (Ps$^-$), which is presently operated at the Max-Planck-Institute for nuclear physics [3]. Two positron lifetime experiments (PLEPS and SPM) will be transferred from the Universität der Bundeswehr to the reactor in the beginning of 2005 [4].

First Positrons at NEPOMUC !

The intense positron source NEPOMUC is based on absorption of high-energy prompt γ-rays from thermal neutron capture in ^{113}Cd [4]. For this purpose, a cadmium cap is placed inside the tip of the inclined beam tube SR 11 in the heavy water moderator tank (see figure 4.4). Inside the cadmium cap a structure of platinum foils is mounted in order to convert the high-energy γ-radiation into positron-electron pairs. Due to the negative positron work function, moderation in annealed platinum
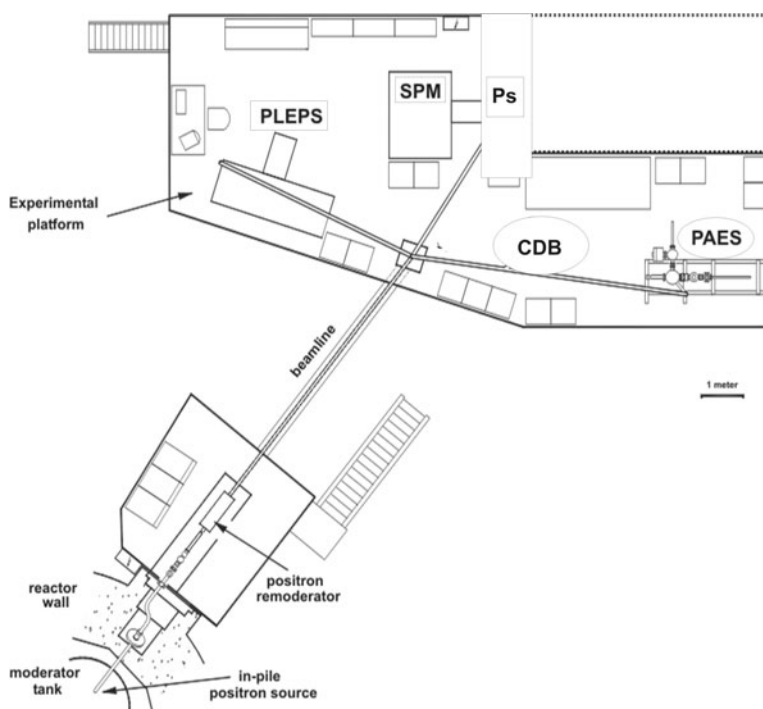

Figure 4.3: Overview of the positron beam facility NEPOMUC. First installed experiments are a CDB spectrometer and a PAES analysis chamber, which are built and operated by E21/TUM. The positron lifetime experiments PLEPS and SPM (Universität der Bundeswehr, München) as well as the (Ps$^-$)-apparatus (MPI for nuclear physics, Heidelberg) will be transferred to the reactor in 2005
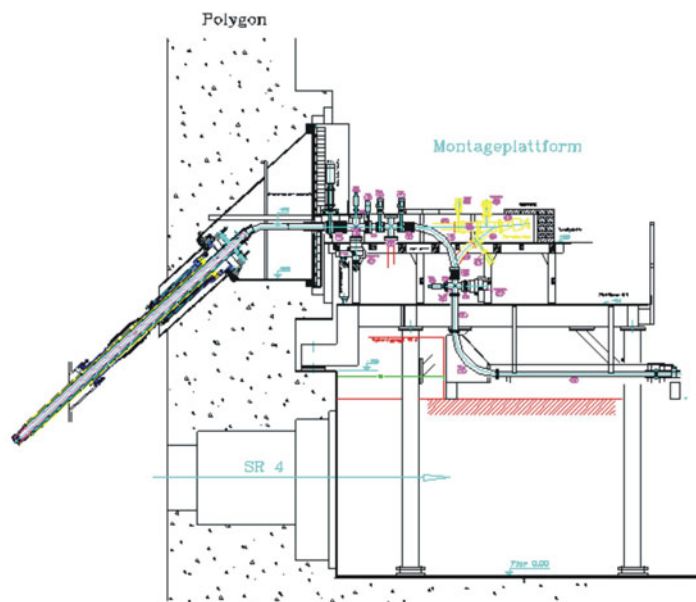
Figure 4.4: Cross sectional view of the inclined beamtube SR 11: The in-pile positron source is mounted inside the tip. After acceleration the positron beam is magnetically guided to the platform outside the biological shield of the reactor.

leads to emission of monoenergetic positrons.

After acceleration to an energy between a few eV and 1 keV by electrical lenses the positron beam is magnetically guided in a solenoid field of typically 7 mT. The beam passes three bents in the biological shield of the reactor in order to eliminate background of fast neutrons and γ-radiation.

Beam Diagnostic Instruments

Intensity and positron beam profile measurements were performed at the first accessible position outside the biological shield. A movable aluminium plate and an aperture were mounted inside the vacuum beamline in order to vary the beam profile. NaI-scintillators were positioned perpendicular to the movable Al-plate. Hence, the beam intensity could be determined by the detection of the 511 keV γ-radiation of positrons that annihilate at the

aluminium plate, which acts as positron target when it is positioned in the beam line.

The beam profile is determined with a micro channel plate (MCP) detector and a CCD-camera. Elec-

trons were repelled by a negative voltage at the MCP-entrance in order to obtain an almost background free signal of positrons hitting the MCP-detector.

Positron Intensity and Beam Profile Measurements

In April 2004 first positrons were detected at low reactor power of 15 kW. Hence, beam parameters such as magnetic solenoid and correction fields as well as acceleration voltages could be optimized. Figure 4.5 shows the raw data of the detected γ-radiation. The photopeak and Compton events due to the 511 keV annihilation radiation are clearly visible. The background accords to a measurement without magnetic guiding field, which was expected to be very low due to the massive heavy concrete shield around the beam tube.

In summer 2004 intensity measurements were performed at the nominal reactor power of 20 MW. Due to limitations of the ap-
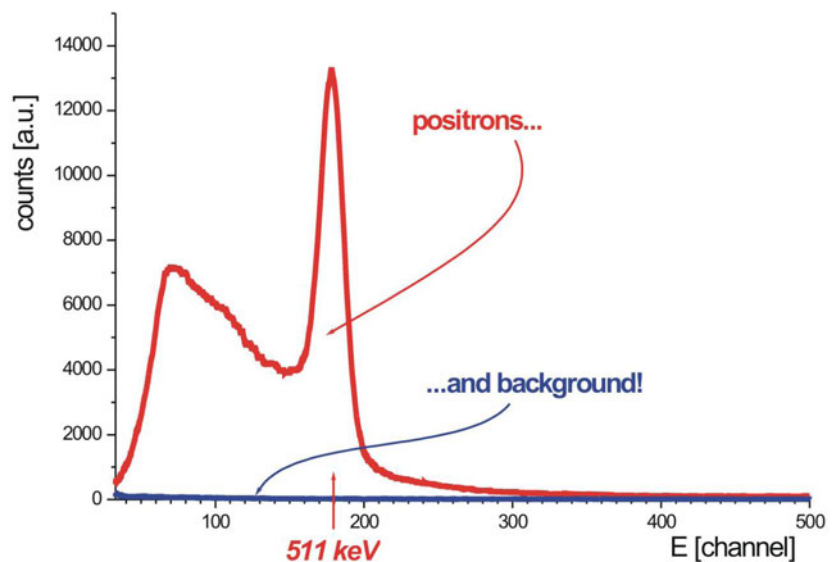

Figure 4.5: Detection of positrons: Photopeak and Compton events due to the 511 keV annihilation radiation.
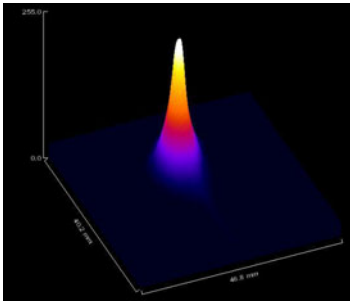
Figure 4.6: Intensity profile of the monoenergetic positron beam at 1 keV and a longitudinal magnetic field of 6 mT. The beam diameter amounts to about 7 mm.

plied voltage the maximum primary beam energy was set to 1 keV, which perfectly fits the Coincident Doppler broadening experiment (see [2]). The highest measured intensity was about 10^8 moderated positrons per second.

The intensity profile of the monoenergetic positron beam at 1 keV was recorded in a longitudinal magnetic field of 6 mT with the MCP-detector. The beam shows a slightly elliptical contour with an estimated diameter of about 6-8 mm (see figure 4.6).

In another experiment the positron beam was extracted at much lower energy of 30 eV in order to accomplish the requirements of the PAES (Positron annihilation induced Auger-electron spectroscopy) facility [5]. For both energies, 30 eV as well as 1 keV, the positron beam was guided to the instruments on the experimental platform.

[1] Hugenschmidt, C., Straßer, B., Schreckenbach, K.   *Radiat. Phys. Chem.*, 68, (2003), 627–629.

[2] Stadlbauer, M.   *Aufbau eines ortsauflösenden Doppler-Koinzidenzspektrometers zur Untersuchung der Positronenzerstrahlung.*   Diplomarbeit, TU München (**2004**).

[3] Schwalm, D., Fleischer, F., Lestinsky, M., Degreif, K., Gwinner, G., Liechtenstein, V., Plenge, F., Scheit, H. *Nucl. Instr. Meth. B*, 221, (2004), 185–194.

[4] Hugenschmidt, C., Kögel, G., Repper, R., Schreckenbach, K., Sperr, P., Straßer, B., Triftshäuser, W. *Nucl. Instr. Meth. B*, 221, (2004), 160–164.

[5] Straßer, B., Hugenschmidt, C., Schreckenbach, K. *Mat. Sci. For.*, 363-365, (2001), 686–688.

4.3 Development of a Coincident Doppler Spectrometer with Spacial Resolution at the Intense Positron Source NEPOMUC

Martin Stadlbauer [1], **Christoph Hugenschmidt** [1,2], **Klaus Schreckenbach** [1,2]
[1]E21, Physik-Department, TU München
[2]ZWE FRM-II, TU München

A CDB-spectrometer was developed in order to enable elemental specific defect spectroscopy by positron annihilation in matter. If a positron is implanted into a metallic sample it thermalizes within picoseconds. After diffusion through hundreds of lattice constants, it annihilates with an electron in the sample into 2 γ-Quanta with energies of 511 keV. Due to the electron momenta the emitted γ-radiation is Doppler shifted. The Doppler shift decreases, if the positron is trapped at a defect due to the lower annihilation probability with core electrons which have high momenta. Hence defects can be studied by measuring the Doppler-broadened 511 keV annihilation line [1]. Moreover, the accurate measurement of high Doppler shifts, i.e. high electron momenta, reveals chemical info at the annihilation site [2]. Our new Doppler spectrometer with two facing germanium detectors allows to focus the positron beam NEPOMUC and to position the sample in vacuum in order to measure Doppler spectra with spacial resolution of about 2 mm.

Experimental Setup

The positron beam is guided in an evacuated tube along a longitudinal magnetic guiding field. The intensity as well as the diameter of the beam is determined by a 2 mm aperture. In order to vary the penetration depth of the positrons, the sample potential can be chosen between 0 and -20 kV. Consequently there exists an electric field in the vacuum chamber which would disturb magnetic focussing. For this reason the magnetic field of the beam tube is screened by μ-metal and the positrons are nonadiabatically released from the guiding field by a magnetic field terminator. An electric focussing unit consisting of an Einzel lens forms the positron beam and reduces it to a diameter of about 2 mm.

The spacial resolution is achieved by positioning the sample   in the
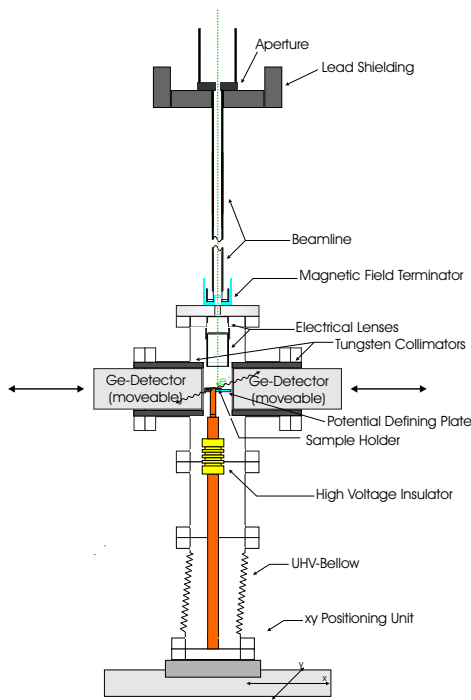
Figure 4.7: Scheme of the CDB experiment.

positron beam crosses the border between aluminium and tungsten. These measurements show, that the beam consists of an intense centre of about 2 mm diameter which is surrounded by a bigger halo, what was ascertained by the comparison with a theoretically supposed homogeneous beam.

The next measurement was performed with a thermally treated brass sample. It was heated on one end to about 800 K and cooled on the other side. The achieved spectra of four different positions on the sample were normalized to annealed zinc and compared with pure copper. As figure 4.8 shows, the curves of copper and zinc differ strongly in the region of high Doppler shift, i.e. E > 513 keV, as a consequence of the different electron momentum distribution in both materials. The four curves of the brass sample are approaching the copper curve as the position of the positron beam reaches the heated side of the sample.
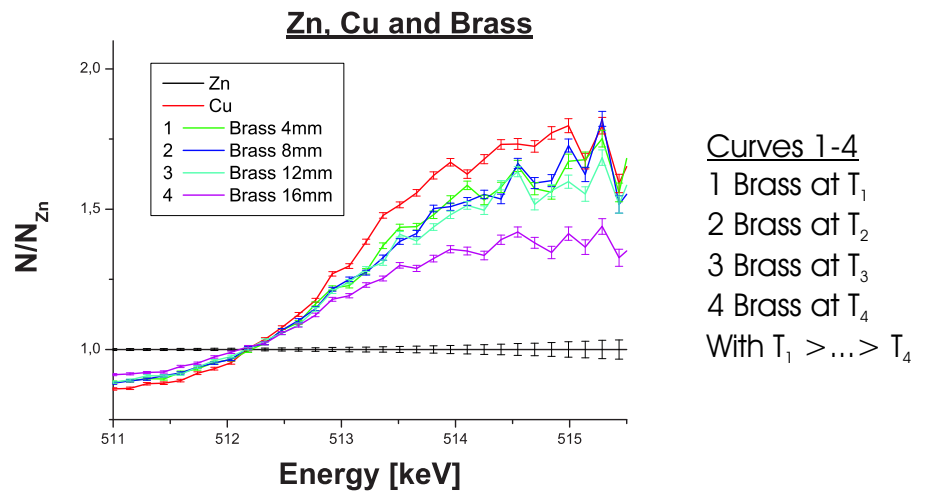
One possible reason for this behaviour is the decrease of the zinc concentration in heated brass due to the low vapour pressure of zinc. In addition the observed behaviour may also be a consequence of a partially annealing during the heating process which would lead to different defect densities.

Further measurements will be performed in order to investigate the contribution of varying defect concentrations.

[1] Schulz, P., Lynn, K. *Rev. Mod. Phys.*, 60, (1988), 701–773.

[2] Asoka-Kumar, P., Alatalo, M., Ghosh, V. J., Krusemann, A. C., Nielsen, B., Lynn, K. G. *Phys. Rev. Let.,* 77, (1996), 2097–2100.

vacuum chamber perpendicular to the beam direction. The translation of the sample holder is accomplished with a stepper motor controlled positioning unit. Figure 4.7 shows a cross sectional view of the sample chamber.

First Measurements

In order to measure the diameter of the positron beam, a sample was prepared which consists of tungsten stripes glued on aluminium. Since the electron momenta of aluminium and tungsten are different, the shape of the annihilation line of both materials is unequal. Hence, the varying broadness of the annihilation line reveals the beam structure, when the sample position is varied and the

Figure 4.8: Annihilation spectra of pure copper, zinc and thermally treated brass.

4.4 A solid Deuterium UCN Source at the TRIGA Mainz

S. Paul[1], **W. Heil**[2], **J.V. Kratz**[3], **E. Gutsmiedl**[1], **I. Altarev**[1], **A. Frei**[1], **J. Hartmann**[1], **W. Schmid**[1], **Y. Sobolev**[2],
G. Hampel[3], **D. Tortorella**[1], **N. Wiehl**[3], **K. Eberhardt**[3]

[1]Physik Department E18, TU München
[2]Institut für Physik, Universität Mainz
[3]Institut für Kernchemie, Universität Mainz

A strong source for ultracold neutrons (UCN) [1] shall be built for the research reactor FRM-II. This source, called Mini-D_2, will be installed at the beam tube SR4, that is horizontally pointing directly to the already existing cold neutron source. For converting cold neutrons to UCN a solid D_2 converter with 200 cm^3 volume at a temperature of 5K is frozen out at the beginning of this beam tube, near to the cold source. The inner part of the beam tube (diameter 6 cm, length 8 m) is cooled to 30K and covered with beryllium in order to store and accumulate UCN and to bring them to different experiments. Simulations indicate, that with this setup UCN densities up to 10^4 cm^{-3} can be reached. For a test of this conversion mechanism, a smaller setup has been build and is currently operated at the pulsed TRIGA reactor in Mainz. This test setup contains all essential parts that will later be used for the FRM-II UCN-source, such as the converter, the storage tube, the D_2-gas system and the SPC-system.

The solid Deuterium UCN Source(SDUCNS) was installed at the TRIGA Mainz in late autumn 2004. First cool down tests (freezing out the deuterium gas at 5-8 K) were done successfully in December 2004.

A first measurement with neutrons from the TRIGA reactor in the pulse mode [2] was also performed in December 2004. This measurement indicated some problems with the UCN Silicon detectors, which are covered with a converter foil (Ti foil with ^{6}Li/^{62}Ni-multilayer) [3], and the data acquisition electronics.

After the disassembling of the cryostat, the UCN detector system was checked. It turned out, that the converter foil of the Si detector was broken. Also the data acquisition electronics was checked with a Si-detector and a alpha-source, and has been re-adjusted.

A new bigger UCN detector will be supplied with a new converter aluminium foil, which is covered with a pure Li6 layer. This detector will be installed outside of the cryostat, connected with a UCN guide (1.5 m – 2 m away from the cryostat), in order to reduce the thermal and epithermal neutron background.

[1] Paul, S., *et al.* In *3rd UCN Workshop, Pushkin, St. Petersburg, Russia* (**2000**).

[2] Eberhardt, K., Kronenberg, A. *Applied Science and Education, Kerntechnik.*

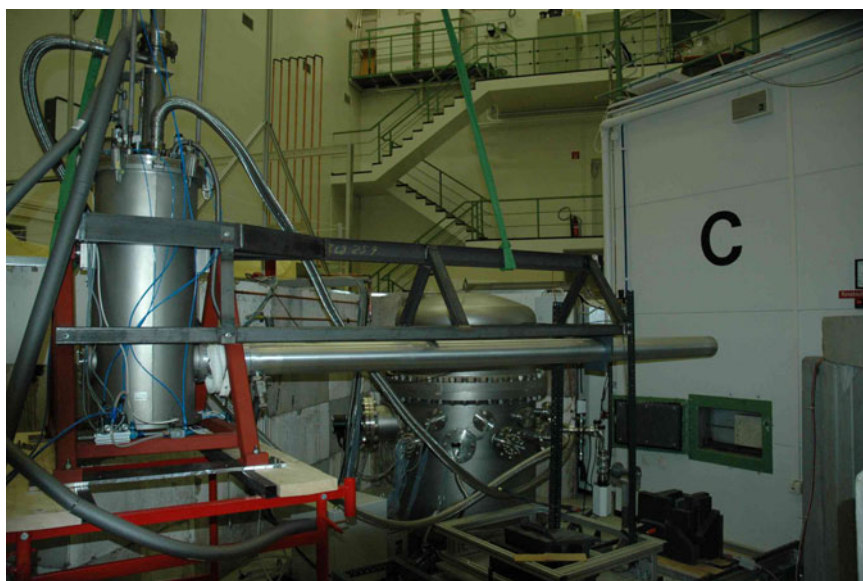[3] Petzold, G., *et al. 3rd UCN Workshop, Pushkin, St. Petersburg, Russia*, 65(5-6), (2000), 269–274.

Figure 4.9: Solid Deuterium UCN Source at the beam channel C of the TRIGA reactor Mainz

5 Radiography and Irradiation

5.1 Coded masks in neutron radiography

F. Grünauer [1]
[1]E21, Physik-Department TU München

Nearly all neutron radiography facilities use a setup similar to a single pinhole camera. With such facilities a compromise between high flux at the detector plane and high spatial resolution has to be made: High resolution can be obtained with a
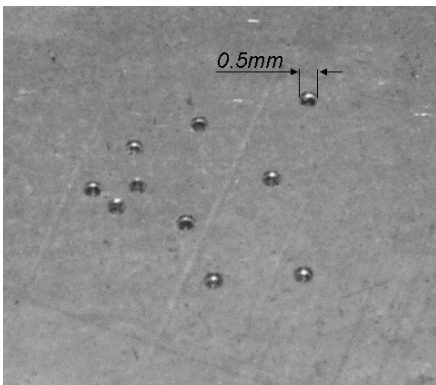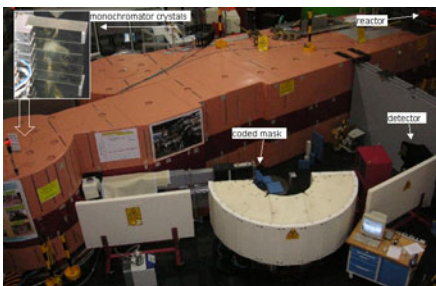

Figure 5.1: Multiple pinhole aperture

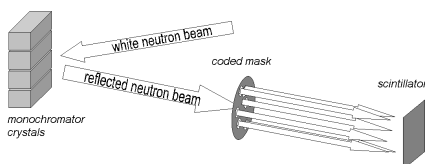Figure 5.2: Setup at the powder diffractometer SPODI

Figure 5.3: Schematic overview of the setup

small aperture diameter D and a large distance L between aperture and object. As flux at the object plane is proportional to $(D/L)^2$, high resolution needs a long exposure time and yields a poor signal to noise ratio. Low L/D ratios provide a low noise level but the resulting image is blurred. Investigations were carried out by Monte Carlo simulations whether other configurations can overcome the single pinhole dilemma. In X-ray astronomy ring shaped masks, random array masks, uniformly redundant array (URA) masks, etc. are used to overcome the problem. The simulations show, that these types of apertures are less advantageous in neutron radiography, where large and structured objects are in the focus of interest. However it could be shown, that a multiple pinhole mask with minimized autocorrelation (Fig. 5.1; non redundant array) together with an improved reconstruction algorithm, provide significant better results. This new approach with regard to neutron radiography was introduced at FRM-II. The following example shows a radiography of an arrangement of Ge-crystals (Fig 5.4). The setup is used as monochromator at the powder diffractometer SPODI.

The example shows, that the signal to noise ratio of a neutron radiography can be increased without
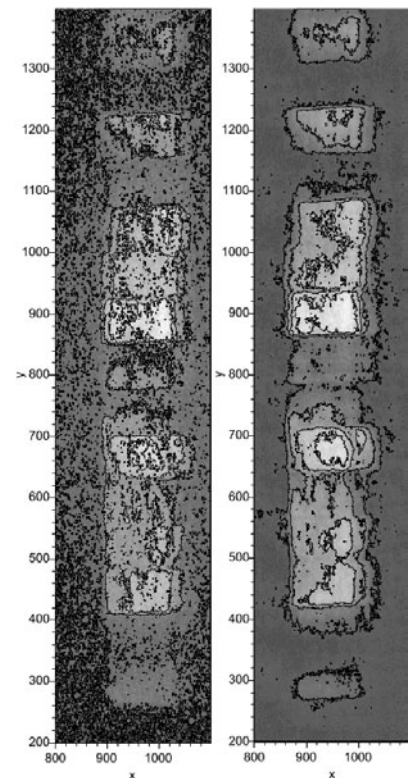

Figure 5.4: Left hand side: Projection of the monochromator crystals using a single hole aperture (hole diameter=0.5mm). Right hand side: Reconstruction of the projection obtained by the coded 10 hole aperture (hole diameter=0.5mm). In both cases the exposure time was 8280 s.

major loss of resolution (Fig. 4). This can be useful for several applications in neutron radiography, e.g. in phase contrast radiography, where the necessity of a very small aperture limits intensity, or in dynamic radiography, where exposure time is limited by the observed process.

5.2 Non-destructive testing with phase contrast radiography at ANTARES

Eberhard Lehmann[2], **Klaus Lorenz**[1], **Erich Steichele**[1], **Peter Vontobel**[2]
[1]E21, Physik-Departmentm TU München
[2]Paul-Scherrer-Institut, Villigen, Switzerland

The refractive index $n = 1 - \delta - i\beta$ of a material consists in general of a real and an imaginary part. The imaginary part causes the attenuation of the neutron beam, what is used in conventional radiographies to visualize the structure of an object. The real part leads to a phase shift φ of the neutron with regard to propagation in free space. At edges and interfaces this leads to great deviations of the wavefronts of an incoming wave. If the detector has a certain distance from the object (in the near field region), an increase in the contrast at edges and interfaces occurs [1]. This interference effect is the so called phase contrast.

Experimental setup

To get phase contrast, the radiography setup has to fulfill two basic requirements:

1. High transversal spatial coherence
   This can be realized easily with a pinhole and a large distance between the pinhole and the object.
2. Detector plane in the near field region
   The distance between sample and detector must not be to

small (else you get only absorption contrast) and it must not be too large (else you come in the fresnel region).

At ANTARES the high lateral coherence is achieved by inserting an aperture with a very small pinhole in the neutron beam. If the diameter of the pinhole is D and the distance between pinhole and sample is L, the lateral coherence length is $l_{coh} = (L/D)\lambda$, where λ is the wavelength of the neutrons. To be able to vary this parameter easily, an aperture wheel was constructed for the ANTARES facility (see fig. 5.5). With this revolver-like device, eight different apertures can be positioned quickly and precisely in the neutron beam. Besides the single pinholes with different diameters, coded apertures are used in the aperture wheel. With the help of these multi-hole apertures, the exposure time for phase contrast radiographies can be reduced.

Applications of phase contrast imaging

The enhanced contrast at edges and interfaces in phase contrast images can be very useful for the non-destructive testing of objects, especially for materials with low attenuation coefficients like aluminium.

The additional contrast at edges is only one feature of this non-interferometric technique. It also allows the measurement of the phase shift φ the neutrons experienced
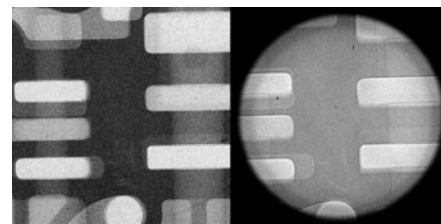

Figure 5.6: Comparison of a conventional radiography (left) and a phase contrast radiography (right) of a cast aluminum sample.

on their way through the sample. The technique to do this phase retrieval is based on the transport-of-intensity-equation (TIE) [2]. Therefore at least two phase contrast radiographies in different sample-to-detector-distances z have to be done. Out of these intensity distributions $I_z(X, Y)$ in the different detector planes, the phase shift is calculated with the TIE [3]. For this phase retrieval, the neutrons do not have to be monochromatic [4]. With this technique it becomes possible to get contrast even between materials with a similar attenuation coefficient (see fig. 5.7).

[1] Cowley. *Diffraction Physics* (Oxford University Press, **1975**).

[2] Teague, M. R. *J. Opt. Soc. Am.*, 73, (1983), 1434–1441.

[3] Allman, B. E., McMahon, P. J., Nugent, K. A., Paganin, D., Jacobson, D. L., Arif, M., Werner, S. A. *Nature*, 408, (2000), 158–159.

[4] McMahon, P. J., Allman, B. E., Jacobson, D. L., Arif, M., Werner, S. A., Nugent, K. A. *Phys. Rev. Lett.*, 91.
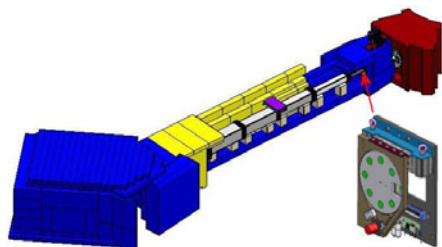
Figure 5.5: Implementation of the aperture wheel in ANTARES.

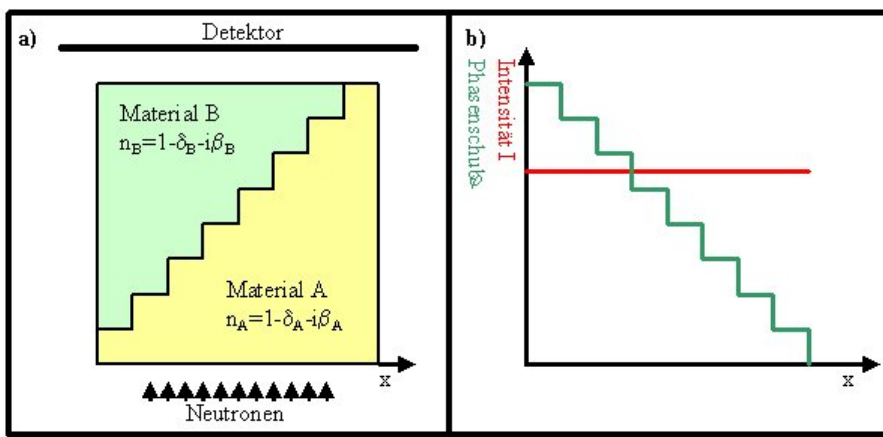Figure 5.7: An example for the application of quantitative phase contrast imaging.

5.3 NECTAR – Neutron Computer Tomography And Radiography

T. Bücherl [1], **Ch. Lierse von Gostomski** [1], **E. Calzada** [2]
[1]Institut für Radiochemie, TU München
[2]ZWE FRM-II, TU München

General

The NEutron Computer Tomography And Radiography (NECTAR) facility using fission neutrons is set up at the converter facility in the experimental hall (beam tube SR 10). It has to share the available beam time with the facility for medical application, also located at SR 10.

Activities

In 2004, only very few measuring time was available, basically used for radiation protection measurements, i.e. the determination of the gamma and neutron dose rates at the outer walls of the shielding bunker. Based on these results and the requirement that the combined gamma and neutron dose rate must be less than 5 μSv/h at the outer side of the bunker walls the beam stop was designed and is actually under construction. A control cabin housing the control unit, detector electronics and a working place was provisionally placed on the back wall of the bunker. The overhead travelling crane capable of handling up to 1000 kg was installed end of 2004. For this, the detector manipulator and storage system and parts of the object manipulator had to be removed.

First results

During the radiation protection measurements it was possible to record some first radiographs. The first object, a step wedge of 10 cm height made of polyethylene, aluminium, iron and lead with steps of 0.5 cm depth each, was placed directly in front of the detector (a scintillator screen in combination with a nitrogen cooled CCD camera). The measurement time was 1 minute per frame, 10 frames in total were measured. The resulting radiograph after normalisation and data processing is shown in figure 5.8. Figure 5.9 shows the resulting radiograph (without normalisation) of a motor.
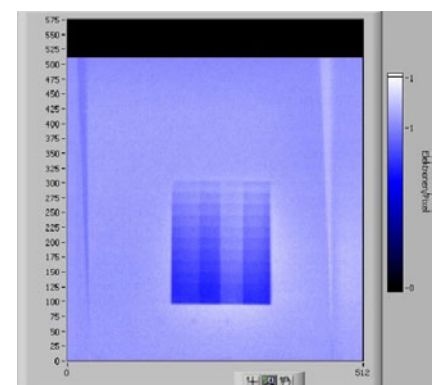
Figure 5.8: Normalized radiograph of a step wedge made of lead, iron, aluminium and polyethylene (from left to right). The height of the step wedge is 10 cm, the depth of each step 0.5 cm. The two wedges on the left and right of the image are caused by a shifted boron carbide plate that was placed in front of the scintillator screen to suppress thermal neutrons due to moderation in the material of the step wedge (basically in the polyethylene).

The measuring parameters were the same as for the step wedge.

Outlook

The rebuilding and precise adjustment of all components of the facility will be performed together with the final positioning of the control cabin. With availability of beam time the performance of the facility for fission neutron radiography and tomography will be determined. This includes the determination of the influence of beam hardening, scattering and other effects on the measuring results for different materials. Based on these results an optimisation and further improvement will be performed.
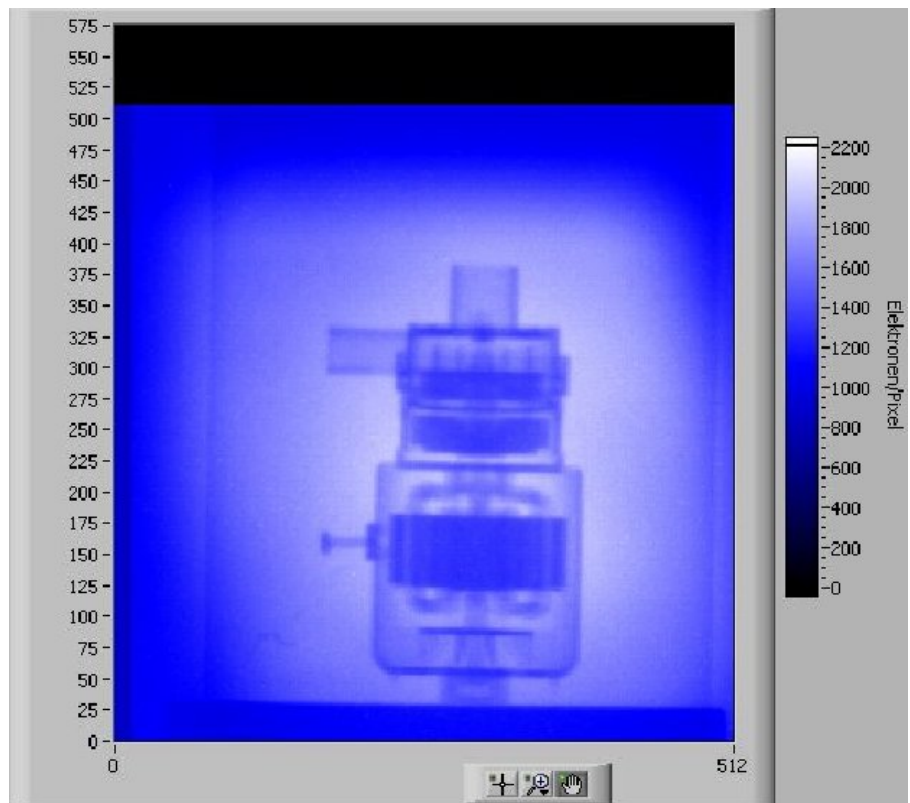

Figure 5.9: Radiograph of a motor of about 9 cm diameter and 18 cm height.

5.4 Fission Neutron Source (Converter facility)

F. M. Wagner[1], **W. Waschkowski**[1]
[1]ZWE FRM II, TU München

The thermal-to-fast neutron converter consists of two uranium plates mounted in about 1 m distance from the reactor core. The same type of fuel is used as in the reactor fuel element, i.e., 93 % enriched U-235 as uranium silicide aluminium dispersion, cladded with aluminium. The total uranium mass is 540 g. The thermal neutrons from the core induce fission processes. The generated fission neutrons reach the irradiation site without being moderated. The converter plates can be removed from the moderator tank in order to pre-serve the uranium (see Fig. 5.10) in case the facility is not in use.

In 2004, during several months, the facility has been put into operation together with the step-wise increase of the reactor power. A large number of checks have been performed, partly together with the representatives of Siemens/Framatome, and with experts from TÜV-Süd. The most important functions and parameters were the thermal power of the converter and the related thermo hydraulic properties, the influence on the reactivity of the reactor core, the neutron and gamma dose rates in the beam, the homogeneity of the beam, and radiation protection measurements within and around the irradiation rooms.

The maximum thermal power of the converter was about 83 kW. At this power, the cooling water is heated by 2.0 K only. The reactivity of the reactor is measurably changed during the movement of the converter plates, but the control rod of the reactor quickly compensates the change so that other experiments are not disturbed.

The results of the first beam measurements show that the converter facility according to the design. The

40-leaf-collimator could not yet be tested in full extent. Currently we are qualifying the facility according to German legisalation for medical apparatuses. Only after the declaration of conformity and a further special permission, the converter facility as a whole is ready for the medical application to patients with near-surface tumours. The current status allows to start with physical irradiations and measurements, e.g., radiography and dosimetry.

In December, a diploma student has started to develop a further filter and to evaluate the beam quality with scientific methods covering also the medical requirements (spectral analysis and phantom measurements). This will give the radiological basis for the treatment of patients.
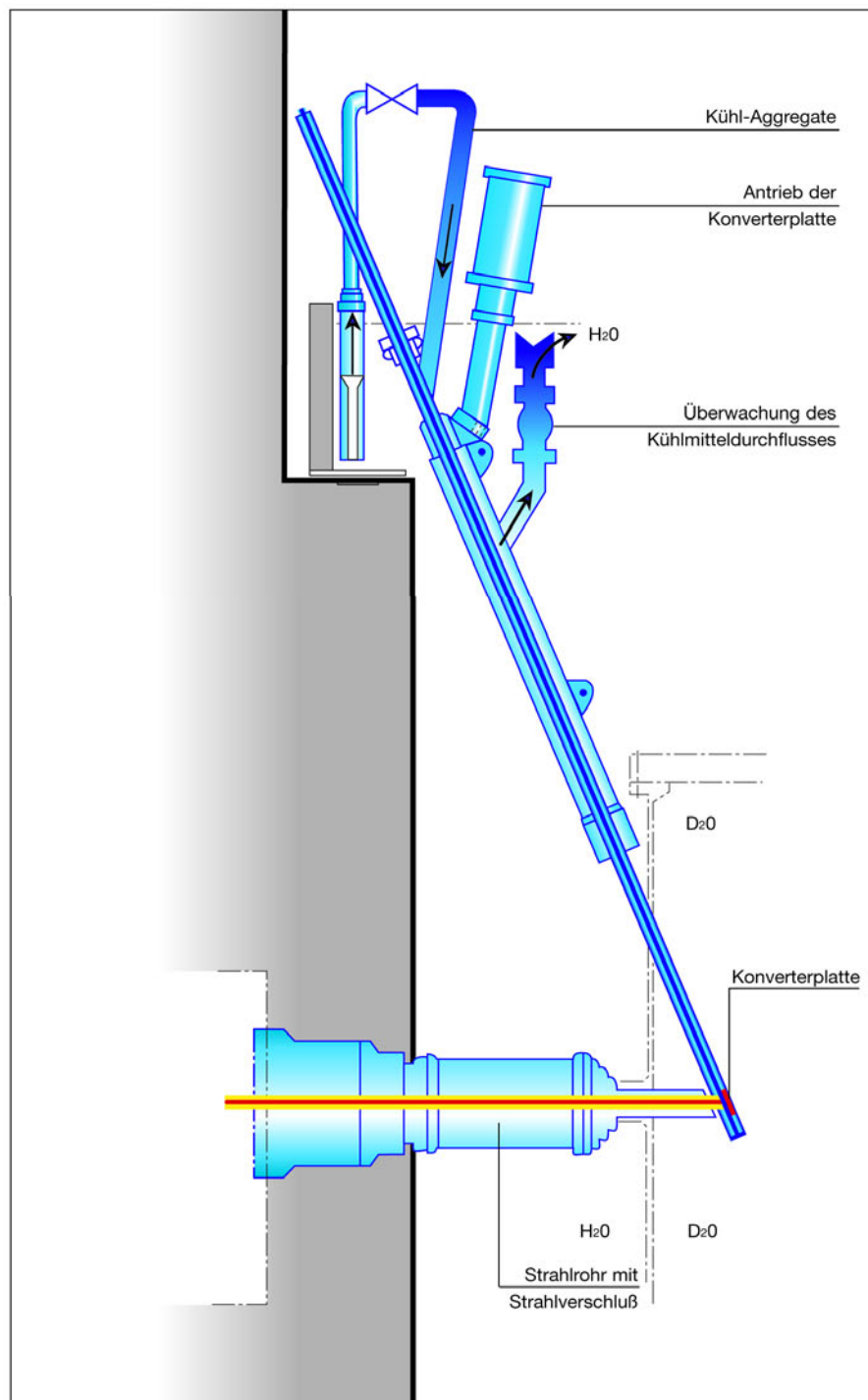

Figure 5.10: Schematic view of the converter

5.5 Irradiation Facilities

H. Gerstenberg[1], **X. Li**[1], **G. Langenstück**[1], **M. Oberndorfer**[1]
[1]ZWE FRM-II, TU München

During the year 2004 the irradiation facilities being part of the initial equipment of the FRM-II reactor underwent their nuclear start-up. In particular these facilities are

- the pneumatic rabbit system RPA,
- the capsule irradiation facility KBA,
- the test rig of the silicon doping facility SDA,
- the transport rabbit system serving as quick connection between FRM-II and the institute for radiochemistry (RCM).

Altogether the nuclear taking into operation of these facilities comprises 17 various checks most of which had to be carried out at different levels of reactor power.

In addition in the very beginning of reactor operation neutron flux measurements were carried out in the framework of the calibration of the reactor power. Thus the very first experiment at the FRM-II was the irradiation of Al:Au and Al:Co wires acting as neutron flux monitors on March 3, i.e. only one day after the date of the first criticality.

Pneumatic Rabbit System RPA

The pneumatic rabbit system consists of six independent irradiation channels, which are suited to be loaded by identical polyethylene capsules. Due to their different positions within the heavy water moderator tank these irradiation channels offer thermal neutron flux densities between $5.1 \times 10^{12}\ cm^{-2}s^{-1}$

Channel	Φ_{th}	Φ_{epi}	Φ_f	$(unit\!:\!cm^{-2}s^{-1})$
RPA-1	3.5×10^{13}	9.6×10^{09}	2.0×10^{09}	
RPA-2	1.5×10^{13}	4.8×10^{09}	4.3×10^{08}	
RPA-3	5.1×10^{12}	1.4×10^{09}	7.2×10^{07}	
RPA-4	6.8×10^{13}	3.3×10^{11}	4.3×10^{10}	
RPA-5	3.9×10^{13}	1.4×10^{10}	5.2×10^{09}	
RPA-6	7.0×10^{12}	1.8×10^{09}	1.5×10^{08}	

Table 5.1: Flux data for the RPA systems

and $6.8 \times 10^{13}\ cm^{-2}s^{-1}$ at full reactor power of 20 MW. The ratio between thermal and fast neutron flux densities is $\gg 1000$ for all of the irradiation channels. The detailed results of the neutron flux measurements are shown in table 5.1.

Besides the measurement of the neutron flux densities the suitability of the shielding in the decay and handling positions for irradiated samples, the maximum heating of samples during irradiation and the contamination status of the tube system was checked during the nuclear start-up phase. It is a peculiarity of the the RPA that before irradiation the air contained in the irradiation capsules is exchanged by CO_2 in order to avoid an increased dose rate due to the production of Ar-41. The effectivity of this exchange process was determined by the irradiation of an empty capsule and subsequent gamma spectrometric analysis to be better than 95%. Finally by means of the irradiation of a Cd-lined capsule the maximum influence of a RPA sample on the reactivity of the reactor was established to be as small as 2 pcm. From this experiment it turned out that RPA capsules can be loaded into and unloaded from the irradiation position

during reactor operation no matter what kind of sample is contained in the capsule.

Capsule Irradiation Facility KBA

The capsule irradiation facility is a pool water driven rabbit device to be used for long term irradiations. It exhibits two irradiation positions both of which can be loaded by up to five Al irradiation capsules. This facility had to undergo a taking into operation program similar to the one of the pneumatic rabbit device. In order to keep the very tight time limits during the nuclear start-up of the FRM-II the neutron flux densities were so far only measured in the two lowest positions of each irradiation channel. The results are shown in table 5.2.

In further steps it was established similar to the procedures described above for the RPA facility that the heating of the water cooled KBA capsules during irradiation is far below critical values and that the influence of the loading and unloading of capsules on the reactivity of the reactor is 7 pcm in maximum and therefore small enough to allow these procedures at reactor opera-

Channel	Φ_{th}	Φ_{epi}	Φ_f	$(unit : cm^{-2}s^{-1})$
KBA1-1	1.3×10^{14}	2.6×10^{11}	3.9×10^{11}	
KBA1-2	9.3×10^{13}	9.9×10^{10}	2.0×10^{11}	
KBA2-1	1.1×10^{14}	7.5×10^{10}	2.1×10^{11}	
KBA2-2	7.7×10^{13}	3.9×10^{10}	1.0×10^{11}	

Table 5.2: Flux data for the KBA systems

Figure 5.11: Positions of flux monitors in the test ingots.

tion for all kinds of sample materials.

In the KBA facility the decay of the freshly irradiated samples takes place within the storage pool of the FRM-II in a distance of approximately 4 m below the surface of the pool. It showed up that the shielding of this position is sufficient to guarantee the very strict dose rate limits of maximally 10 $\mu Sv/h$ for the working area above the decay positions.

Summary

In 2004 a total of 114 irradiations were carried out at the FRM-II. About 40 of which were part of the nuclear start-up procedure of the reactor. It was established that generally speaking the irradiation facilities work properly and that these facilities are prepared to enter into routine operation.

After completion of the nuclear start-up procedures the FRM-II was operated several weeks at nominal power of 20 MW. Already during this period the first irradiations for scientific purposes were carried out. The users of the irradiation service were not only scientists working at the FRM-II but also external customers like the Institute for Radiochemistry of the Technische Universität München (RCM) or the geological institute of the Universität Bremen.

Silicon doping Facility SDA

The silicon doping facility (SDA) will serve for neutron transmutation doping of the semiconductor Si. During the nuclear start-up phase of the reactor, the following checks were carried out on this facility at different levels of reactor power by using a simplified test rig:

- Determination of neutron flux at the irradiation position (200 kW, 2 MW, 20 MW),
- Measurement of temperature within the ingots (10 MW, 20 MW),
- Influence on the reactor reactivity (200 kW, 10 MW, 20 MW).

The neutron flux distribution in the Si ingots was determined experimentally. Flux monitors (Al:Au, Zr) were placed at different positions within two test Si ingots which were rotated on their own axis with 5-6 rotations per minute during the irradiation. The test ingots had a diameter of 15 cm and a total length of 50 cm. Fig. 5.11 shows the positions of the flux monitors in the test ingots. Al:Au standard wires with high concentration of 0.2% Au were used at the low levels of reactor power and the irradiation time was also increased to 2 hours accordingly, so that we could get suitable conditions in the γ-counting. In the other start-up steps the Au-concentration was reduced to 0.1% and the irra-
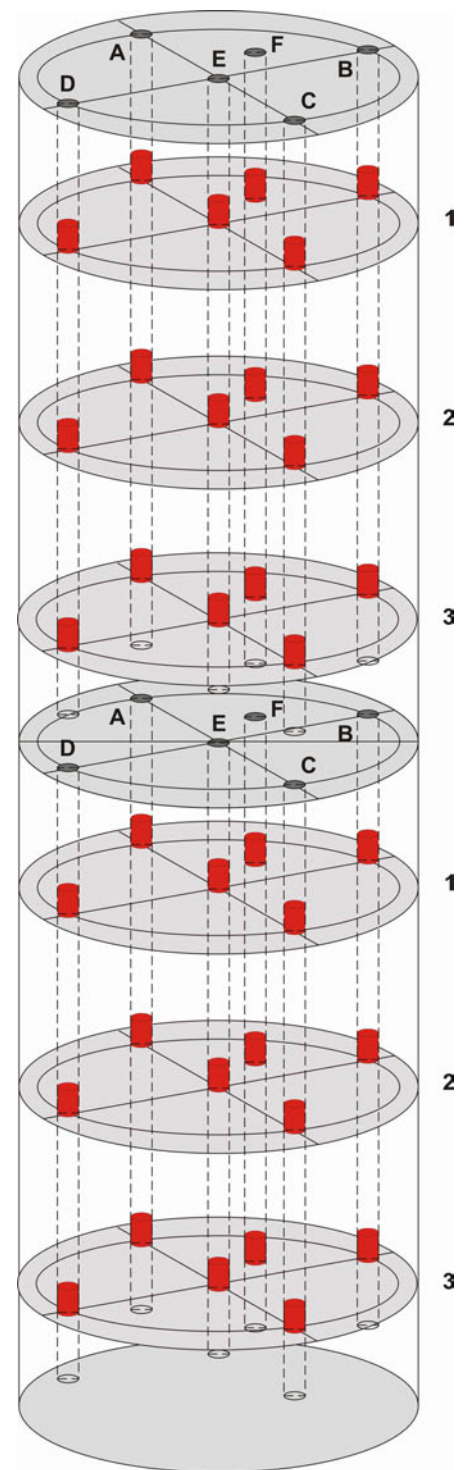
diation time to 40 minutes. The γ-countings of the monitors were performed in the institute for radiochemistry (RCM) and the calculation method of MULTIFLUX [1] was used to determine the absolute val-
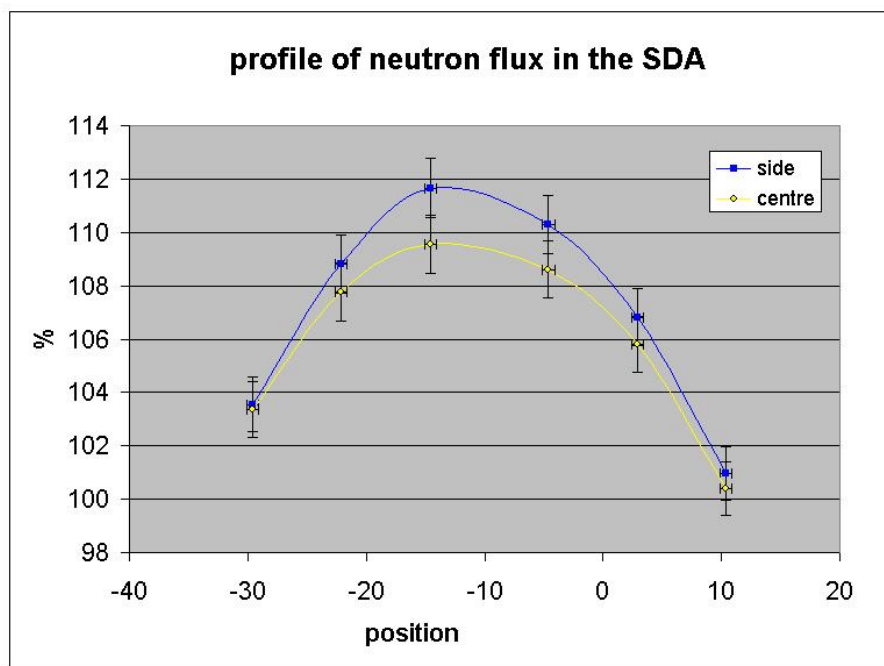
Figure 5.12: Profile of neutron flux in the SDA.

ues of thermal and epithermal neutron flux densities. An extrapolation of the measuremed valuess shows a maximal thermal neutron flux density of $1.7 \times 10^{13} \ cm^{-2} s^{-1}$ in the middle of the doping position at 20 MW.

The inhomogeneity of neutron flux within the test ingots was determined by comparing the specific activity of the Au-standards mounted at different positions. The axial difference between the middle level and the both edges of the test ingots was about 12%. The radial difference was smaller than 3% within the 6"-ingots. Based on the values of the flux profile (fig. 5.12), the shape of the Ni-absorber which should reduce the inhomogeneity of the neutron flux below 5% was calculated by means of a Monte-Carlo calculation. The Ni-layer will be spread on the Al-liner. A prototype of such an absorber has the simplified shape of a trapezium (fig. 5.13) and will be made by the company Leistner. Because the maximal wall thickness of

the Ni-layer is 1 mm and the liner will be exposed in a high neutron field for a long time, the quality control of the fabrication will be strictly arranged. The first test liner will be

mounted on the outside of the irradiation container of the SDA-test rig and will be tested in the next reactor cycle. The final Si doping facility offering a semi automatic operation will be completed in the second half of 2005 after the liner is optimized. The documents of the construction must be verified by the TÜV at first.

The irradiation position of the ingots is exposed to a very strong γ-field in the moderator tank. Therefore the local temperature in the Si ingots increases due to the γ-heating from the close surrounding. The temperature was measured by using special thermal melt crayons. Small crayon samples with different melting points were packed in quartz ampoules and placed within the ingots at different positions like the flux monitors. The measurement results show a maximal temperature of ca. 110°C in the middle of the ingots at 19,5 MW. An effective cooling system will be built in the final Si doping facility for long time
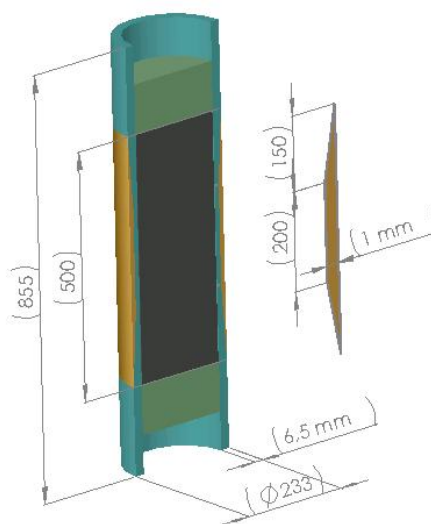

Figure 5.13: The first test liner with Ni-layer.

irradiations in routine operation.

Already in the first step of the reactor start-up the influence of the Si-ingots on the reactor reactivity was investigated during the drive-in and drive-out of the test ingots in the moderator tank. The change of the reactivity was very small because of the relative far distance of 100 cm from the middle of the doping facility to the reactor core. The maximal change of ± 10 pcm was measured at 19,5 MW. That means that the handling of the doping facility does not bring any risk for the reactor security.

[1] Lin, X., Baumgärtner, F., Li, X. *J. Radioanal. Nucl. Chem. Art.*, 215, (1996), 179.

Figure 5.14: View of the RPA control room.

6 Scientific Highlights

6.1 Effects of high-pressure hydrogen charging on the structure and lattice dynamics of austenitic stainless steels

M. Hoelzel [1,2], **V. Rajevac** [1], **S.A. Danilkin** [3], **H. Ehrenberg** [1], **D.M. Toebbens** [3], **T.J. Udovic** [4], **H. Fuess** [1], **H. Wipf** [5]

[1]Material- und Geowissenschaften,TU Darmstadt

[2]ZWE FRM-II, TU München

[3]SF2, Hahn-Meitner-Institut, Berlin

[4]NIST Center for Neutron Research, National Institute of Standards and Technology, Gaithersburg, MD

[5]Institut für Festkörperphysik, TU Darmstadt

Austenitic stainless steels are very widely applied due to their high corrosion resistance and good mechanical properties. Their applications reach from sets of cutlery to pressure vessels, marine screw propellers and turbines. The degradation of mechanical properties due to the uptake of hydrogen from the environment is a severe problem for a lot of applications. Among the postulated mechanisms of hydrogen embrittlement in austenitic stainless steels, the hydrogen-induced formation of brittle hydride and martensite phases is under discussion.

In this work, steel samples have been studied, which were hydrogenated under high pressures in order to investigate the phase transformation behaviour due to hydrogen chargings. The results were compared with literature data based on electrolytically hydrogenated samples [1, 2, 3, 4, 5, 6]. High-pressure hydrogenations lead to quite homogeneous hydrogen distributions in the bulk, while electrolytical hydrogen chargings result in a hydrogen deposition on the surface with strong gradients in the hydrogen concentration. The effects of hydrogen on the structure and lattice dynamics in austenitic stainless steels Fe/Cr18/Ni10 and Fe/Cr25/Ni20 have been investigated by elastic and inelastic neutron scattering as well as by X-ray diffraction. Inelastic neutron scattering is a very sensitive technique to study hydrogen, giving information on the formation of hydrides which are complementary to the results obtained by diffraction.

It was found that hydrogen and deuterium atoms occupy exclusively the octahedral interstitial sites in both steels. In the frame of accuracy, no hydrogen-induced phase transformations have been observed in steel Fe/Cr25/Ni20 for the whole range of hydrogen concentrations up to H/Me = 1. In case of Fe/Cr18/Ni10, the formation of ε-martensite occurred due to hydrogenations at 3.0 GPa and 7.0 GPa,
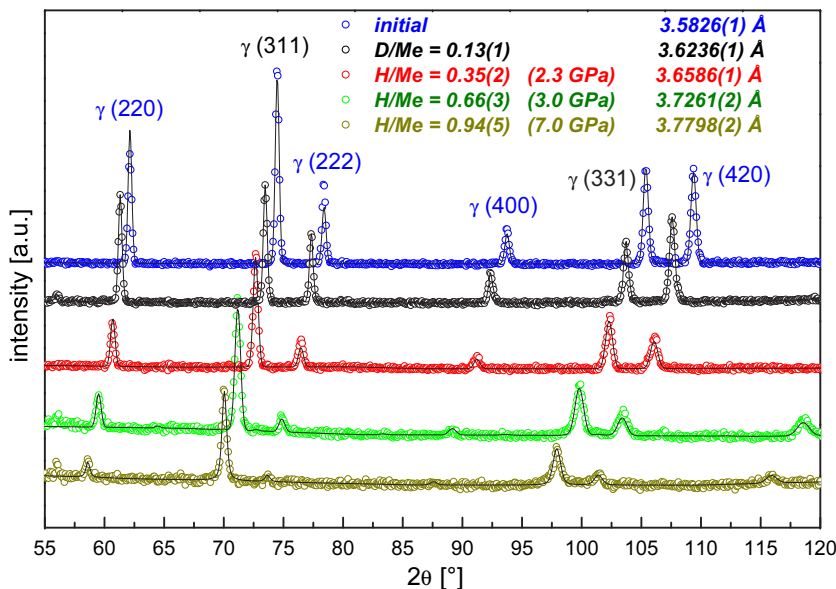

Figure 6.1: Measured (circles) and calculated (lines) neutron diffraction patterns for 310 stainless steel (Fe/Cr25/Ni20) charged with different hydrogen (deuterium) contents.
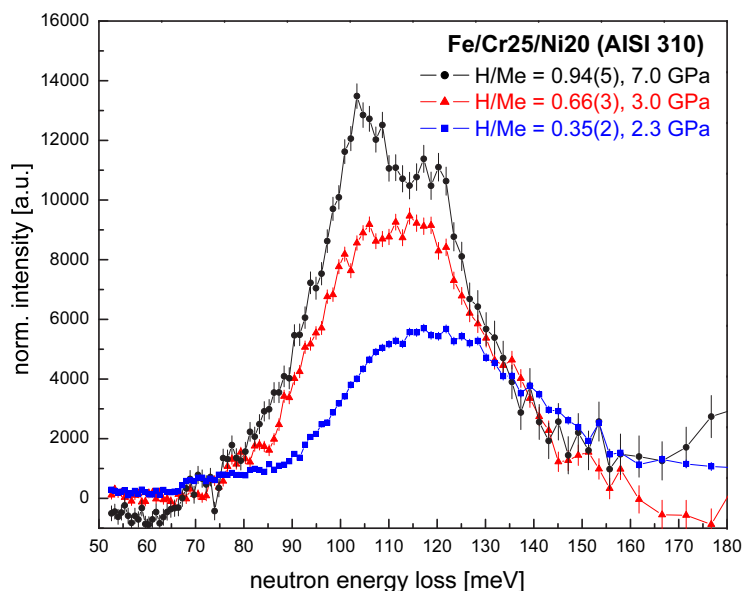
Figure 6.2: Inelastic neutron scattering spectra for 310 stainless steel (Fe/Cr25/Ni20) charged with different hydrogen (deuterium) contents, after background subraction.

corresponding to hydrogen contents of H/Me = 0.56 and H/Me = 1.03, respectively [7]. Additionally, the formation of ε-martensite was observed in Fe/Cr18/Ni10 after subjection to 4.0 GPa without the presence of hydrogen.

Neither the elastic, nor the inelastic neutron scattering experiments gave indications for hydrides. In the vibrational spectra a continuous decrease of the vibrational energies of the optical modes has been observed for increasing Me - H interatomic distances. In both steels, the optical modes in the samples with highest hydrogen contents showed a splitting into a two-component profile, which could be explained by longitudinal and transverse optical branches. In all samples, the peaks corresponding to the optical modes showed a significant broadening compared to the instrumental resolution. Supposedly, this broadening was mainly determined by the modification of the vibrational energies due to different configurations of metal atoms around hydrogen atoms [8, 9].

Even at maximum hydrogen contents, the high-pressure charged samples revealed a lower tendency for the formation of ε-martensite compared to electrolytically hydrogenation. The results indicate, that the formation of ε-martensite is less determined by the absolute hydrogen concentration rather than the stress states resulting from the particular hydrogen distributions.

In this work, several results have been achieved which contradict the postulated hydrogen-induced formation of hydride and martensite phases in austenitic stainless steels:

At first, no hydrides have been detected in both Fe/Cr25/Ni20 and Fe/Cr18/Ni10 steels. Secondly, no phase transformations have been found at all in steel Fe/Cr25/Ni20 for the whole range of hydrogen concentrations up to H/Me = 1. Moreover, in steel Fe/Cr18/Ni10 martensitic transformations could be achieved by high pressures even in the absence of hydrogen.

[1] Sugiyama, S., Ohkubo, H., Takenaka, M., Ohsawa, K., Ansari, M. I., Tsukada, N., Kuramoto, E. *J. Nuclear Mat.*, 283-287, (2000), 863.

[2] Mathias, H., Katz, Y., Nadiv, S. *Metal Science*, 12, (1978), 129.

[3] Kamachi, K. *Trans. ISIJ*, 18, (1978), 485.

[4] Gavriljuk, V. G., Hänninen, H., Tereshchenko, A. S., Ullakko, K. *Scripta Metall. et Mater.*, 28, (1993), 247.

[5] Narita, N., Altstetter, C. J., Birnbaum, H. K. *Metal. Trans. A*, 13A, (1982), 1355.

[6] Ulmer, D. G., Altstetter, C. J. *Acta metal. mater.*, 41(7), (1993), 2235.

[7] Hoelzel, M., Danilkin, S., Ehrenberg, H., Toebbens, D. M., Udovic, T. J., Fuess, H., Wipf, H. *Mat. Sci. & Eng. A*, 384, (2004), 255.

[8] Rajevac, V., Hoelzel, M., Danilkin, S. A., Hoser, A., Fuess, H. *J. Phys. C: Cond. Matter.*, 16, (2004), 2609.

[9] Hoelzel, M., Rajevac, V., Danilkin, S. A., Udovic, T. J., Wipf, H., Fuess, H. *submitted to J. Phys.: Cond Matter.*

6.2 Reinvestigation of magnetic critical phenomena in MnSi

D. Lamago[2,1], **R. Georgii**[2,1], **P. Böni**[1], **O. Okorokov**[3], **Yu.O. Chetverikov**[3], **H. Eckerlebe**[4], **P. K. Pranzas**[4]

[1]E21, Physik-Departmentm TU München
[2]ZWE FRM-II, TU München
[3]Petersburg Nuclear Physics Institute, Gatchina, Russia
[4]GKSS-Forschungszentrum, Geesthacht

The predictions of Kawamura [1] on the existence of new universality classes for magnetic systems with chiral symmetry motivated several theoretical and experimental investigations of critical phenomena in helical magnets. In spite of some experimental validation of the hypothesis of new chiral universality classes, the Kawamuras predictions are still subject of controversy. Azaria et al. [2] suggest that the lack of universality of experimental results on Ho, Dy and Tb can be understood as the consequence of a tricritical mean-field behavior for the Heisenberg-like spin-order. Experimental and theoretical investigations of the magnetic critical behavior in the intermetallic compound MnSi could help to explain the phase transitions in helimagnets since MnSi is known as a typical chiral magnet and exhibits a complex magnetic transition at 29 K. Here we report on critical small angle po-
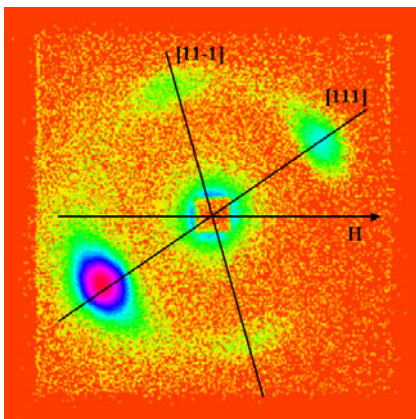

Figure 6.3: SANS scattering patterns observed in MnSi at zero field for $T = 17$ K.

larized neutron scattering measurements of a single crystal of MnSi. A precise alignment of the single crystal allows to study the critical behavior of each magnetic satellite separately and thus to evaluate with high accuracy the critical exponents of the phase transition. The measurements were performed at the GKSS research center (SANS-2) and at the FRM-II (MIRA).

The high quality single crystal was oriented in such a way that two axes [111] were set in a plane perpendicular to the incident beam. The possibility to rotate the sample was given by a low temperature piezo-rotator of *Attocube Systems* [3]. The sample could be rotated only around the vertical axis, it was not possible to tilt the sample. This set-up allowed us to select a magnetic satellite of interest and then to perform a field and/or a temperature scan. In our previous experiment it was quite difficult to satisfactorily align the crystal since there were no goniometer available.

Fig. 6.3 displays a typical diffraction pattern of a helical magnet at zero field for $T = 17$ K. We denote the appearance of four magnetic peaks due to the reflection of the chiral vectors collinear to the two [111] axes. There are no additional peaks as in our previous measurements, which indicates a better crystal orientation. First measurements on the Instrument MIRA at the FRM-2 display a similar scattering pattern (see Fig. 6.4).
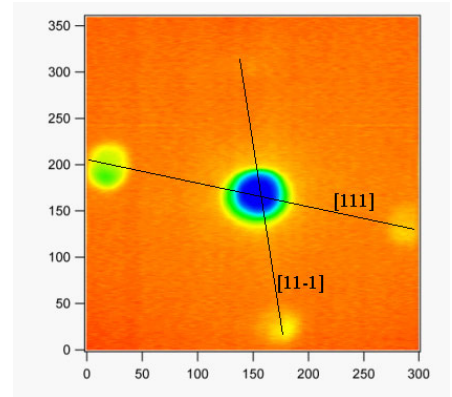

Figure 6.4: Scattering patterns observed in MnSi on the instrument MIRA at zero field for $T = 27$ K.

The sample was then rotated in such a way that only the magnetic satellites along one of the [111] direction were visible (not shown). It should be noticed that the other peaks were not dissolved completely since it was not possible to tilt the sample. In this geometry we used polarised neutrons and changed the magnetic field from $H = 0$ to 600 mT. As soon as a magnetic field is applied, the selected satellites move towards the direction of the field so that at $H_c = 350$ mT the peaks collapses to the direction of the magnetic field and only one satellite is visible as shown in Fig.6.5 (case with flipper on). The intensity of this peak begin to decrease with further increase of the magnetic field and finally vanished, i.e. no scattering is observed anymore. From the dependence of the scattering intensity with the reduced magnetic field $I \propto (H - H_C)^{\beta}$, we find the critical exponent $\beta = 0.23 \pm 0.013$ of the phase
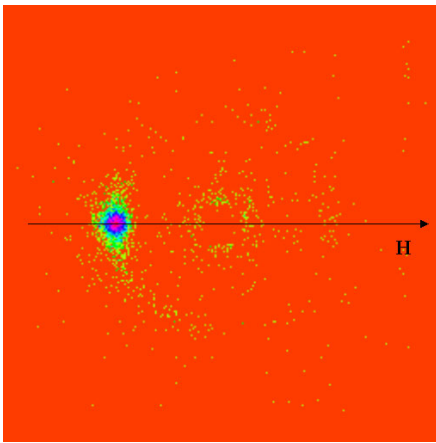
Figure 6.5: SANS scattering patterns at $H = 350\,\text{mT}$ for $T = 17\,\text{K}$.

transition due to the wave-vector rotation towards the [111] direction.

[1] Kawamura, H. *J. Appl. Phys.*, 63, (1988), 3086.

[2] Azaria, P., Delamotte, B., Jolicoeur, T. *J. Appl. Phys.*, 69, (1991), 8.

[3] http://www.attocube.com.

6.3 Polarized SANS measurements of the flux line lattice in Niobium

Sebastian Mühlbauer [1], **Robert Georgii** [1,2]
[1]E21, Physik-Departmentm TU München
[2]ZWE FRM-II, TU München

Intention

Magnetic structures of superconductors have great importance in helping to understand the mechanism of superconductivity, especially of the modern cuprate superconductors like YBaCuO. These superconductors belong to the so called type II superconductors, which are penetrated by external fields in the region of $H_{c1} < H < H_{c2}$ in form of flux or vortex lines. The ideal flux line lattice (FLL) is described by a hexagonal symmetry that may be disturbed owing to e. g. the crystal lattice of the bulk superconductor, possible crystal defects, lattice distortions or the surface roughness of the material. As the critical field or current density is lowered near to such crystal anomalies, they act as pinning centres for flux lines.[1]

Experiments

The flux line lattice (FLL) of a superconducting niobium single crystal has been measured in SANS (small angle neutron scattering) geometry on the instrument MIRA at the FRM II. With SANS, especially using long wavelengths, it is possible to gain direct information about the magnetic structure of the sample.

Experimental setup

To provide a suitable sample environment for the FLL measurements, a pair of Helmholtz coils with current supply and a closed cycle cryostat with temperature controller were adapted to MIRA. The temperature can be driven from 3.5 K to ambient temperature (stability below 0.02 K), and a magnetic field up to 0.15 T can be applied parallel and vertical to the neutron beam (see Fig. 6.6).

Results

With a two dimensional position sensitive detector, the scattered intensity was recorded. In order to put the sample in the Shubnikov-phase, a external magnetic field, oriented parallel to the incident neutron beam, was applied.
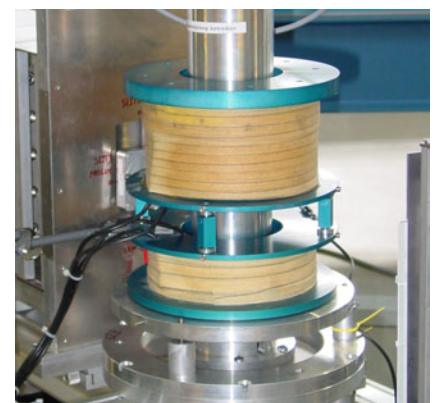

Figure 6.6: The closed cycle cryostat mounted together with the small Helmholtz coil system on the sample table on MIRA

The field strength was varied from zero to 0.15 Tesla, the temperature range was 3.5 K to 9.5 K. For a incident wavelength of 10 Å the observed magnetic peaks show a sixfold symmetry (separated by 60°), corresponding to $|Q| \approx 0.01$ Å at 6.5 K and 0.15 T (see Fig. 6.7.

Outlook

In addition to the conducted SANS experiments in 2004, it is planned to do polarized SANS on the sample in order to get a deeper insight in the chirality of the FLL. It is also planned to investigate the vortex behavior near to the critical field H_{c2}. The latter experiment shall add information whether a melting transition of the FLL takes place at H_{c2} [2]. Niobium was chosen because of its well known behaviour, to get used to the instrument´s capabilities for future measurements on high T_c superconductors.

[1] Buckel, W. *Supraleitung* (VCH).

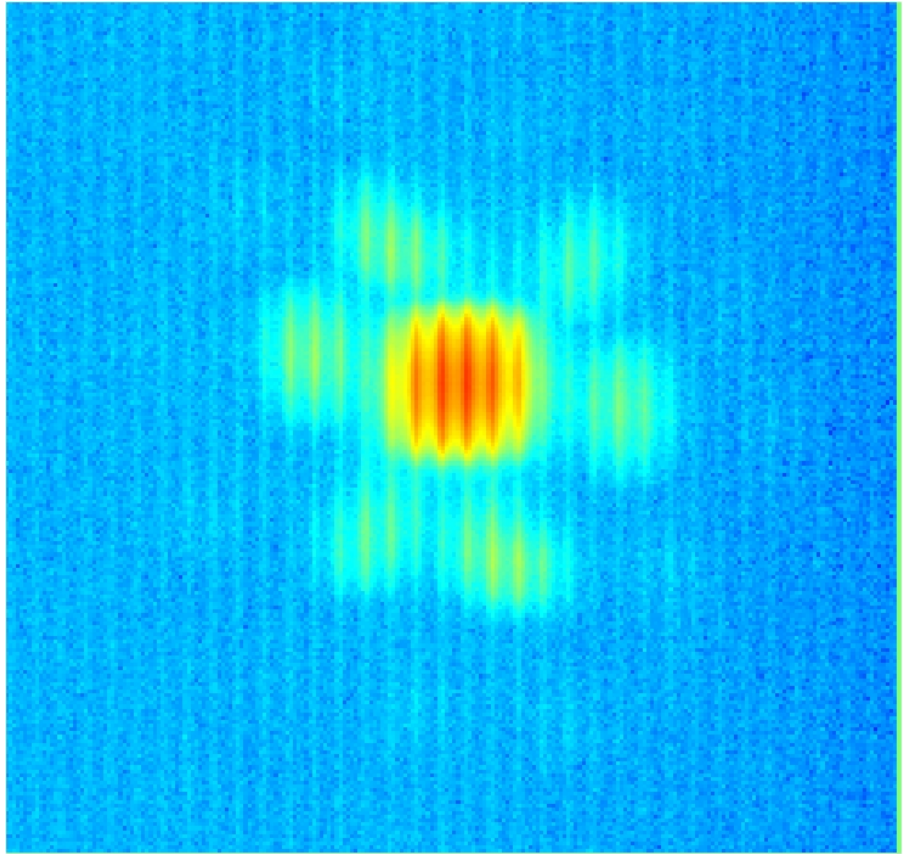[2] Lynn, J. W., *et al. Phys. Rev. Lett.*, 72, (1994), 3413.

Figure 6.7: SANS picture of the FLL of niobium on MIRA. The sixfold symmetry is observed. The first order peaks are centered around the direct beam, second order peaks are visible, but of low scattering intensity. The lined structure results from the anode wires of the detector.

7 People, Facts and Figures

7.1 Facts and figures

J. Neuhaus[1]
[1]ZWE FRM-II, TU München

User office

The first call for proposals was published in October 2004. It covered 14 instruments for neutron experiments and 3 instruments using a positron beam. At the deadline of 1^{rst} of November we received 119 proposals demanding 1089 days of beam time. The first call for proposals covered the cycles no. 2 and 3 and explicitly asked for *friendly users* to test and optimize the instruments. In view of the ongoing commitioning and the different progress on the instruments we had to limit the number of days per instrument between 35 and 52 to be allocated to external users. The selection of the proposals was done by external referees (member list see 7.2). In view of the large number of proposals we had to split the referees into two groups. For the future selection committees these groups will be divided more specifically to scientific areas. Altogether 688 days could be
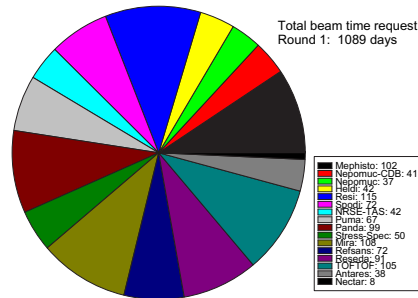

Figure 7.1: Number of proposals per instrument in round 1.

allocated.

The FRM-II participates in the Framework 6 programme (FP6) of the European Community in the *Neutron Myon Integrated Infrastructure Initiative* (NMI3). Main part is the programme to grant access for European (non German) user groups to perform experiments at our institute. We received 19 proposals out of which 13 were approved by the referees. Here we could allocate 88 days of beam time.

Visits and events

In the year 2004 we organized as every year, together with other institutes from the campus in Garching an open house day on October, 23rd. This day 419 visitors were guided through the experimental halls and were informed about the use of the FRM-II during lectures in the physics department. All together we welcomed 3463 visitors

during the year 2004 . This still large number presents a more than 20reduction compared to the preceding year, which reflects the access restrictions during the startup of the reactor. Noteworthy is the large portion of students (705) and pupils (417) on the total amount of visitors in 2004.
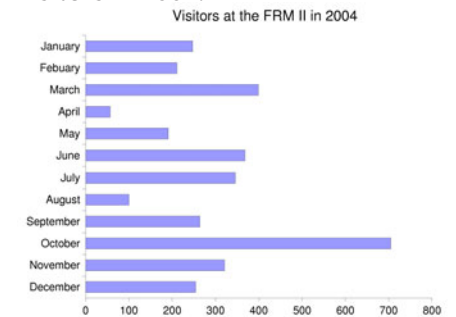

Figure 7.2: Number of visitors in 2004

For the public relation of the FRM-II the most important event clearly has been the official inauguration on June 9th. Here about 1000 guests joined the ceremony at the campus in Garching. Further prominent visits were the summer interview of Minister-President Dr. Edmund Stoiber taken partly at the experimental hall of the FRM-II and broadcasted on the German television channel ZDF August 5th. During the second half of 2004 the Bavarian television has recorded a 30 minute television film about the FRM-II which was broadcasted in February 2005.

7.2 Committees

Strategierat FRM-II

Chairman

Prof. Dr. Gernot Heger
Institut für Kristallographie

RWTH Aachen

Members

Ministerialdirigent Jürgen Großkreutz
Bayerisches Staatsministerium für Wissenschaft,
Forschung und Kunst

MRin Dr. Ulrike Kirste
Bayerisches Staatsministerium für Wissenschaft,
Forschung und Kunst
(since July 2004)

Dr. Rainer Köpke
Bundesministerium für Bildung und Forschung

Prof. Dr. Georg Büldt
Institut für Biologische Informationsverarbeitung
Forschungszentrum Jülich

Prof. Dr. Dosch
Max-Planck-Institut für Metallforschung

Prof. Dr. Dieter Richter
Institut für Festkörperphysik
Forschungszentrum Jülich

Prof. Dr. Dirk Schwalm
Max-Planck-Institut für Kernphysik, Heidelberg

Prof. Dr. Helmut Schwarz
Institute for Chemistry
Technische Universität Berlin

Prof. Dr. Dr. Michael Wannenmacher
Radiologische Klinik und Poliklinik
Abteilung Strahlentherapie
Universität Heidelberg

Dr. Heinz Voggenreiter
Director
Institute of Structures and Design
German Aerospace Center (DLR) Stuttgart

Prof. Dr. Götz Eckold
Institute of Physical Chemistry
Universität Göttingen
(Speaker Instrumentation advisory board)

Guests

Prof. Dr. Dr. Wolfgang A. Herrmann
Präsident der Technischen Universität München

Dr.-Ing. Rainer Kuch
Zentrale Verwaltung
Technische Universität München

Dr. Michael Klimke
Zentrale Verwaltung
Technische Universität München

Prof. Dr. Winfried Petry
ZWE FRM-II
Technische Universität München

Prof. Dr. Klaus Schreckenbach
ZWE FRM-II
Technische Universität München

Guido Engelke
ZWE FRM-II
Technische Universität München

Dr. Viola Klamroth
ZWE FRM-II
Technische Universität München

Committee for Industrial and Medical Use

Members

Automobile Industry
Dr.-Ing. Rainer Simon
BMW AG München

Dr.-Ing. Maik Broda
Ford Forschungszentrum Aachen

Aerospace Industry
Dr.-Ing. Rainer Rauh
Airbus Deutschland Bremen

Chemistry and Environment
Dr. Jens Rieger
BASF AG Ludwigshafen

Dr. Ralph Gilles
TU München ZWE FRM-II
http://www.frm2.tum.de/industrie

Dr. Heinz Voggenreiter
German Aerospace Center (DLR) Stuttgart

Committee for Evaluation of Beamtime Proposals

Members

Prof. Markus Braden
Physikalisches Institut
Universität zu Köln

Prof. Michael Monkenbusch
Institut für Festkörperforschung
Forschungszentrum Jülich

Prof. Heinz-Günther Brokmeier
Institut für Werkstoffforschung
GKSS - Forschungszentrum Geesthacht

Prof. Werner Paulus
Structures et Propriétés de la Matière
Université de Rennes 1

PD Mechthild Enderle
Institut Laue Langevin
Grenoble

Prof. Günther Roth
Institut für Kristallographie
RWTH Aachen

Prof. Jan Jolie
Institute of Nuclear Physics
Universität zu Köln

Prof. Wolfgang Scherer
Institut für Chemische Physik
Universität Augsburg

Prof. Bernhard Keimer
Max-Planck-Institut für Festkörperforschung
Stuttgart

Prof. Wolfgang Schmahl
Mineralogie und Kristallographie
Ruhr-Universität Bochum

Prof. Karl Maier
Helmholtz-Institut für Strahlen- und Kernphysik
Bonn

Prof. Jeremy Smith
Fachbereich Computational Molecular Biophysics
Universität Heidelberg

Prof. Monika Willert-Porada   PD Katharina Theis-Bröhl
Lehrstuhl für Werkstoffverarbeitung   Festkörperphysik
Universität Bayreuth   Ruhr-Universität Bochum

Scientific Secretaries

Dr. Ralph Gilles   Dr. Peter Link
ZWE FRM-II   ZWE FRM-II

TUM Advisory Board

Chairman

Prof. Dr. Ewald Werner
Lehrstuhl für Werkstoffkunde und -mechanik
Technische Universität München

Members

Prof. Dr. Peter Böni
Physik Department E21
Technische Universität München

Prof. Dr. Andreas Türler
Institut für Radiochemie
Technische Universität München

Prof. Dr. Markus Schwaiger
Nuklearmedizinische Klinik und Poliklinik
Klinikum rechts der Isar
Technische Universität München

Prof. Dr. Bernhard Wolf
Heinz Nixdorf-Lehrstuhl für medizinische Elektronik
Technische Universität München

Prof. Dr. Arne Skerra
Lehrstuhl für Biologische Chemie
Technische Universität München

Guests

Dr. Michael Klimke
University Management
Technische Universität München

Guido Engelke
ZWE FRM-II
Technische Universität München

Prof. Winfried Petry
ZWE FRM-II
Technische Universität München

Prof. Klaus Schreckenbach
ZWE FRM-II
Technische Universität München

Instrumentation Advisory Board

Chairman

Prof. Dr. Götz Eckold
Institute for Physical Chemistry
Georg-August-Universität Göttingen

Members

Prof. Dr. Dieter Habs
Sektion Physik
Ludwig-Maximilian-Universität München

Prof. Dr. Peter Böni
Physik Department E21
Technische Universität München

Prof. Dr. Dirk Dubbers
Physikalisches Institut
Universität Heidelberg

Dr. Hans Graf
Abteilung NE
Hahn-Meitner-Institut, Berlin

Prof. Dr. Andreas Magerl
Chair for Crystallography and Structural Physics
Friedrich-Alexander-Universität Erlangen-Nürnberg

Prof. Dr. Gottfried Münzenberg
Gesellschaft für Schwerionenforschung mbH, Darmstadt

Prof. Dr. Wolfgang Scherer
Lehrstuhl für Chemische Physik
Universität Augsburg

Dr. habil. Dieter Schwahn
Institut für Festkörperforschung
Forschungszentrum Jülich

Prof. Dr. Markus Schwaiger
Lehrstuhl für Nuklearmedizin
Technische Universität München

Prof. Dr. Andreas Türler
Institut für Radiochemie
Technische Universität München

Dr. habil. Regine Willumeit
GKSS Forschungszentrum, Geesthacht

Guests

Dr. Michael Klimke
Zentrale Verwaltung
Technische Universität München

Dr. Klaus Feldmann
BEO-PFR
Forschungszentrum Jülich

Ministerialdirigent Jürgen Großkreutz
Bayerisches Staatsministerium für Wissenschaft,
Forschung und Kunst

MRin Dr. Ulrike Kirste
Bayerisches Staatsministerium für Wissenschaft,
Forschung und Kunst

Prof. Dr. Gernot Heger
Institut für Kristallographie
RWTH Aachen

RR Felix Köhl
Bayerisches Staatsministerium für Wissenschaft,
Forschung und Kunst

Dr. Jürgen Neuhaus
ZWE-FRM-II
Technische Universität München

Prof. Dr. Winfried Petry
ZWE-FRM-II
Technische Universität München

Guido Engelke
ZWE FRM-II
Technische Universität München

Prof. Dr. Klaus Schreckenbach
ZWE FRM-II
Technische Universität München

Prof. Dr. W. Press
Institut Laue Langevin
Grenoble, France

Prof. Dr. Tasso Springer

Secretary

Dr. Peter Link   ZWE FRM-II

7.3 Staff

Board of Directors

Scientific Director
Prof. Dr. W. Petry

Technical Director
Prof. Dr. K. Schreckenbach

Administrative Director
G. Engelke

Experiments

Head
Prof. Dr. W. Petry

Secretaries
W. Wittowetz
E. Jörg-Müller

Coordination
Dr. J. Neuhaus
H. Türck

Instruments
N. Arend
H. Bamberger
S. Bayraki (MPI-Stuttgart)
J. Brunner
K. Buchner (MPI-Stuttgart)
Dr. T. Bücherl (RCI, TUM)
W. Bünten (FZ-Jülich)
E. Calzada
D. Etzdorf
J. Franke (MPI-Stuttgart)
Dr. A.-M. Gaspar
Dr. R. Georgii
Dr. R. Gilles
Dr. M.Haese-Seiler (GKSS)
Dr. W. Häußler

F. Hibsch
Dr. M. Hofmann
Dr. M. Hölzel (TU Darmstadt)
Dr. K. Hradil (Univ. Göttingen)
Dr. C. Hugenschmidt
Dr. V. Hutanu
Dr. T. Keller (MPI-Stuttgart)
Dr. V. Kudryaschov
B. Krimmer
D. Lamago
Dr. P. Link
Dr. Loeper-Kabasakal
K. Lorenz
R. Lorenz
A. Mantwill
T. Mehaddene
Dr. M. Meven
S. Mühlbauer
A. Müller
Dr. A. Ostermann
Dr. B. Pedersen
Dr. J. Rebelo-Kornmeier
R. Repper
J. Ringe
Dr. P. Rottländer (FZ-Jülich)
Dr. A. Rühm (MPI Stuttgart)

Dr. B. Schillinger
Dr. M. Schlapp (TU Darmstadt)
H. Schneider (Univ. Göttingen)
Dr. A. Schneidewind (TU Dresden)
G. Seidl
M. Stadlbauer
B. Straßer
Dr. T. Unruh
H. Wagensonner
F.M. Wagner
Dr. W. Waschkowski
Dr. U. Wildgruber (MPI-Stuttgart)

Detectors and electronic
Dr. K. Zeitelhack
Dr. I. Defendi
S. Egerland
Dr. A. Kastenmüller
D. Maier
M. Panradl
Th. Schöffel

Sample environment
Dr. J. Peters
H. Kolb
A. Müller

A. Pscheidt
A. Schmidt
J. Wetzlaff

Neutron optics
Prof. Dr. G. Borchert
C. Breunig
H. Hofmann
E. Kahle
O. Lykhvar

Administration

Head
G. Engelke

Secretary
C. Zeller

Reactor operation

Head
Prof. Dr. K. Schreckenbach

Secretaries
K. Lüttig
M. Neuberger
S. Rubsch

Management
Dr. H. Gerstenberg (irradiation and sources)
Dr. J. Meier (reactor projects)
Dr. C. Morkel (reactor operation)

Shift members
F. Gründer
A. Bancsov
A. Benke
M. Danner
J.-M. Favoli
M. Flieher
H. Groß
L. Herdam
F. Hofstetter
K. Höglauer
T. Kalk
G. Kaltenegger
U. Kappenberg

Dr. S. Masalovich
A. Urban

IT Services
J. Krüger
H. Wenninger
J. Beckmann
J. Ertl
J. Dettbarn
S. Galinski

Members
B. Bendak
B. Gallenberger
I. Heinath
H. Niedermeier
R. Obermeier

F. Kewitz
M. G. Krümpelmann
J. Kund
A. Lochinger
G. Mauermann
A. Meilinger
M. Moser
L. Rottenkolber
G. Schlittenbauer

Technical services
N. Waasmaier
K. Pfaff
J. Aigner
D. Bahmet
H. Gampfer
W. Glashauser
J. Groß
G. Guld
B. Heck
M. Kleidorfer
W. Kluge
H. Kollmannsberger
J.-L. Kraus
R. Maier
K. Otto
A. Schindler

H. Gilde
J. Mittermaier
R. Müller
J. Pulz
S. Roth
M. Stowasser
B. Wildmoser
F. Zöbisch

Public relations
Dr. V. Klamroth (ZV TUM)
I. Scholz (ZV TUM)
A. Schaumlöffel

Visitorservice
J. Jeske
U. Kurz

R. Schlecht jun.
J. Schreiner
C. Strobl
G. Wagner
A. Weber
J. Wetzl
N. Wiegner
C. Ziller

Electrics and electronics
R. Schätzlein
G. Aigner
W. Buchner
Ü. Sarikaya
H. Schwaighofer

Irradiation and sources
Dr. H. Gerstenberg
Dr. E. Gutsmiedl
Dr. X. Li
C. Müller
M. Oberndorfer
D. Päthe
W. Lange
G. Langenstück
F.-M. Wagner
A. Wirtz

Reactor projects
Dr. J. Meier
M. Schmitt
M. Ullrich

Documentation
V. Zill
J. Jung

Instrument Safety
R. Lorenz

Technical design
F.-L. Tralmer
J. Fink

H. Fußstetter
J. Jüttner
K. Lichtenstein

Workshops
C. Herzog
U. Stiegel
A. Begic
M. Fuß
A. Huber
A. Scharl
R. Schlecht sen.
M. Tessaro

Radiation protection
Dr. H. Zeising
S. Dambeck
W. Dollrieß
H. Hottmann
B. Neugebauer
H.-J. Werth
S. Wolff

Chemical laboratory
Dr. F. Dienstbach
U. Jaser
C. Auer
R. Bertsch

Reactor physics

Prof. Dr. K. Böning   Dr. A. Röhrmoser   N. Wieschalla

Security department

L. Stienen   J. Stephani

Imprint